An ESR and ENDOR study of spin relaxation of semiquinones in liquid solution*

Daniel S. Leniart

Instrument Division, Varian Associates, Palo Alto, California 94303

Henry D. Connor

Department of Chemistry, Kentucky Wesleyan College, Owensboro, Kentucky 42301

Jack H. Freed

Department of Chemistry, Cornell University, Ithaca, New York 14850
(Received 6 December 1974)

A quantitative test of the ENDOR theory for free radicals in solution has been developed experimentally using the semiquinone (SQ) radical anions of parabenzo- (PBSQ), duro- (DSQ), and 2,5-dimethyl-*para*-benzo- (2,5-DPMBSQ) dissolved in ethyl alcohol (EtOH) and dimethoxyethane (DME) solvents. It is shown that, in general, an ENDOR signal arising from a molecule containing four or less equivalent nuclei, such as PBSQ, can be analyzed rigorously whereas a molecule containing more than four equivalent nuclei, such as DSQ, which, in principle, could be analyzed rigorously, practically is best analyzed using approximate forms of the ENDOR theory. It is shown that 2,5-DMPBSQ may be analyzed using a combination of both the rigorous and approximate forms of the ENDOR theory. The analysis involves calculation of the ENDOR relaxation parameters, T_{2n}, Ω_n, and $\Omega_{e,n}$, from the experimental ENDOR percent enhancement and linewidth studies. A comparison was made by performing the ESR linewidth and saturation studies to obtain values of W_e, the electron spin–lattice relaxation probability, and W_n, the nuclear spin-relaxation probability and then using this information to predict the observed ENDOR relaxation parameters in terms of the theory. The over-all behavior of the experimental results was found to be fully consistent with the general trends predicted by the theory and expected from the quantitative measurements obtained from the ESR studies. This work describes in detail the instrumentation and experimental methods necessary to measure relaxation parameters of organic free radicals in solution. A comprehensive section describing the effects of modulation amplitude, microwave power, coherence broadening or splitting, and pulse rate is given along with methods for analyzing ENDOR line shapes in their presence. The results and analyses of all ESR and ENDOR experiments are described in detail. Analysis of the rotational correlation time τ_R, obtained from the ESR studies, shows the radical anions in DME solution are most likely solvated and affected by the counterion and/or supporting electrolyte while PBSQ in EtOH is most likely dissociated. A comparison of the experimental and theoretical magnitudes of W_e leads to the possibility that for small molecules in liquids a Brownian model of reorientation by infinitesimal jumps need not be satisfactory and that jumps of large angle would be needed to better fit the experimental data. The effect of Heisenberg exchange on ENDOR signals is analyzed and discussed in detail, leading to the conclusion that the intermolecular electron–electron dipolar interaction as well as Heisenberg exchange make contributions to the concentration dependent portion of the linewidth. However, the latter contributes much more to the ESR linewidths as compared to the ENDOR widths for PBSQ in EtOH. The above analysis is modified to include charge effects. Finally it is shown that for methyl group ENDOR cross relaxation from modulation of the isotropic hyperfine splitting via methyl group rotation is not the dominant nuclear relaxation mechanism and all methyl group ENDOR analyses are consistent with a W_n derived from the pseudosecular terms of the anisotropic electron–nuclear dipolar interaction.

I. INTRODUCTION

In a series of detailed theoretical papers, the theory for saturation and double resonance for the ESR spectra of free radicals in solution has been developed.[1–5] Detailed confirmational experiments for saturation and for electron–electron double resonance (ELDOR) have already been reported.[6–8] The case of electron–nuclear double resonance (ENDOR) has perhaps been most extensively studied theoretically in part because of its greater complexity. The general features of the ENDOR theory have been shown to be reasonably consistent with the original observations of Hyde,[9,1,2] and various rf coherence phenomena, peculiar to ENDOR and predicted by the theory, have been found to be in accord with experimental observation.[3]

The present work was undertaken to provide a quantitative experimental test of the ENDOR theory. The over-all conception is based on the recognition that the ENDOR signals (viz., the magnitudes of their enhancements and their shapes) are predicted to be completely determined by the magnitudes of the various spin-relaxation processes as well as by the strengths of the applied oscillating fields. Furthermore, it should be possible, in favorable cases, to completely determine the needed information on the spin–relaxation processes from detailed studies of ESR linewidths and saturation behavior.

Our detailed studies have been carried out on the semiquinones: *para*-benzosemiquinone (PBSQ), durosemiquinone (DSQ), and 2, 5-dimethylsemiquinone (2, 5 DMSQ). These were chosen because of the basic simplicity of their ESR and ENDOR signals, because it was relatively convenient to obtain nearly all the needed relaxation information from the ESR spectra, and because they would allow for some intercomparison of different types of ENDOR signals (e.g., ring protons vs methyl protons). We have already reported on various other aspects of the ENDOR spectra arising from a

variety of semiquinones. The ENDOR analysis is (when applied rigorously as we intended in this work) quite complex.[11] In fact, only in the simple case of PBSQ was it convenient to perform the complete rigorous analysis.[11,12] In view of this problem, another objective in this work was to test and develop approximate methods of analysis, wherever possible, to aid in dealing with the more complex cases. The theoretical basis for such approximate methods has already been dealt with in part in V,[5] but is extended here.

It will be seen that, in general, rather good agreement is obtained between theory and experiment, especially in view of the considerable difficulties involved. Some of the basic conclusions of this work have already been briefly summarized in a recent review article.[13]

We present in Sec. II a description of the experimental methodology and hardware that was used. In particular, we give a detailed discussion of features of the modified Varian ENDOR spectrometer in our laboratory in order that the ENDOR percent enhancement measurement is fully understood. The important problem of accurate measurement of the nuclear rf field at the sample is also discussed there. In Sec. III, various other important experimental variables in the ENDOR experiment are discussed. These include field modulation amplitude effects, microwave power effects, coherence effects, and pulse rate effects. The detailed discussion of the experimental results and their analysis is given in Sec. IV. This section first gives the analysis of the unsaturated ESR linewidths, and it shows how the important quantity W_n, the lattice induced nuclear spin flip rate, may be estimated from these linewidths. Also, the Heisenberg exchange frequency, ω_{HE}, is obtained for the more concentrated radical solutions. The saturation measurements and the concomitant data analysis yielding W_e, the lattice-induced electron spin flip rate, are then discussed. This includes various approximate methods for analyzing the saturation data. In the last part of that section, the results on the ENDOR linewidths and percent enhancements are presented, and they are analyzed in terms of the complete theory, or various approximate forms of it, as well as the pertinent relaxation parameters (e.g., W_e, W_n, and ω_{HE}) already obtained from the ESR analyses. Further discussion of the results in terms of rotational diffusion, weak Heisenberg exchange and intermolecular dipolar interactions, and methyl group internal rotations, appears in Sec. V. A summary of the work and general conclusions that can be drawn, including ideas for further study, appear in Sec. VI.

II. EXPERIMENTAL METHODS

A. Sample preparation

The duroquinone (DQ) was obtained from Aldrich Chemical Company. It was purified by two recrystallizations from 95% ethanol followed by a vacuum sublimation. Samples prepared in this manner were determined to be polarographically pure. The *p*-benzoquinone was prepared by oxidation of the hydroquinone (Aldrich). It was purified in the same manner as DQ. The 2, 5-dimethyl-*p*-benzoquinone was obtained from Eastman Organic Chemicals and was used without further purification.

The dimethoxyethane (DME) was Eastman White Label and was purified by usual methods.[14] The absolute ethanol was obtained from U. S. Industrial Chemicals Company and was dried by refluxing with Drierite. It was stored under vacuum over molecular sieves. The *n*-hexane was spectrophotometric grade and was obtained from Fisher Scientific Company. The polarograph-grade tetrabutylammonium perchlorate (TBAP) was obtained from Southwestern Analytical Chemical Company and was purified by successive recrystallizations from a 50% (by volume) methanol, 50% water solution and from analytical reagent ethyl acetate. After the recrystallizations, the compound was dried at 100 °C in a vacuum oven.

The DSQ and PBSQ in DME solutions were prepared by the electrochemical techniques described elsewhere.[12] The solutions were 0.1*M* in TBAP unless noted otherwise.

The ethanolic solutions of the semiquinones were prepared in a slightly different manner from that described by Das *et al.*[10] Complete details of the methods are given by Connor.[12]

B. Instrumentation

1. *ESR and ENDOR spectrometers*

We have employed a Varian ENDOR accessory and a Varian E-12 ESR spectrometer in the studies reported here, although in our initial work a Varian V-4500-10A spectrometer was utilized. A brief description of certain aspects of the equipment and operating procedures will be given to facilitate the understanding of later discussions. A more detailed discussion of the ENDOR–ESR instrumentation is given by Leniart.[11]

The ENDOR spectrometer is composed of three sections; magnetic field control, rf pulse generation, and signal detection. The field control section consists of an E-203 field controller stabilized by a field frequency lock. The rf pulse generation section is described in detail by Leniart.[11] For our work, it should be noted that this section has controls which permit the variation of the rf pulse amplitude and the rf duty cycle (pulse width). Alteration of the electronic circuitry permits one to have either a 35 Hz or 6 kHz rf pulse rate. The configuration of the detection section is dependent upon the rf pulse rate used. In the initial work, a 6 kHz gate was placed between the preamplifier and the 6 kHz receiver when the pulse rate was 6 kHz. After the ENDOR accessory was connected to the E-12 spectrometer, it was possible to completely shield the cavity region with 0.002 in copper foil and consequently eliminate all rf interference. It was then found that the 6 kHz gate did not improve the ENDOR signal to noise ratio. The gate also had a detrimental effect in that it drifted out of balance during the course of an experiment. This change in the gating caused variations in the ENDOR amplitudes. Thus, in all of our experiments utilizing 6 kHz rf puls-

ing, the 6 kHz gate was not in the circuitry and the signal passed directly from the preamp to the 6 kHz receiver. In all ENDOR work with 35 Hz rf pulsing, there was a 35 Hz gate between the 6 kHz phase detector and the 35 Hz receiver. The 6 kHz phase detector output could be either ac or dc-coupled to the 35 Hz gate.

The 9 GHz ESR saturation and linewidth studies were carried out with the Varian E-12 ESR spectrometer. A modulation frequency of 10 kHz was used in all of these experiments. The modulation amplitude was maintained at a value less than one-tenth of the ESR linewidth. The magnetic field sweep was calibrated from the splittings of a DSQ in DME sample.

The 35 GHz linewidth studies were carried out with a Varian V-4503 bridge and the V-4500-10A spectrometer system.

In the 9 GHz experiments, the temperature of the sample was maintained at the desired value using a Varian E-257 temperature control unit. The temperature was measured at the center of the cavity with a copper–constantan thermocouple and was stable to $\pm 1\,^{\circ}\mathrm{C}$. A Varian V-4557 (an older version of the E-257 unit) temperature controller with a modified nitrogen gas transfer system was used to cool the sample in the 35 GHz experiments.

At first, the ENDOR linewidth ($\Delta_{1/2,1/2}$) data was recorded on an x–y recorder whose x axis was driven by the analog form of the nuclear rf frequency. This type of x-axis drive was used to correct for nonlinearity in the rf sweep unit. In the later experiments reported here, however, the time base x axis on the x–y recorder was used, because the frequency drive originally used decreased the signal to noise. The noise increase is due to the irregularity in the counter output as a result of its averaging in zero frequency values when the rf pulse is not on. This problem was most significant when the ENDOR lines were very narrow, and it was necessary to sweep the rf frequency very slowly. We found that for the ENDOR lines which we have studied, the deviation of the rf frequency sweep from linearity over the region of the ENDOR lineshape was insignificant. In all ENDOR experiments, the $\Delta_{1/2,1/2}$'s were determined from frequency calibration marks placed on each side of the ENDOR line in the vicinity of the half-height.

2. Radio frequency field measurements

The magnitude of the nuclear rf field at the sample was measured by two independent methods: (1) an rf probe provided by Varian Associates with the ENDOR accessory, and (2) the use of an rf coherence effect.

a. Probe. The probe was positioned so that its output as viewed on a Tektronix 585 oscilloscope was a maximum. There was a $50\,\Omega$ termination connected in parallel with the probe. In order to calibrate this probe, a probe with a 2-turn loop of diameter 5.3 mm which could be connected to the oscilloscope through a two foot twisted lead was prepared. No termination was used with this probe. Care was taken to insure that no rf was picked up by the leads. Comparison of the output and diameter of the two probes under identical conditions gave a correction factor of 1.46 ± 0.10 for the output of the Varian probe. Thus, for the Varian probe,

$$E_{\mathrm{real}} = E_{\mathrm{observed}} \times 1.46 \ . \tag{2.1}$$

The value of B_n was calculated from the relationship

$$B_n = \tfrac{1}{4} E_{\mathrm{real}} / NA\omega_0 \ , \tag{2.2}$$

where N is the number of turns in the probe, A is the area of the loop, and ω_0 is the angular frequency of the rf field.

Since the servo system which controls the capacitor (see Leniart) in the resonant L–C circuit shifts the capacitor slightly away from resonance when the rf frequency sweep is off, the rf frequency was swept when the rf amplitude was being measured.

The vertical sensitivity of the oscilloscope used to measure the output of the probe was calibrated with the standard oscillator in the oscilloscope before and after each measurement of the rf power. The calibration of the oscilloscope was observed to vary by as much as 10% from one experiment to the next, so one must recalibrate compared to the standard oscillator.

b. Coherence effect. Freed *et al.*[3] have calculated that the ENDOR line begins to exhibit an rf coherence splitting when the value of $\gamma_n B_n \cong \frac{1}{2} T_{2,n}$ (where $T_{2,n}^{-1} = \Delta_{n(1/2,1/2)}$ is the NMR width). More accurate computer simulations for the PBSQ system (see below) showed that when $\gamma_n B_n = \frac{1}{2} T_{2,n}$, then the spectrum is predicted to have a central dip which is 2% of the total signal amplitude, and this result is not very sensitive to changes in relaxation parameters. Experimental spectra were obtained with the rf coherence dip of 2%, and the value of B_n was then determined from $d_n = \frac{1}{2} T_{2,n}(\mathrm{exptl})$. The rf magnetic field B_n, as measured by the coherence effect was 0.66 of the value obtained with the calibrated Varian probe. It is our belief that the coherence effect result, which *directly* reflects B_n *at the sample*, is the more reliable of the two methods, although we indicate below how both measurements affect the analysis of our results.

C. Concentration measurements

Eastman *et al.* have described the basic methods of determining radical concentrations by utilizing ESR and optical spectroscopy.[6] It was necessary to modify their methods because of the lack of stability of the radical systems which we studied. This lack of stability precluded the possibility of determining the extinction coefficient of a radical in a given solvent by ESR and optical measurements and then using exclusively optical measurements to determine the concentrations of other samples of the same system.

A KTCNE in DME sample served as a convenient secondary standard. The sample tube was equipped with a Pyrocell No. 6008 rectangular cell with a 1 mm light path for optical measurements and a 3 mm o.d. Pyrex sidearm for ESR measurements. The extinction coefficient of KTCNE in DME was determined by (1) a solvent switching technique utilizing the known value of the extinction coefficient of KTCNE in acetonitrile (ACN) and

optical measurements, and (2) by the method of Eastman *et al.*,[7] which first relies on a spin concentration measurement by ESR methods. In the solvent-switching method, a sample cell containing two auxiliary calibrated tanks has a weighed amount of KTCNE in the central tank with measured volumes of acetonitrile (ACN) and DME in each of the two auxiliary tanks. The KTCNE is first dissolved in ACN, the absorbance taken; the ACN is distilled out and the DME is distilled in and the new absorbance is taken. The process is then repeated to obtain a new absorbance with ACN to check whether any KTCNE has been decomposed or lost. The molar extinction coefficient ϵ of KTCNE in DME at 4350 Å was thus determined by Method 1 to be 7310 ± 300 and by Method 2 to be 7800 ± 700. The former result was considered more reliable than that from Method 2 and was used in all subsequent measurements.

In the determination of the concentration of an unstable free radical solution, the back cavity of the dual sample cavity was maintained at − 40 °C by the V-4540 temperature controller. The front cavity containing the standard KTCNE–DME sample was maintained at room temperature. The ESR absorptions were obtained for the standard sample and the unstable sample in the front and back cavities, respectively. Since the unstable sample would decompose if placed in the front cavity, it was necessary to develop a correction factor from which the ESR absorption area for the unstable sample in the front cavity could be determined. A second correction factor was necessary to account for changes in the microwave field distribution in the dual sample cavity because of the temperature difference of the two cavities.

The two correction factors are concerned with differences in the microwave and modulation fields in the two cavities. Only the solvent in the solutions which we were measuring affects the microwave field. The modulation field is not affected by the sample. Thus, a sample containing a more stable free radical but the same solvent was substituted for the unstable sample in the determinations of the correction factors by straightforward procedures.[15,12]

D. ENDOR measurements

1. *Initial setup*

In general, all ENDOR spectra are composed of two symmetric groups of lines with respect to a swept nuclear radio frequency, each group equally spaced above and below the free proton precession frequency. The more intense, high frequency ENDOR lines were monitored in these studies, since the low frequency partner lines added no additional spectroscopic information and were more difficult to obtain experimentally because of a drop in amplitude of the rf drive as the frequency was lowered.[16]

The first step of the experimental setup technique was to obtain an oscilloscope display of the normal first derivative ESR spectrum. The dc field offset of the field frequency lock unit was adjusted to shift the $M_J = 0$ hyperfine line into the center of the scope display and the audio field modulation (i.e., the second modulating field, regulating the oscilloscope x axis, necessary for a display) amplitude was reduced until only a single extremum of the $M_J = 0$ hyperfine line filled the display. The sample temperature and rf power were then selected and the ENDOR cavity was allowed to equilibrate in temperature. (In fact, to assure that one sat on an ESR extremum throughout the rf frequency sweep, the cavity was allowed to equilibrate in temperature after each change of rf power.) Next the microwave power incident upon the sample was increased until the ESR first derivative amplitude was maximized. Finally, the radio frequency was swept at a given rate using an appropriate time constant; generally the sweep rates were 125 to 250 kHz/min, with a time constant of 3 sec. Once the ENDOR signal was obtained, the microwave power and modulation amplitude were readjusted to maximize the ENDOR signal to noise ratio.

Upon changing the temperature at the sample, the entire procedure given above was repeated since the experimental parameters needed for maximum signal amplitude (ESR and ENDOR) may be temperature dependent. Section III describes some of the subtleties associated with the experimental variables (modulation amplitude, microwave power, etc.) employed in the ENDOR experiment.

2. *Linewidth studies*

In each ENDOR configuration, i.e., 35 Hz field modulation, 6 kHz rf pulsing and 6 kHz field modulation, 35 Hz rf pulsing, ENDOR signals were obtained at a particular sample temperature for a series of rf powers. At any given rf power, the radio frequency was swept through the ENDOR signal four times in a given direction (sweeping a certain direction usually provided a better tracking of the rf oscillator by the servo system to maintain the LC resonant condition of the rf power amplifier). The field modulation amplitude that gave the largest obtainable ENDOR signal height often results in overmodulation of the ESR spectrum. Care was taken to insure that the modulation amplitude did not affect the ENDOR line shape (however, it does affect the ENDOR enhancement; see Sec. III). The narrowest ENDOR line measured experimentally (DSQ (EtOH) at − 30 °C) showed a half-width at half-height of $\Delta_{1/2,1/2} \cong 35$ kHz, or (since $\gamma_H = 4.2$ kHz/G) a linewidth of ~8 G. The value of the modulation amplitude employed during this particular experiment was 0.5 ± 0.16 G peak to peak and several runs were made using values just above and just below 0.5 ± 0.16 G to confirm the fact that the ENDOR line shape was unaffected. Table I compares the line shape of an experimental ENDOR signal to a true Lorentzian.

After verifying the line shape (noting, however, the deviation from Lorentzian character becomes more pronounced at high rf powers, see Ref. 3), an attempt was made to relate the ENDOR half-width at half-height to the experimentally measured rf power in the following manner:

$$\Delta_{1/2,1/2} = \sqrt{S}\,/T_{2n}\,, \tag{2.3}$$

where S is the nuclear saturation factor given by

$$S = 1 + (\Delta_n T_{2n})^2 + d_n^2(\Omega_n - \Omega_{e,n}^2\,\delta)T_{2n} \tag{2.4}$$

TABLE I. A comparison of ENDOR and Lorentzian line shapes for PBSQ.

Fraction of absorption amplitude	$\Delta/\Delta_{1/2,1/2}$ (Lorentzian)	$\Delta/\Delta_{1/2,1/2}$ (ENDOR)[b]	% deviation[c] from Lorentzian	$\Delta/\Delta_{1/2,1/2}$ (ENDOR)[d]	% deviation[c] from Lorentzian
0.9	0.337	0.379	12.5	0.324	3.9
0.8	0.507	0.526	3.7	0.543	7.1
0.7	0.667	0.695	4.2	0.667	0.0
0.6	0.832	0.853	2.5	0.857	3.0
0.5	1.000	1.000	0.0	1.000	0.0
0.4	1.248	1.189	4.7	1.257	0.7
0.3	1.525	1.453	4.7	1.495	2.0
0.2	1.960	1.853	5.5	1.952	0.4
0.1	2.871	2.695	6.1	2.838	1.1

[a] $\Delta_{1/2,1/2}$ is the half-width at half-height. Δ is the half-width at a particular fraction of the absorption amplitude.
[b] The absorption mode of configuration one was used (15 kHz field modulation and 40 Hz pulsing).
[c] % error $= ((R_L - R_{exptl})/R_L) \times 100$, where R is the reduced width $(\Delta/\Delta_{1/2,1/2})$ of a true Lorentzian (L) or experimental (exptl) line shape.
[d] The absorption mode of configuration two was used (40 Hz field modulation and 6 kHz pulsing).

and

$$\Delta_n = (\omega_n - \omega_0) , \tag{2.5a}$$

$$d_n = \tfrac{1}{2}\gamma_n B_n J_- , \tag{2.5b}$$

$$\delta^{-1} = \Omega_e + 1.33(T_{2e} d_e^2)^{-1} , \tag{2.5c}$$

while $(\Omega_n - \Omega_{e,n}^2 \delta)$ are the saturation parameters that represent the "effective" nuclear T_{1n}. Thus, when the nuclear resonance condition ($\Delta_n = 0$) is fulfilled, Eq. (2.3) can be rewritten in a manner similar to that used to analyze progressive saturation data (see, e.g., Ref. 17):

$$\Delta_{1/2,1/2}^2 = \frac{1}{T_{2n}^2} + \frac{\Omega_n'}{T_{2n}} d_n^2 , \tag{2.6a}$$

where

$$\Omega_n' = \Omega_n - \Omega_{e,n}^2 \delta . \tag{2.6b}$$

Experimentally, one measures $\Delta_{1/2,1/2}$ for a series of d_n leading to a plot of $\Delta_{1/2,1/2}^2$ vs d_n^2 having an intercept at zero rf power ($B_n = 0$) proportional to the true ENDOR linewidth and a slope proportional to the effective nuclear spin–lattice relaxation time. The generalized form of Eq. (2.6a),

$$\Delta_{1/2,1/2}^2 = i + mB_n^2 , \tag{2.7}$$

can be used to analyze any Lorentzian ENDOR line shape. Thus, by varying the rf power, a nuclear saturation technique can be devised whereby data may be obtained, the proper interpretation of which leads to relaxation parameters pertaining to ENDOR phenomena. The results are given in Sec. IV. C.

3. *Percent enhancement measurements*

a. The absolute method. The method of measurement of the absolute percent enhancement (PE) with 35 Hz radio frequency pulsing will be described by following the course of the signal coming from the crystal detector.

When one is doing an ENDOR experiment, the dc magnetic field, H_0, is set at one of the maxima of the first derivative ESR signal and the nuclear rf frequency is swept. If the rf frequency sweep is held at the point of maximum ENDOR amplitude (center of nuclear resonance), the components of the crystal signal are a 6 kHz ESR component with amplitude B and a 6 kHz–35 Hz ENDOR component of amplitude A (see Fig. 1). The 6 kHz parts of both components are amplified and detected in the 6 kHz phase detector. The amplification of the 6 kHz phase detector is represented by the factor X (see Fig. 1). The signals leaving the 6 kHz phase detector have amplitudes XA and XB. The output of the 6 kHz phase detector goes to the function selector switch which ac couples the 6 kHz phase detector to the 35 Hz gate. The dc ESR signal is stopped at the function selector switch and only the dc-35 Hz ENDOR signal passes into the gate. Since the gate is open only when the nuclear rf is on, the rf-induced signal passes through it to the audio phase detector where it is amplified, detected, and displayed on the recorder. If the gain of the audio phase detector is represented by Y, the final signal amplitude is XYA.

If the function selector switch is changed to the gated position, the 6 kHz phase detector is dc decoupled to the 35 Hz gate, and both the dc ESR signal of amplitude XB and the dc-35 Hz ENDOR signal of amplitude XA are incident on the gate. As in the ENDOR experiment, the ENDOR signal passes through the gate to the audio phase detector. In this configuration, the dc ESR signal is chopped by the gate. The signal incident on the 35 Hz phase detector has two components, dc-35 Hz ENDOR of amplitude XA and 35 Hz chopped dc ESR of amplitude XB. The output of the audio detector unit in this case would be $XY(A+B)$. If the nuclear rf frequency were set beyond the observable wings of the ENDOR line, the output of the audio unit would contain no ENDOR component and would have amplitude XYB.

In the experimental measurement, the dc magnetic field is varied. The audio phase detector output is then either an enhanced or unenhanced ESR spectrum, depending upon the value of the rf frequency. Since the amplitude of the on-nuclear resonance ESR (ENESR) is

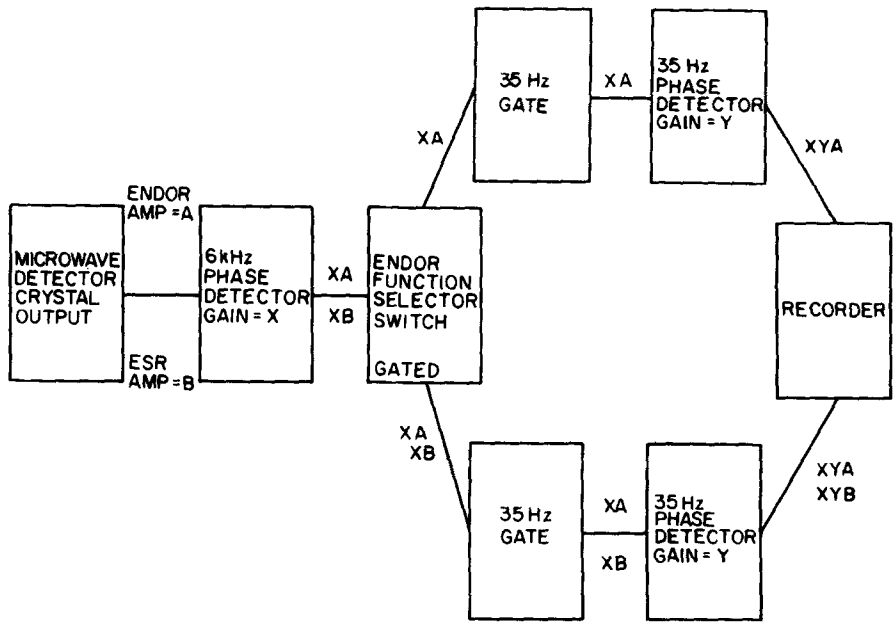

FIG. 1. A block diagram of the ESR/ENDOR apparatus used to determine the ENDOR percent enhancement while pulsing the rf frequency at 35 Hz with a 10% duty cycle and modulating the dc field at 6 kHz.

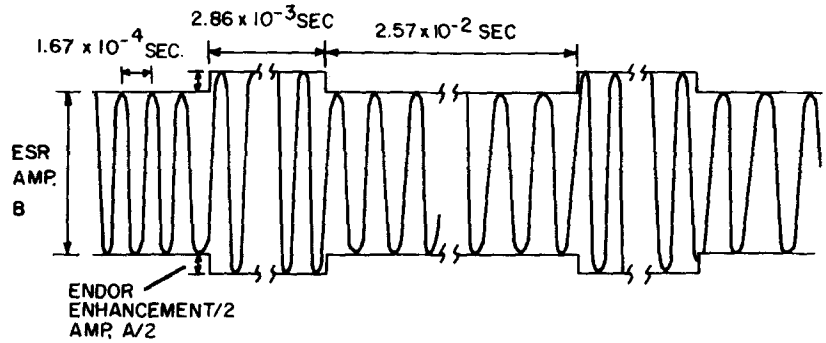

given by $XY(A+B)$ and the off-nuclear resonance value (UNENESR) is XYB, the PE($=A/B$) is obtained as follows:

$$\mathrm{PE} = \frac{(\mathrm{ENESR}) - (\mathrm{UNENESR})}{(\mathrm{UNENESR})} , \tag{2.8}$$

$$\mathrm{PE} = \frac{XY(A+B) - XYB}{XYB} = A/B . \tag{2.9}$$

Our initial PE measurements by Leniart were done as described above. It was found that data could be reproduced with only about 40% accuracy. At the time of those initial measurements, it was recognized that the rf frequency chosen for the off-nuclear resonance ESR signal affected the PE. The data in each of the PE vs temperature curves was taken at one off-nuclear resonance rf frequency.

It was found that changes in rf interference induced by changing the position of grounding cables affected the dependence of the PE on the value of the off-nuclear resonance rf frequency. Since charges in rf line filters had no effect on this dependence, it was decided that it arose from radiation from the cavity region being received by an "antenna" in the ENDOR detection unit. This explains the variation of % enhancement with the value of the off-nuclear resonance rf frequency, since the pickup of an antenna is frequency dependent.

Before the ENDOR unit was connected to the E-12 spectrometer, it was impossible to eliminate the transmitted rf interference signals by shielding. Thus it was necessary to devise a correction which would minimize the dependence of the PE on the value of the off-nuclear resonance rf frequency in order to improve the reproducibility of the results. We found that the contribution to the PE from rf interference could be determined by carrying out the PE measurement as described above with the microwave power lowered to such a value that no signal would be observed in a regular ENDOR experiment. When this "rf interference PE" was subtracted from the uncorrected PE, the error in the precision of our data dropped from 40% to 10%. After the ENDOR unit was connected to the E-12 spectrometer, where the wider magnet permitted more complete shielding, this correction was no longer necessary.

b. Relative method. In the 6 kHz rf pulsing configuration, it is not possible to do the PE measurement described above. The 6 kHz–35 Hz ENDOR and 35 Hz ESR signal pass from the detector crystal to the 6 kHz phase detector and then to the audio (35 Hz) phase detector. As shown in Fig. 2, the 35 Hz ESR signal does not pass through the 6 kHz phase detector. Thus, we have used relative measurements to determine the PE with this

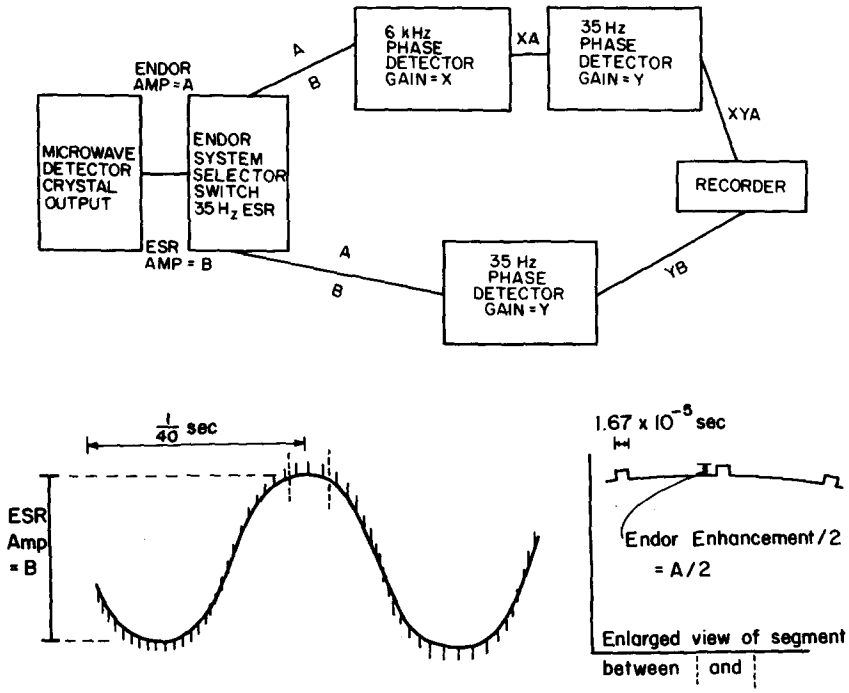

FIG. 2. A block diagram of the ESR/ENDOR apparatus used to determine the ENDOR percent enhancement while pulsing the rf frequency at 6 kHz with a 25% duty cycle and modulating the dc field at 35 Hz.

ENDOR configuration. It was necessary to do most of the experiments in this configuration, because it has a signal to noise ratio 2 to 3 (E-12 ENDOR) times that of the 35 Hz rf pulsing configuration and is significantly more stable.

The reasons for the difference in signal to noise ratios are based on the effects of rf interference (rfi). The first methods of shielding involved placing grounding cables between various points on the spectrometer until the rfi was minimized. Later we found that more rfi could be eliminated by enclosing as much of the cavity as possible with 0.002 in. copper foil. This change in shielding dropped the signal to noise difference of the two configurations from 10 to 5 (V4504 ENDOR). Finally, when the ENDOR was connected to the E-12 spectrometer, and the cavity could be completely surrounded by the copper foil, the signal to noise difference between the two configurations could be occasionally reduced to less than 2. The stability of the 35 Hz rf pulsing configuration was still much less than that of the 6 kHz rf pulsing configuration, because of the transitory appearance of a zero beat which would render all experiments impossible. All results involving use of this configuration were obtained when conditions were optimal.

A dilute sample of DSQ in EtOH whose PE had been measured with the 35 Hz rf pulsing configuration was used as a standard in the relative measurements with the 6 kHz rf pulsing configuration. The relative method involved the determination of the ENDOR and 35 Hz ESR amplitudes of the standard and the unknown. The gains of the 6 kHz and 35 Hz phase detection units are again denoted by X and Y. The output signals as indicated in Fig. 2 are then XYA and YB. The same amplifier and recorder gains were used in all experiments. The 35 Hz field modulation amplitude and the microwave power settings used in these measurements were very important and will be discussed in detail later. The PE of the unknown was determined as follows:

$$\left.\begin{matrix}\text{ENDOR}-XYA\\ \text{ESR}-YB\end{matrix}\right\}\ \text{Data for unknown},$$

$$\left.\begin{matrix}\text{ENDOR}-XYM\\ \text{ESR}-YN\end{matrix}\right\}\ \text{Data for standard},\qquad (2.10)$$

$$\text{PE known}$$

$$\text{Unknown PE} = (XYA)(YN)(\text{Std. PE})(YB)(XYM)\ .$$

In the 35 Hz rf pulsing configuration, all signals followed the same course and thus a change in the gain of an amplifier would affect both the ENDOR and ESR signal. Only a change in gain between the on-nuclear resonance and off-nuclear resonance measurements would give erroneous results. The precautions taken to avoid this occurrence were (a) the equipment was turned on several hours before a measurement was taken so that it could reach thermal equilibrium in the room; (b) the experiments were done as rapidly as possible—a complete measurement of 3 on-nuclear and 3 off-nuclear resonance ESR lines was done in 3 min; and (c) the measurements in (b) were done many times and repeated on different days to test their reproducibility.

As stated in (b) above, one complete measurement of the PE required 3 min of work. However, this absolute measurement could be carried out only on systems exhibiting large percent enhancements at low rf power such as dilute DSQ in EtOH (cf., Fig. 26). Thus, it was necessary to make the relative measurements of all other PE's using the 6 kHz rf pulsing configuration even though it took much longer, approximately 1 h. There was a

$\frac{1}{4}$ h time gap between the use of the 6 kHz amplifier for the standard and its use for the unknown. A change in the gain of this amplifier during this period would not be detected and thus the results would be erroneous. The precautions listed above were taken in these measurements also. We found that the 6 kHz amplifier gain never changed if the instrument, including the nuclear rf power amplifier, was allowed to warm up for several hours before any measurements were made. Because of its high voltages, the power amplifier could not be operated continuously. It was necessary to turn it off after each day's work was concluded. In order to minimize the amount of day-to-day recalibration, a measurement was taken which made the unknown a secondary standard. The PE of the unknown was determined over the temperature range of interest for one value of B_n^2 by the relative method. This value of B_n^2 was included in those used in the complete ENDOR linewidth–PE variation with B_n^2 study. Since the value of the PE was known for one data point in each variation of B_n^2 experiment, it was possible to determine the value of the PE at other values of B_n^2 from the ratio of the ENDOR intensities.

For dilute PBSQ in EtOH, the half-life of a sample is comparable to the time required to complete an ENDOR study (~2 h) at $T = -30$ °C. At higher temperatures, the decay is even more rapid. Hence, if only relative ENDOR amplitudes were considered in determining the variation of the PE with B_n^2, there would be substantial error introduced into the studies at $T = -30°$ because of sample decay. In order to compensate for changes in concentration, the 35 Hz ESR signal, with the 35 Hz modulation the same as that used in the ENDOR experiment, was recorded before and after each rf power change in an ENDOR study. The ratio (ENDOR amplitude/35 Hz ESR amplitude) was used instead of the ENDOR amplitude to determine the variation of PE as a function of B_n^2.

E. Microwave field by comparative method

In our ENDOR experiments, it was necessary to know the magnitude of $B_{1_{eff}}^2$, the effective circularly-polarized magnetic field at the sample. These values were obtained, for the ENDOR cavity, by first conducting a saturation experiment (cf. Sec. II. B) on the sample, after the T_1 and T_2 had already been determined by standard methods (cf. Secs. IV. A and B).

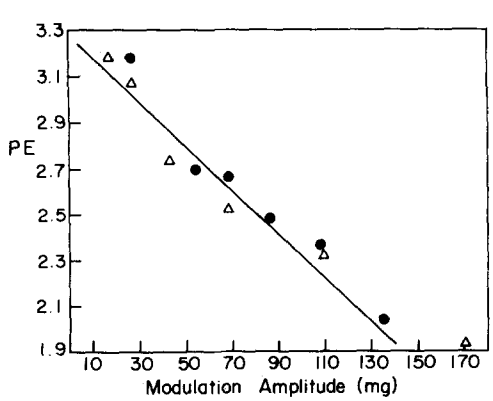

FIG. 3. Percent enhancement of a dilute sample of DSQ in EtOH at $T = -40$ °C and $B_n^2 = 4.4$ G^2 plotted as a function of modulation amplitude. ●=6 kHz rf pulsing. Δ=35 Hz rf pulsing.

TABLE II. Determination of overmodulation correction factor using a dilute solution of DSQ in EtOH.

Temperature (°C)	Pulse rate	Correction factor[a]
−40	35 Hz	1.67 ± 0.09
−50	35 Hz	1.72 ± 0.15
−60	35 Hz	1.57 ± 0.06
−40	6 kHz	1.63 ± 0.07
−50	6 kHz	1.66 ± 0.05
−60	6 kHz	1.56 ± 0.09

[a]Factor by which the PE of an overmodulated ESR line is decreased from the maximum PE obtained when modulation amplitude < 10% of the ESR linewidth.

III. VARIABLES IN THE ENDOR EXPERIMENT

A. Modulation amplitude effects

1. Experimental

In Fig. 3, the PE of a dilute sample of DSQ in EtOH at $T = -40$ °C and B_n^2 as determined with the two ENDOR configurations is plotted as a function of modulation amplitude. The ENDOR linewidth was found to be independent of modulation amplitude. Also, the modulation amplitude (MA) effects are the same whether 6 kHz or 35 Hz was used for the rf pulsing. We would have preferred to do the ENDOR PE vs B_n^2 experiments in the region of low MA where the PE is invariant with MA. Although the PE is a maximum in this region, the ENDOR amplitude is approximately $\frac{1}{4}$ of its maximum value. Since accurate measurements would have been extremely difficult in many cases because of weak ENDOR signals due to lower signal to noise ratios, we determined a correction factor enabling one to convert the overmodulated data to modulation-amplitude independent values.

In order to insure reproducibility of our results, we chose to do all of our ENDOR linewidth–PE studies with a MA which maximized the ESR amplitude. Thus, in all experiments the ratio of modulation amplitude to ESR linewidth was the same. Since the PE is a function of this ratio, the ratio of the MA-invariant PE to the overmodulated (ESR amplitude maximized) PE provided the necessary correction factor.

The PE of the standard, dilute DSQ in EtOH that was used in the relative measurements of PE was corrected using this factor. The correction of the standard was all that was required as long as all data taken in the relative measurements were overmodulated.

Table II lists our results for several measurements of the correction factor, showing that it is reproducible under a variety of conditions.

It is possible to estimate the effect of overmodulation

of the ESR on the PE by a simple analysis valid for a steady-state experiment, and this is given below. For our case of interest (case 3), the PE for a modulation amplitude which maximized the ESR amplitude is predicted to be 75% of the PE of an undermodulated ESR line. Our experimental results of Table II yield a value of 60%.

The reasonable agreement between the calculated and experimental results encourages us in the applicability of a simple correction factor. We attribute the differences between the two to some instrumental effects which are not taken into consideration in our calculation [e.g., variation in modulation amplitude along the sample for the ENDOR cavity, which has a comparatively long (~1 in.) active region along the sample axis].

2. Theoretical

It is possible to calculate the effect of overmodulation of the ESR signal on ENDOR enhancements. In his study of modulation broadening of unsaturated Lorentzian spectra, Wahlquist[18] finds the amplitude $[(a_1)_p]$ of the first derivative of a Lorentzian as a function of modulation amplitude to be given by

$$(a_1)_p = \pm (3/2)(2/H_{1/2})^2\{(u_p-2)/u_p(2u_p-3)\}^{1/2} , \quad (3.1)$$

where

$$u_p = 2 + 4/3\beta^2 + 4/3\beta(\beta^2+3/4)^{1/2} \quad (3.2)$$

and

$$\beta = \tfrac{1}{2} H_{1/2}/H_\omega . \quad (3.3)$$

Here $H_{1/2}$ is the full-width at half-height of the absorption and H_ω is the amplitude of the sinusoidal modulation with circular frequency.

Wahlquist's treatment is for an unsaturated Lorentzian where the absorption function can be written as

$$v = -\pi|\gamma| H_2 M_0 f_{H_{1/2}}(\Delta\omega) , \quad (3.4)$$

where $f_{H_{1/2}}(\Delta\omega)$ is the normalized Lorentz shape function with full-width at half intensity $H_{1/2}$. In our ENDOR experiments, the ESR line is strongly saturated and hence the absorption must be written for a steady-state experiment as

$$v' = -\pi|\gamma| H_1 M_0 f_{H_{1/2}}(\Delta\omega)/(1+\gamma^2 H_1^2 T_1 T_2) . \quad (3.5)$$

The $H_{1/2}$ in the normalized Lorentz function $f_{H_{1/2}}(\Delta\omega)$ is then

$$H'_{1/2} = H_{1/2}(1+\gamma^2 T_1 T_2)^{1/2} \equiv H_{1/2} z^{1/2} , \quad (3.6)$$

where $H_{1/2}$ is $1/T_2$, the width in the absence of measureable saturation. The differences between unsaturated and saturated line shapes thus appear in the linewidth of the normalized Lorentz function and in the dependence of the absorption amplitude upon the microwave magnetic field H_1. To convert Wahlquist's results to the saturated case we must substitute $H'_{1/2}$ for $H_{1/2}$ and renormalize the amplitude function by multiplying it by $Z^{-1/2}$, thus giving us

$$(a_1)'_p = \pm (3/2)(2/H'_{1/2})^2 z^{-1/2}\{(u_p-2)/u_p(2u_p-3)\}^{1/2} , \quad (3.7)$$

$$u_p = 2 + 4/3\beta^2 + 4/3\beta(\beta^2+3/4)^{1/2} , \quad (3.8)$$

$$\beta = \tfrac{1}{2} H'_{1/2}/H_\omega . \quad (3.9)$$

The ENDOR effect can be treated as a perturbation in $H_{1/2}$ or z induced by the nuclear rf field. The presence of the rf field (at nuclear resonance) decreases the degree of saturation of the ESR line, thereby causing z to decrease. This decrease in effective saturation causes an increase in signal amplitude, which is the PE observed in ENDOR.

We can introduce this change in $H'_{1/2}$ into the equations by redefining β as

$$\beta = \beta' + \epsilon \qquad \beta \gg \epsilon , \quad (3.10)$$

where ϵ is due to the rf-induced linewidth change. That is

$$H'_{1/2} = 2\beta H_\omega = 2(\beta'+\epsilon) H_\omega . \quad (3.11)$$

Case (1): The first case which we shall discuss occurs when the modulating field is much smaller than the ESR linewidth so that $\beta \gg 1$. Then we can reduce u_p to

$$u_p \cong 2.5 + (8/3)\beta^2 . \quad (3.12)$$

Equation (3.7) then becomes

$$(a_1)'_p \cong (3^{3/2} z^{-1/2}/2\beta)(1/H'^2_{1/2}) . \quad (3.13)$$

Substituting in Eqs. (3.10) and (3.11), we get

$$(a_1)'_p = (3^{3/2} z^{-1/2}/8H_\omega^2 \beta'^3)(1 - 3\epsilon/\beta') . \quad (3.14)$$

In order to determine the dependence of $z^{-1/2}$ on β' and ϵ, we must utilize Eqs. (3.6) and (3.11) to obtain

$$z^{-1/2} \cong \frac{H_{1/2}}{2H_\omega\beta'}(1 - \epsilon/\beta') . \quad (3.15)$$

Introducing this value for $z^{-1/2}$ into Eq. (3.14) and retaining only those terms that are first order in ϵ/β', we get

$$(a_1)_p = \frac{3\sqrt{3}\, H_{1/2}(1 - 4\epsilon/\beta')}{16 H_\omega^3 \beta'^4} . \quad (3.16)$$

Hence, we see that for the case where the modulation field is much smaller than the ESR linewidth, the PE is $4\epsilon/\beta'$ or 4% if we choose $\epsilon/\beta' = 0.01$. By a similar analysis we obtain results for three other cases.

Case (2): modulation amplitude equal to the ESR linewidth. Let $\beta = 1 + \epsilon$. Here,

$$(a_1)'_p \cong 0.22(H_{1/2}/H_\omega^3)(1.0 - 3.43\epsilon) \quad (3.17)$$

or PE is $3.43\epsilon/\beta'$.

Case (3): modulation amplitude that maximizes the ESR signal. Let $\beta = \frac{1}{2}(1.0 + \epsilon')$, $(\epsilon' = \frac{1}{2}\epsilon)$. Here,

$$(a_1)'_p \cong 2H_{1/2}(1 - 3\epsilon')H_\omega^3 \quad (3.18)$$

or PE is $3\epsilon/\beta'$.

Case (4): strong overmodulation of the ESR signal. Let $\beta \ll 1$:

$$(a_1)'_p \cong (3/3^{1/4} 4H_\omega^3 \beta^{5/2})(1 - 5\epsilon/2\beta') \quad (3.19)$$

or PE is $2.5\epsilon/\beta'$.

B. Microwave power effects on the ENDOR signal

The theoretical analysis of ENDOR spectra has shown that for a single spin of $I = \frac{1}{2}$ or for "average ENDOR,"

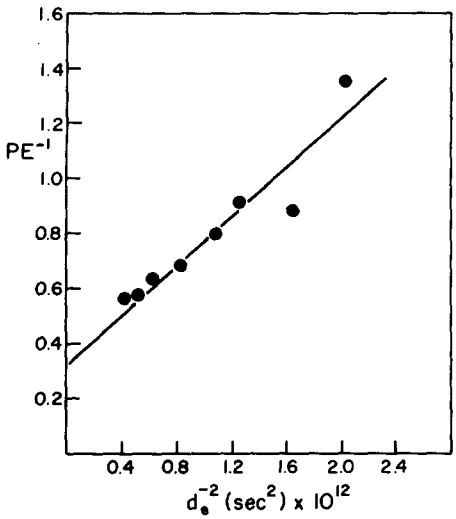

FIG. 4. PE^{-1} plotted as a function of d_e^{-2} for a dilute solution of PBSQ in EtOH with $B_n^2 = 4.0$ G^2 and $T = -40$ °C.

one has[1,5]

$$(PE)^{-1} = r + sB_e^{-2} , \tag{3.20}$$

where r and s are dependent upon the relaxation properties, NMR frequency, and B_n^2, provided one holds the ESR frequency and B_0 constant. Computer simulations of more general cases for PBSQ have also predicted such a linear dependence on B_e^{-2}. A typical experimental result which demonstrates this relationship is given in Fig. 4, while in Fig. 5 the asymptotic behavior of PE with B_e^2 for large B_e^2 is illustrated.

Ideally, studies of the variation of the PE as a function of nuclear rf power should have been carried out in the region where the approximation $d_e^2 \to \infty$ could be utilized. In order to reach this limit, we would have had to use microwave powers which would have produced microwave coherence broadening of the ENDOR lines. Since we did not wish to distort our ENDOR line shapes, we did not make our ENDOR measurements in that region.

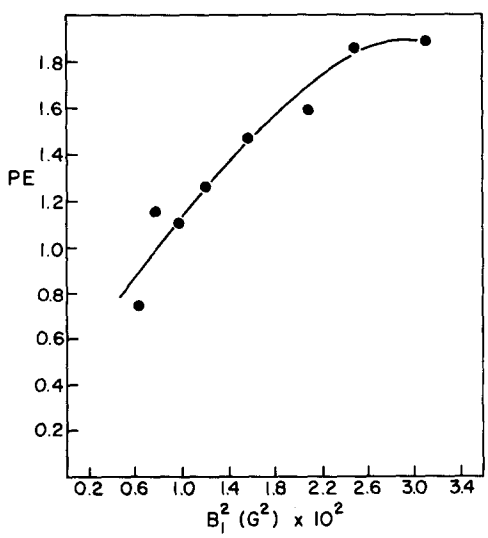

FIG. 5. Percent enhancement plotted as a function of B_1^2 for a dilute solution of PBSQ in EtOH with $B_1^2 = 4.0$ G^2 and $T = -40$ °C.

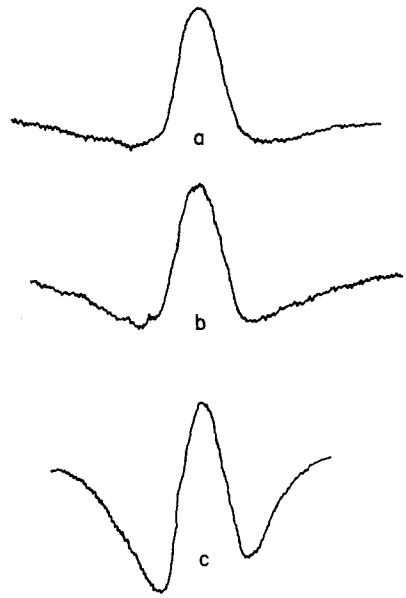

FIG. 6. Distorted ENDOR line shapes caused by coherence effects. (a) High B_1^2, long T_{2e}, medium B_n^2; (b) High B_1^2, long T_{2e}, high B_n^2; (c) Low B_1^2, long T_{2e}, high B_n^2.

In order to be able to reproduce our experimental results, we used the point of maximum ESR derivative amplitude as a function of microwave power as the point of reference in all ENDOR experiments. At each temperature the ESR amplitude was maximized with respect to microwave power.

In order to improve the ENDOR signal to noise, the microwave power used in the ENDOR experiment was set at twice the value needed to maximize the ESR amplitude.

C. Coherence effects and ENDOR line shapes

In our experiments with narrow-line ESR samples, it was rather easy to distort the ENDOR lineshape from that of a simple Lorentzian when the nuclear rf power is high. Typical examples are given in Fig. 6. We are able to predict such line shapes from our general computer solution. It is instructive, however, to study the analytical results for a single $I = \frac{1}{2}$ case. Then for $\Delta_e = 0$ and no ESR saturation, one has[3]

$$Z_e'' = \frac{q\omega_e d_e T_{2e}(T_{2x}^2 \Delta_n^2 + 1 + T_{2e} T_{2x} d_n^2)}{(T_{2w}^2 \Delta_n^2 + (1 + T_{2e} T_{2x} d_n^2)^2)} . \tag{3.21}$$

One can usually simplify this expression by setting $T_{2x} \cong T_{2e}$. The longest T_{2e} observed in the quinone systems was 1.6×10^{-6} sec. The maximum B_n for our ENDOR uint is 6.4 G (Varian probe). Hence

$$d_n = 10.5 \times 10^4 \text{ sec}^{-1}$$

and

$$(d_n T_{2e})^2 = 0.028 .$$

Thus, we see that $(d_n T_{2e})^2 \ll 1$. Then Eq. (3.21) may be simplified to

$$Z_e'' = q\omega_e d_e T_{2e} 1 - \frac{T_{2e}^2 d_n^2}{1 + T_{2e}^2 \Delta_n^2} . \tag{3.22}$$

Equation (3.22) indicates that the ESR amplitude decreases as d_n^2 increases. We also see that this rf-induced effect has a Lorentzian line shape with a half-width at half-height the same as the ESR line. Since the ESR amplitude is reduced, the phase of the coherence line will be opposite to the phase of the usual ENDOR-enhanced line. Also, the coherence line will be broader than the ENDOR line since $T_{2e} \ll T_{2n}$ (typical values are ENDOR $\Delta_{1/2,1/2} = 25$ kHz, ESR $\Delta_{1/2,1/2} = 112$ kHz). The sum of two such lines gives line shapes like those in Fig. 6.

The broad coherence line increases in amplitude as the nuclear rf power increases. The best method of observation of this line is achieved by using low microwave powers and high nuclear rf powers. The coherence reduction signal is independent of microwave power, but the normal ENDOR signal is weaker. Similarly, the high value of B_1^2 used in the ENDOR experiments helped to minimize the effect of the coherence line on the ENDOR line shape. The high duty cycle and comparatively low nuclear rf powers used in the ENDOR experiments also minimized the distortion of the ENDOR line shape.[19]

This coherence effect is not the same as that utilized to calibrate the rf field (cf. Sec. II). The latter is based upon the nuclear rf field shifting the ENDOR frequencies, and it requires an ENDOR transition from two or more equivalent protons. The former is based upon the nuclear rf field shifting the ESR frequencies, and it can result from the ENDOR of a single proton. Cf. Ref. 3 for further discussion.

In general, coherence effects interfere with the relaxation studies, because they distort the line shapes, destroying any simple dependences the ENDOR line shapes may have on rf power. Consequently, our relaxation experiments were performed at sufficiently low values of B_n to guarantee that the coherence effects were not present.

In the absence of coherence effects, the ENDOR line shape was found to be very nearly Lorentzian. We give in Table I typical experimental ENDOR line shape results demonstrating this.

D. Pulse rate effects

Freed[1] has given a qualitative discussion concerning transient effects in pulsed rf ENDOR experiments. He found that for pulse times $t \sim W_e^{-1}$, the ESR signal could be enhanced because of "heating up" of the spin systems. The rf pulse duration for 6 kHz pulses at 10% duty cycle is 1.5×10^{-5} sec. The nuclear relaxation parameters $T_{2,n}$ and Ω_n for a dilute solution of DSQ in EtOH at -50 °C are 56×10^{-7} and 25×10^{-7} sec (see below). (The values for $T_{2,e}$ and $T_{1,e}$ are 0.61×10^{-7} and 20×10^{-7}.) Since the values of Ω_n and $T_{1,e}$ for this system are so large (generally larger than for PBSQ), it was felt that steady state conditions might not be obtained when 6 kHz pulsing is used; thus, transient phenomena might be observed. However, no enhancement from heating up the spin system by lowering the 6 kHz rf pulsing duty cycle from 10% to 5% was observed. (All enhancements were corrected for signal to noise changes resulting from changes in duty cycle by multiplying them by the appropriate ratio of the duty cycles.)

The ENDOR linewidth of this system was found to decrease as the duty cycle was increased from 5% to 20%. At duty cycles from 20% to 50%, there was *no change* in width or amplitude. As the width decreased the amplitude increased so that the area under the absorption remained the same. The temperature of the sample was varied and the linewidth–duty cycle effect remained. Other systems with shorter nuclear relaxation times exhibited the same dependence, although to a lesser extent (possibly because the ENDOR widths were larger).

The only effect on the ENDOR enhancement occurred in the duty cycle region where the linewidth varied. The ENDOR enhancement varied so that the area under the signal remained constant.

The behavior of this duty-cycle effect, which disappears for duty cycles > 20%, has led us to the conclusion that it is originating in the detection system. Experiments undertaken to locate the instrumental source of the effect were not successful, so the possibility that the effect could originate there was not eliminated.

Since we were unable to locate and thus eliminate the source of the duty cycle dependence, we carried out all of our measurements with the duty cycle at 25% (i.e., in the duty cycle region where no effect on the ENDOR signal is observed).

In order to verify that data obtained with 6 kHz rf pulsing was reliable, we repeated some of the ENDOR measurements utilizing both configurations. The DSQ in EtOH system (see above) was utilized, since its large Ω_n implied it would be most likely to show a frequency effect. The ENDOR linewidths and PE's were measured at various rf powers and two temperatures (-50 and -60 °C) using both configurations. The intercepts and slopes of the ENDOR linewidths squared vs d_n^2 [cf. Eqs. (4.27) and (4.30)] were compared, as was the relative variation of PE with rf power (d_n^2). (The absolute PE is, as already noted, not obtained with the 6 kHz pulsing configuration.) All of the results were indeed comparable within the limits of the experimental error.

IV. RESULTS AND ANALYSIS

A. ESR linewidths

While the ESR lines in the spectra studied in this work are multiple or degenerate lines, it was found, by comparing the theoretical analyses based upon our computer simultations, that they are adequately treated as average Lorentzians with average unsaturated widths. This is expected because the dominant contributions to the widths are nuclear-spin independent (see below).[20]

The experimental widths for PBSQ and DSQ have a width variation amongst the hyperfine lines which obeys the simple relation

$$\langle T_2^{-1}(\bar{M})\rangle = A + B\bar{M} + C\bar{M}^2 + T_2^{-1}(\bar{M})_{\mathrm{HE}}\,, \tag{4.1}$$

where $\bar{M}$ is the spectral index number.[21] The parameters A, B, and C are predicted from the theory of ESR

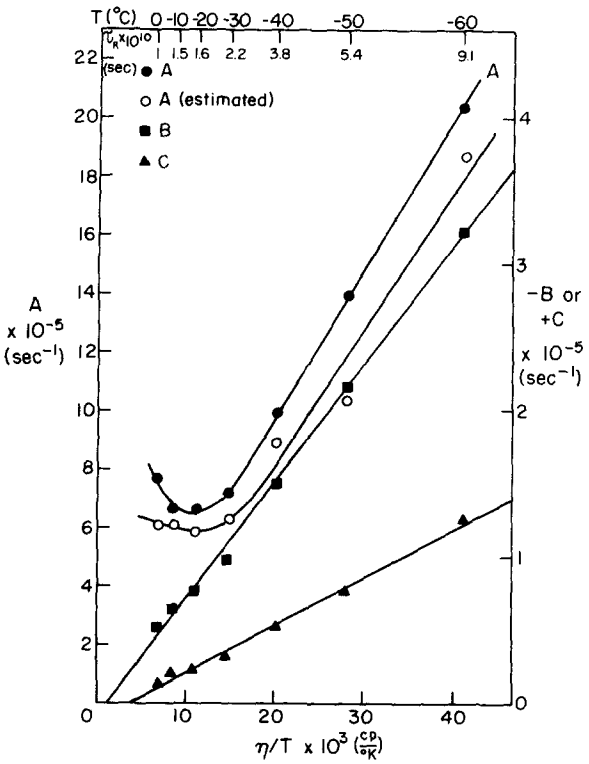

FIG. 7. The ESR linewidth parameters A, B, and C for a dilute solution of PBSQ in EtOH as a function of η/T.

linewidths to be given by[20,22]

$$A = (8/3)j^G(0)\,B_0^2 + f_D + X\,, \tag{4.2a}$$

$$B = (16/3)j_a^{DG}(0)\,B_0\,, \tag{4.2b}$$

$$C = (8/3)j_{aa}^{D}(0)\,\Gamma_{ab}\,. \tag{4.2c}$$

Here

$$\Gamma_{ab} = (1/3)\left[1 + 2\left|j_{ab}^{D}(0)/j_{aa}^{D}(0)\right|\right] \quad \text{for PBSQ} \tag{4.3a}$$

and

$$\Gamma_{ab} = (5/11)\left[1 + (6/5)\left|j_{ab}^{D}(0)/j_{aa}^{D}(0)\right|\right] \quad \text{for DSQ}\,, \tag{4.3b}$$

while

$$f_D = 34/9\,j_{aa}^{D}(0) - 16/9 j_{ab}^{D}(0) \quad \text{for PBSQ} \tag{4.4a}$$

and

$$f_D = 114/11 j_{aa}^{D}(0) - 48/11 j_{ab}^{D}(0) \quad \text{for DSQ}\,. \tag{4.4b}$$

The average ESR linewidths for 2, 5 DMPBSQ obey

$$\langle T_2^{-1}(M_R, M_M)\rangle = A + B_M \bar{M}_M + B_R \bar{M}_R + C_M \bar{M}_M^2 + C_R \bar{M}_R^2 + C_{M,R}\bar{M}_M\bar{M}_R + (T_2^{-1})_{HE}\,, \tag{4.5}$$

where we have distinguished between ring protons and methyl protons by the subscripts R and M, respectively. Here

$$B_i = (16/3)j_i^{DG}(0)\,B_0\,, \tag{4.6a}$$

$$C_{ij} = (8/3)j_{ij}^{D}(0) \quad i, j = R, M\,, \tag{4.6b}$$

$$A = (8/3)j^G(0)B_0^2 + 3j_{MM}^{D}(0) + j_{RR}^{D}(0) + X\,. \tag{4.6c}$$

The $j(0)$'s in Eqs. (4.2)–(4.4) and (4.6) are the zero frequency spectral densities that are proportional to τ_R, the rotational correlation time, as well as the appropriate magnetic parameters (see below). The superscripts D, DG, and G represent dipolar, dipolar–g-tensor cross terms, and g-tensor terms. The subscripts in Eqs. (4.2)–(4.4) refer to the group or groups (a or b) of completely-equivalent nuclei being considered. The quantity $(T_2^{-1})_{HE}$ is the width contribution from Heisenberg spin–exchange given by

$$T_2^{-1}(M)_{HE} = \left(\frac{N - 2D_M}{N}\right)\omega_{HE}\,, \tag{4.7}$$

where ω_{HE} is the Heisenberg-exchange frequency, N is the number of spin energy levels, and D_λ the degeneracy of the λth ESR line. The term X represents all other nuclear-spin-independent mechanisms and is usually assumed to be primarily due to spin–rotational relaxation, which may be estimated, assuming a simple Stokes–Einstein model, as

$$T_{2SR}^{-1} = \sum (g_i - g_e)^2/9\tau_R\,. \tag{4.8}$$

In Eqs. (4.2) and (4.6), we have neglected nonsecular dipolar and g-tensor terms, since the rotational motions at the reduced temperatures utilized in our study are too slow for these terms to be important.

The general procedure for separating out the parameters of Eqs. (4.1) and (4.5) is first to study very dilute solutions where $T_2^{-1}(M)_{HE} \approx 0$ as a function of nuclear quantum number, and then to study the concentration-dependent results for $T_2^{-1}(M)_{HE}$.

In our studies on dilute solutions, the central ($M_I = 0$) linewidth was measured accurately, and the widths of the other lines were determined from that width plus the relative amplitudes and degeneracies of the lines in the usual manner. The results for a various dilute solutions are given in Figs. 7–11 as A, B_i, and $C_{i,j}$ vs η/T.

1. PBSQ

The results for B and C of PBSQ in EtOH (cf. Fig. 7) show the usual linear dependence on η/T that is expected when τ_R follows Stokes–Einstein-type behavior, i.e.,

$$\tau_R = (6R)^{-1} = 4\pi\eta a^3\kappa/3kT\,, \tag{4.8'}$$

where R is the rotational diffusion coefficient, a is the effective radius of the solute, while κ is an adjustable parameter ($0 \le \kappa \le 1$) which corrects the macroscopic viscosity η to the "microscopic" viscosity (or alternatively corrects a^3). The results for B and C in DME solvent (cf. Fig. 8) are also linear in η/T at the higher temperatures, but at the lower temperatures some curvature is observed in both B and C, which we attribute to the presence of TBAP which tends to aggregate and thus affects η (see also discussion of results below).

When the magnetic parameters are known, it is possible to extract from a graph of B vs C, (cf. Fig. 12) two components ($\tau_{R_\parallel}^{-1}$ and $\tau_{R_\perp}^{-1}$) of the rotational-diffusion tensor. However, the main point to be made at this time is that the good linear dependence of B vs C for

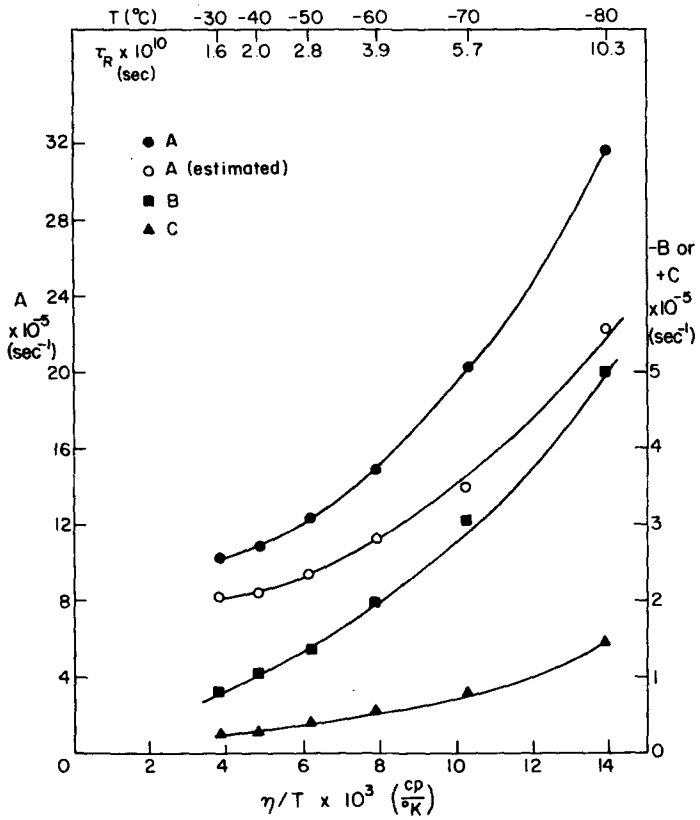

FIG. 8. The ESR linewidth parameter A, B, and C for a dilute solution of PBSQ in DME as a function of η/T.

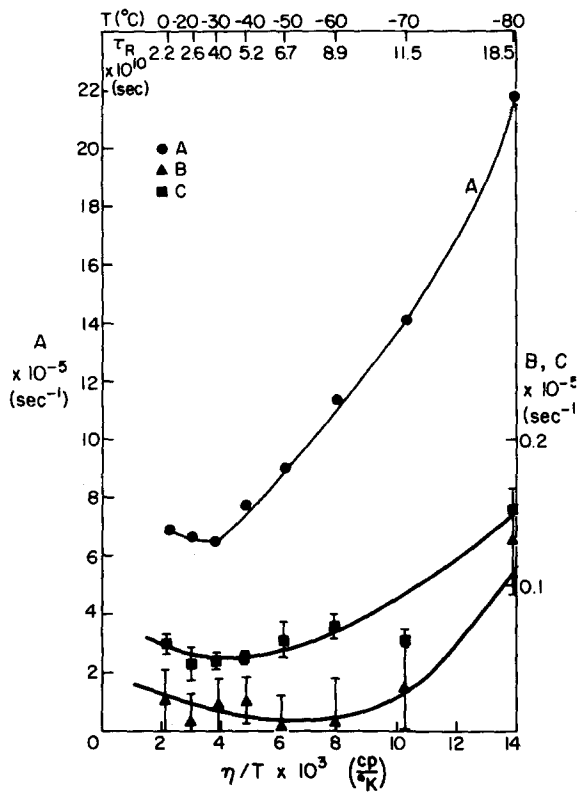

FIG. 10. The ESR linewidth parameter A, B, and C for a dilute solution of DSQ in DME as a function of η/T.

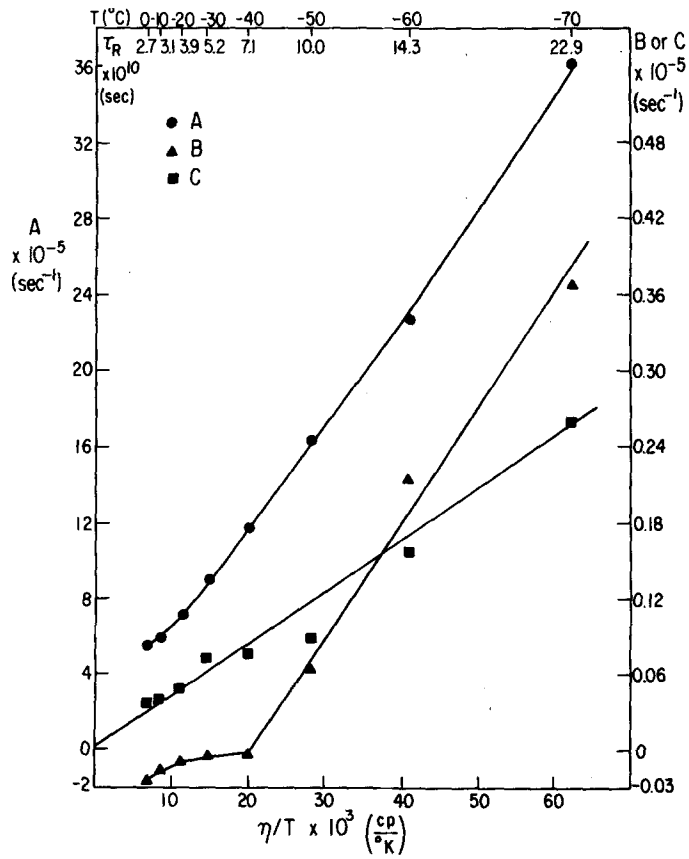

FIG. 9. The ESR linewidth parameters A, B, and C for a dilute solution of DSQ in EtOH as a function of η/T.

both EtOH *and* DME solvents with zero intercept shown in Fig. 12 is good evidence that they are simply determined by the theoretical expressions Eqs. (4.2), and are not affected by subsidiary processes such as modulations of the average $\bar{a}$ and $\bar{g}$ values. (In the case of DME solvent, this helps confirm our assignment of the deviations from linearity with η/T to effects of TBAP on the η.)

By far the most reliable method of extracting out the τ_R's is by first measuring the anisotropic **A** and **g** tensors from rigid limit spectra. This has only been possible in cases of large hf parameters, and the present cases involve hf parameters that are much too small. The alternative procedure is to rely on calculations of these parameters, but they are usually only reliable to within factors of the order of 2 and we also neglect potentially large solvent effects.[23] For the sake of obtaining estimates of τ_R, we have calculated the dipolar parameters utilizing the McConnell–Strathdee[24] method and have obtained, in the notation of Freed and Fraenkel,[20]

$$D_a^{(0)} = -0.186718\times10^7 \text{ sec}^{-1}, \tag{4.9a}$$

$$D_a^{(\pm1)} = 0, \tag{4.9b}$$

$$D_a^{(\pm2)} = (0.162196 \pm 10.102919)\times10^7 \text{ sec}^{-1} \tag{4.9c}$$

[where Eq. (4.9c) is for positions 9 and 11. For positions 10 and 12, the ± signs on the lhs should be reversed.] While Stone's g-tensor theory was utilized to predict the g-tensor components,

$$g_1 = 2.0036 \,, \tag{4.10a}$$

$$g_2 = 2.0074 \,, \tag{4.10b}$$

$$g_3 = 2.0024 \,, \tag{4.10c}$$

in agreement with $g_{av} = 2.0045$ below -66 °C (but it is 2.0046 above that temperature). This leads to the following results:

$$j^D_{aa}(0) = j^D_{bb}(0) = 1.22\times10^{14}\tau_R \,, \tag{4.11a}$$

$$j^D_{ab}(0) = j^D_{ba}(0) = 1.62\times10^{13}\tau_R \,, \tag{4.11b}$$

$$j^{DG}_a(0) = j^{DG}_b(0) = [-0.421209\times10^{13}g^{(0)} + 0.731784 \times10^{13}g^{(2)}]\tau_R \text{ (for all protons)} \,, \tag{4.11c}$$

where $g^{(0)} = (2g_3 - g_1 - g_2)$ and $g^{(2)} = (3/2)(g_1 - g_2)$. Unfortunately, Eq. (4.11c) utilizing the values of Eqs. (4.9) and (4.10) results in the very small difference between two large numbers and is thus very sensitive to even small inaccuracies in these estimates, which can even lead to a sign change in Eq. (4.11c). Thus, B and Eq. (4.11c) are not useful in estimating τ_R in the present case. [Note, however, that about a 30% change in either $g^{(0)}$, $D^{(0)}$, $g^{(2)}$, or $D^{(2)}$ (or some combination) in the proper direction would result in values of τ_R predicted from B which agree with those predicted from C and Eqs. (4.11a) and (4.11b).]

The values of τ_R predicted from C and Eqs. (4.11a), (4.11b), (4.3a), and (4.2b) are shown in Figs. 7 and 8. τ_R varies for PBSQ in EtOH from $\sim10^{-10}$ at 0 °C to $\sim10^{-9}$ sec at -60 °C, and for PBSQ in DME a similar variation is seen from -30 °C to -80 °C.

Now, the main purpose of the current linewidth studies is to obtain the necessary input data for the ENDOR

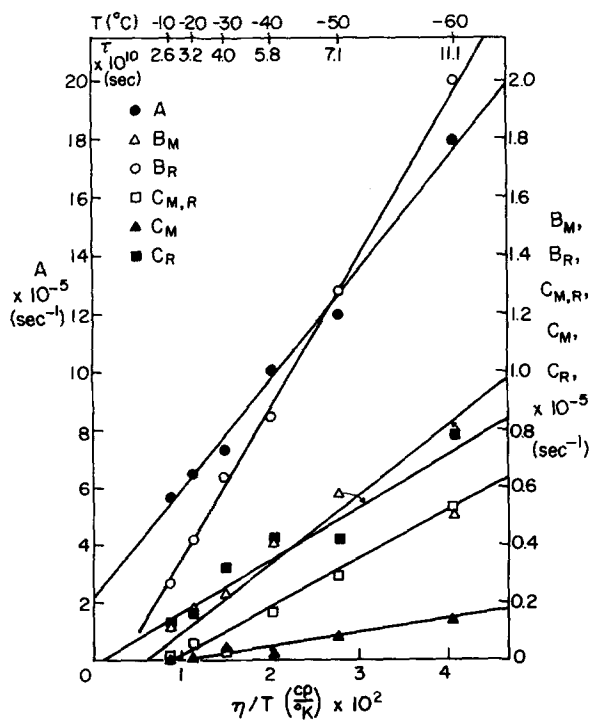

FIG. 11. The ESR linewidth parameter A, B_M, B_R, C_M, C_R, $C_{M,R}$ for a dilute solution of 2,5-DMSQ in EtOH as a function of η/T.

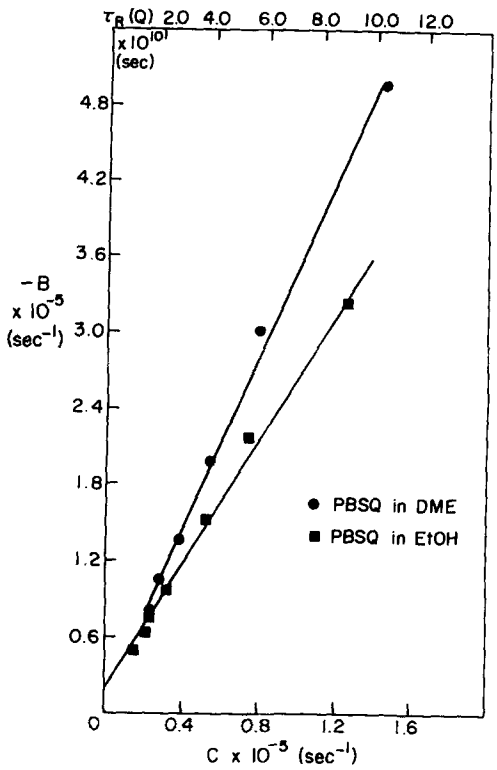

FIG. 12. A graph of the ESR linewidth parameters B vs C for PBSQ in DME and EtOH.

studies. In particular, one needs an estimate of the nuclear-spin-flip term

$$W_n \equiv \tfrac{1}{2} j^D_{aa}(0) \,, \tag{4.12}$$

and this is readily obtained from the experimental results and Eq. (4.2b) without any knowledge of the correct magnetic parameters being required within the multiplicative factor Γ_{ab}. The latter is seen to vary from $\Gamma_{ab} = 1$ [cf. Eq. (4.3a)] for completely correlated nuclei [i.e., $j^D_{ab}(0) = j^D_{aa}(0)$] to $\Gamma_{ab} = 1/3$ for uncorrelated nuclei (i.e., $j^D_{ab} = 0$). We estimate $j^D_{ab}(0) = 0.133 j^D_{aa}(0)$ from Eqs. (4.11a) and (4.11b), i.e., the two different pairs of equivalent nuclei are almost uncorrelated).

We note also that it is possible to predict the value of $A - X$ from Eq. (4.2a) utilizing Eqs. (4.4a), (4.10), (4.11) and the values of τ_R obtained above. One finds that a substantial fraction of A is explained in this manner. If we assume $X \approx T^{-1}_{2SR} \approx 2W_e$, where W_e is the electron-spin-flip rate determined by saturation measurements, then one should predict A itself. Such predictions are shown in Figs. 7 and 8 utilizing the values of W_e discussed below. The predicted values for A show good agreement with experiment in the case of EtOH solvent but are somewhat low for DME solvent. In the latter case, a 50% increase in the τ_R utilized in Eq. (4.2c) would bring the predicted and experimental values for A into good agreement, thus perhaps indicating a solvent effect on the dipolar parameters utilized to estimate τ_R from Eq. (4.2b).

We have also carried out linewidth measurements at 35 GHz on the $M_I = 0$ line. These experiments have clearly demonstrated (by comparison with the X-band

results) that the predominant portion of A is indeed due to the pure secular g-tensor contribution given by the first term in Eq. (4.26) [i.e., $A_{(35\text{ GHz})} \approx (35/9.3)^2 A_{(x\text{ band})} = 14.3 A_{(x\text{ band})}$]. The same result was found to be true for DSQ and 2, 5-DMPBSQ in the solvents utilized.

2. DSQ

The values of A, B, and C vs η/T for DSQ in EtOH and DME are shown in Figs. 9 and 10. One is struck by the very small values of B and C that are observed. The values for B are typically 10–40 times smaller and those for C are 5–10 times smaller than the equivalent results for PBSQ, while the values for A are comparable. In fact, in EtOH solvent, B actually changes sign, from a small negative value for $T \gtrsim -40$ °C to more substantial positive values for $T \lesssim -50$ °C. This is reminiscent of the theoretical prediction of Eq. (4.11c) for PBSQ for which very small (solvent) shifts in the magnetic parameters could cause large changes (including sign) in B. The parameter C, however, seems to be significantly better behaved, despite the large experimental error associated with the measurement of this small quantity. Also, we note that while the ratio of C for DSQ to that for PBSQ varies from about 0.2 at the higher temperatures to about 0.1 at the lower temperatures, that ratio (for given C of PBSQ) is essentially the same in both solvents. Thus, we would conclude that the C's for DSQ are probably not markedly affected by any new solvent-dependent relaxation processes which should be different in a strong hydrogen-bonding solvent (EtOH) vs an aprotic solvent (DME). Thus, we would expect to obtain a reasonable estimate of W_n from Eq. (4.12) utilizing Eq. (4.2b), the experimental results for C, and an estimate of Γ.

We have performed extensive McConnell–Strathdee-type calculations for dipolar parameters on a methyl fragment bonded to a semiquinone ring, involving averaging over the methyl fragment.[25] These results indicate that

$$j^D_{aa,\text{DSQ}}(0)/j^D_{aa,\text{PBSQ}}(0) \cong 0.209\,, \tag{4.13a}$$

$$j^D_{ab,\text{DSQ}}(0)/j_{aa,\text{DSQ}}(0) \cong 0.310\,, \tag{4.13b}$$

$$\Gamma_{ab} = 0.642 \tag{4.13c}$$

for a given τ_R. If, however, Eqs. (4.13a) and (4.13b) (or the more detailed expressions in Ref. 25) are used to estimate τ_R from C, we obtain values of τ_R that are about 2 times smaller than those for PBSQ at the same temperature and solvent. This is the *reverse* trend from that anticipated from the increased size of DSQ, cf. Eq. (4.8).

We have therefore utilized another means for estimating τ_R, based on the experimental values for A. As noted above, it was possible to account for nearly all of A for PBSQ using Eq. (4.2a) with $X \approx 2W_e$, the predominant term being the secular g-tensor contribution. For DSQ, as already noted, a comparison of the 9.3 and 35 GHz $M_I = 0$ linewidths demonstrated that the g-tensor contribution also predominates. Furthermore, one notes that the dipolar contributions in Eq. (4.2a) for DSQ must even be significantly less than for PBSQ. Thus, a reasonable approximation to τ_R may be obtained from Eq. (4.2a) and utilizing the values of W_e obtained from saturation studies as discussed below (the resulting values of X have only a marginal effect except at the higher temperatures studied). We have used the g-tensor values of Eqs. (4.10). The values of τ_R we obtain are shown along the upper coordinate axes in Figs. 9 and 10. They range from about 2.5–3 times *longer* than those for PBSQ at the higher temperatures to about 1.5–2 times *longer* at the lower temperatures, and thus are in the expected direction relative to PBSQ. [Their variation with temperature is in accord with the variation in ratio of C(DSQ)/C(PBSQ) already noted.] Our results for W_e on the PBSQ and DSQ systems are also consistent, with τ_R for DSQ being about twice as long (cf. next section). These results would tend to imply that Eq. (4.13a) is off by roughly a factor of 4. We have no immediate explanation for this discrepancy. Perhaps such effects as weak H bonding of the methyl protons to the adjacent O atom would need to be included to achieve a better estimate of the dipolar coefficients.

An important consideration in the linewidth studies in DME is the sensitivity at low temperatures of the linewidths to the TBAP concentration. This is illustrated in Fig. 13 for DSQ. In order to minimize the broadening observed, we used the minimal amount of TBAP which would stabilize the concentration of radicals that we wished to study. It is likely that the effects of the increased concentration of TBAP counterion is to increase the τ_R for the radical counterion either by increasing the effective η and/or the effective a^3. This would lead to an increase in the g-tensor contributions, which dominate the low temperature widths.

3. 2, 5-DMPBSQ

The experimental parameters defined by Eq. (4.5) are displayed in Fig. 11 for EtOH solvent as a function of η/T. These results are similar to PBSQ and DSQ, respectively, in the case of the ring proton and methyl

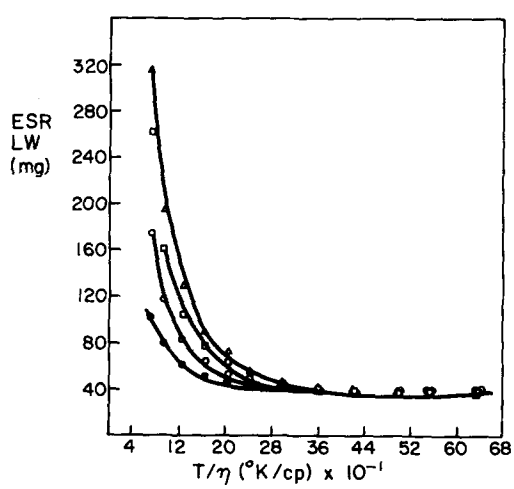

FIG. 13. The linewidths of the $M_I = 0$ ESR line plotted as a function of T/η for a dilute solution of DSQ in DME containing various amounts of TBAP (Δ = 0.03 g/ml TBAP; □ = 0.020 g/ml TBAP; ○ = 0.010 g/ml TBAP; • = 0.001 g/ml TBAP).

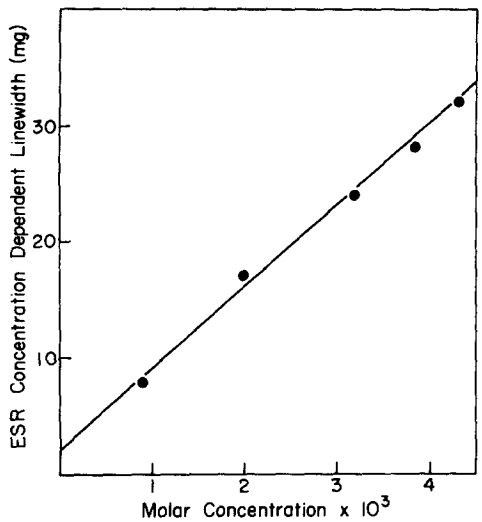

FIG. 14. The concentration dependent component of the $M_I = 0$ ESR linewidth of solutions of PBSQ in EtOH at $T = -50\,^\circ$C plotted as a function of concentration.

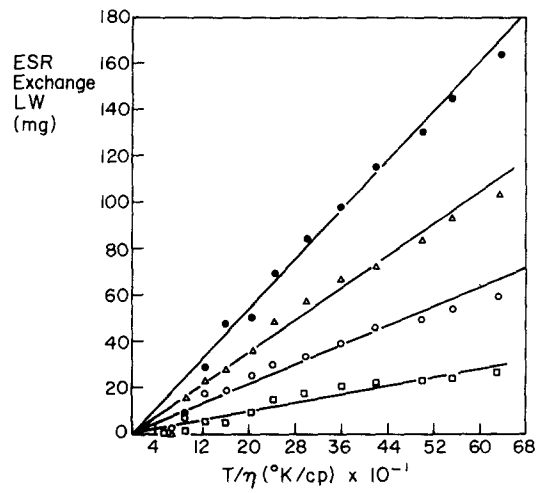

FIG. 16. The exchange component of the $M_I = 0$ ESR line plotted as a function of T/η for solutions of DSQ in DME. • = $9\times10^{-4}M$; Δ = $6.3\times10^{-4}M$; ○ = $3.0\times10^{-4}M$; □ = $1.5\times10^{-4}M$.

proton experimental parameters, as one would expect, so similar comments would apply. We have utilized $C_{R,R}$ and $C_{M,M}$ with Eq. (4.6b) to determine $W_{n,R}$ and $W_{n,M}$ from Eq. (4.12). We have estimated the τ_R from Eq. (4.6c) in the manner discussed for DSQ, and they are shown in Fig. 11. For a given temperature, they lie intermediate between the results for DSQ and PBSQ, as one would expect from size considerations.

4. *Heisenberg exchange*

One obtains ω_{HE} by subtracting out the dilute solution $T_2^{-1}(M)$ from the concentrated $T_2^{-1}(M)$, the difference being $T_2^{-1}(M)_{HE}$ of Eq. (4.7). This procedure has been employed for solutions of DSQ or PBSQ. The simple theory for spin exchange yields[6]

$$\omega_{HE} = \mathfrak{N}k[J^2\tau_1^2/(1+J^2\tau_1^2)]\,, \tag{4.14}$$

where $\mathfrak{N}$ is the radical density (no. spins/ml), k the second-order rate constant for the bimolecular encounters of radicals, J is twice their exchange interaction, and

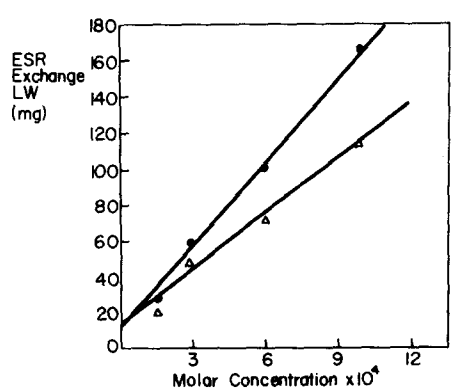

FIG. 15. The exchange component of the $M_I = 0$ ESR line as a function of concentration for solutions of DSQ in DME at $T = -10$ (Δ) and +15 (•) °C.

τ_1 the lifetime of the interacting pair. One usually finds $k \propto T/\eta$, which is expected for simple Brownian diffusion and a Stokes–Einstein model where[6,25a]

$$k^1 = 4\pi dD\,, \tag{4.15}$$

$$\tau_1^{-1} = (6D/d^2)\,, \tag{4.16}$$

and

$$D = kT/6\pi a\eta\,, \tag{4.17}$$

where D is the relative translational diffusion coefficient, and d is the "interaction distance" for exchange. These expressions must be modified to consider charge effects. The linear dependence expected for ω_{HE} on radical concentration is illustrated in Fig. 14 for solutions of PBSQ in EtOH and in Fig. 15 for DSQ in DME. Normally, one expects strong exchange $J^2\tau_1^2 \gg 1$, and $\omega_{HE}/\mathfrak{N} = k \propto T/\eta$. This linear dependence of ω_{HE} on T/η is shown in Fig. 16 for DSQ in DME and in Fig. 17 for PBSQ in DME. However, the results for PBSQ in EtOH were found to be definitely *not* linear in T/η. Instead, one obtains a result in which ω_{HE} is linear in η/T (cf. Fig. 18). Such a result would, for example, be expected if one had weak exchange, i.e., $J^2\tau_1^2 \ll 1$, so Eqs. (4.14)–(4.17) would yield $\omega_{HE}/\mathfrak{N} = kJ^2\tau_1^2 = \pi/9J^2d^5D^{-1} \propto \eta/T$. We discuss this matter further below.

We have determined independent estimates of k for DSQ in DME (+15 °C) from the slopes of Figs. 15 and 16 of $(2.98\pm0.20)\times10^9\,M^{-1}\cdot\text{sec}^{-1}$ and $(2.93\pm0.1)\times10^9\,M^{-1}\cdot\text{sec}^{-1}$, respectively, which agree well. We have, from Fig. 17, a value of $k = 3.52\pm0.12\times10^9\,M^{-1}\cdot\text{sec}^{-1}$ (at 15 °C) for PBSQ in DME. A value of $k = 6.4\times10^9\,M^{-1}\cdot\text{sec}^{-1}$ is predicted for both cases from Eqs. (4.16) and (4.18) if one takes $d = 2a$. The smaller experimental values might be due in part to residual charge effects. The quantity $\omega_{HE}/\mathfrak{N}$ for PBSQ in EtOH has been obtained from Figs. 14 and 18 and yields values of $1.87\pm0.20\times10^8\,M^{-1}\cdot\text{sec}^{-1}$ and $1.40\pm0.20\times10^8\,M^{-1}\cdot\text{sec}^{-1}$, respectively (at −50°), which agree well. The latter was obtained from the slope of the linewidth vs η/T in an exactly analogous manner to that used in the strong ex-

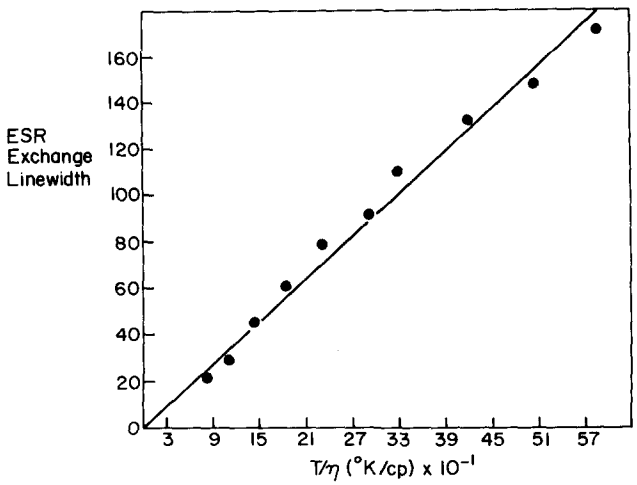

FIG. 17. The exchange component of $M_I = 0$ ESR line of a $1.2 \times 10^{-3} M$ solution of PBSQ in DME plotted as a function of T/η.

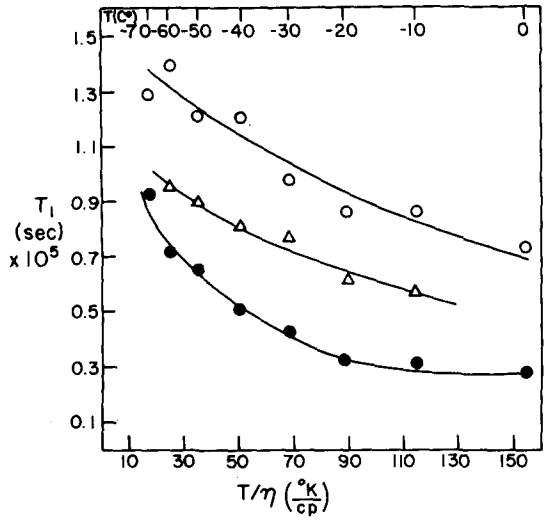

FIG. 19. Variation of T_1 as a function of T/η for solutions of PBSQ (•), DSQ (○), and 2,5-DMPBSQ (Δ) in EtOH.

change cases.

We have already noted the strong dependence of the ESR linewidths below -60 °C in DME on the TBAP concentration (cf. Fig. 13). For that reason, in determining T_2^{-1} (conc.) $- T_2^{-1}$ (dil.) for DSQ in DME, we utilized for each concentrated sample a dilute sample having the same TBAP concentration. The dilute widths utilized for DSQ in DME to obtain Fig. 16 are those shown in Fig. 13. (It is necessary to use greater amounts of TBAP to stabilize the solutions, as the concentration of radical is increased.) Note, however, that the uncertainty in the TBAP concentration of a particular sample, due to the methods of sample preparation, can lead to large uncertainty in the intrinisc width. The PBSQ in DME results were obtained for $T/\mathfrak{N} > 16$ ($T > -50$ °C), where effects from TBAP are not very significant, and were then extrapolated for $T/\mathfrak{N} < 16$.

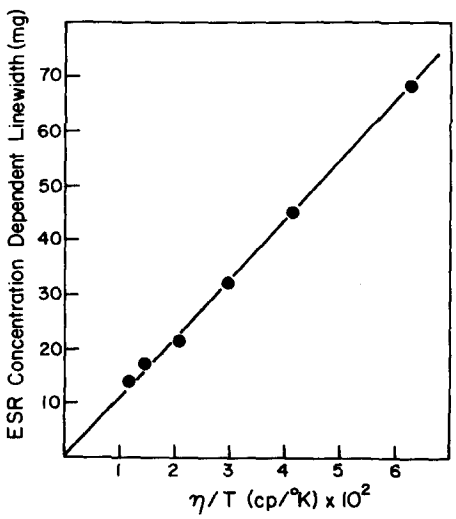

FIG. 18. The concentration dependent component of the $M_I = 0$ ESR linewidth of a $4.27 \times 10^{-3} M$ solution of PBSQ in EtOH plotted as a function of η/T.

B. Saturation measurements and determination of T_1 and T_2

The relaxation times T_1 and T_2 have been determined by the progressive saturation technique which is based on the expression[26]

$$\delta^2 = (4/3\,\gamma_e^2)(1/T_2)^2 + 4/3\,B_1^2(T_1/T_2)\,, \qquad (4.18)$$

where δ is the derivative peak-to-peak width, γ_e is the gyromagnetic ratio of the electron, and B_1 is the circularly polarized magnetic induction and is given by[3]

$$B_{1_{max}}^2 = (\mu H_0^2 Q_0(1 - |\Gamma_0|^2)P_{inc}/2\omega_0) \times 10^8\,\mathrm{G}\,. \qquad (4.19)$$

In Eq. (4.19), Q_0 is the unloaded cavity Q, ω_0 is the cavity resonance frequency, and P_{inc} is the microwave power incident on the cavity. Γ_0 is the power reflection coefficient for the cavity at resonance, H_0^2 is the reduced magnetic field strength, and μ is the permeability of the medium.

The T_1/T_2 ratios determined from Equation (4.18) were corrected for nonuniform microwave modulation fields as well as distortions of the microwave modal pattern by the method described by Kooser *et al.*[26] Only the corrected values of T_1 are reported here.

The experimental fits to Eq. (4.18) yields values of T_2 with a precision of 3%–6% and T_1/T_2 with 10%–20% in the present work. In all cases, only the central line of the ESR spectrum was studied.

The value of $Q_0(1 - |\Gamma_0|^2)$ as a function of temperature for DME reported by Das, Wagner, and Freed[27] as $Q_0(1 - |\Gamma_0|^2) = (3857 \pm 63) + (20 \pm 2)T(-80 \geq T(°C) \leq 23)$ was used in this work. The value for ethanol was found to be 5000 ± 500 for $-20 \geq T(°C) \leq -80$. The method of measurement has been described in detail by Wagner.[28]

We show in Figs. 19–22 T_1 results vs T/η for PBSQ and DSQ in EtOH and DME solvents and 2, 5-DMPBSQ in EtOH.

In general, one may analyze the observed T_1's in terms of both W_e and W_n (or $b \equiv W_n/W_e$) utilizing in gen-

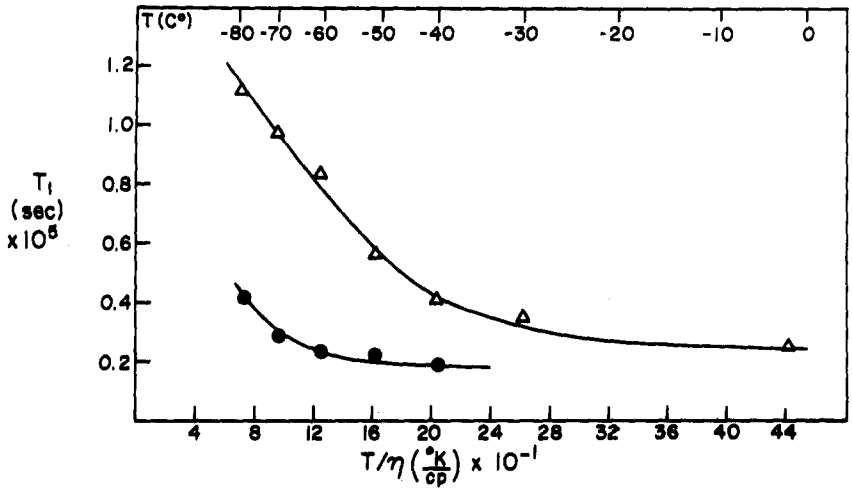

FIG. 20. Variation of T_1 as a function of T/η for solutions of PBSQ (•) and DSQ (Δ) in DME.

eral saturation theories (since the values of τ_R in our work obey $|\tau_R \omega_0| \gg 1$, thus suppressing nonsecular cross relaxation). [The more concentrated solutions involve ω_{HE} (or $b'' \equiv \omega_{HE}/NW_e$) as well.] One learns from the general theories that, for example, the sixfold degenerate central line of PBSQ will saturate as a superposition of Lorentzians, which need not behave as a simple average Lorentzian. This difficulty can exist even when the unsaturated line behaves as an average Lorentzian, as in the present work. This is because the saturation parameters of T_1's for each component may still be markedly different (see below for typical examples), and this is the case predicted for PBSQ at the lower temperatures. We have found it useful to utilize our computer programs for PBSQ based on the general theory to analyze the T_1 results. In general, a superposition of lines of different intrinsic T_1's need not obey Eq. (4.18), which displays a simple quadratic dependence on B_1^2. We have, however, found this quadratic dependence to hold in all our current work. Thus, our computer programs (for a particular set of relaxation parameters) would be run for a range of values of B_1^2, and the results fit to Eq. (4.18) to extract an effective T_1 for comparison with the experimental results. Provided the W_n (and ω_{HE}) are known, this comparison is a means of extracting out W_e from the saturation experiment. In the course of our analyses, we found that certain averaging procedures could be used effectively to deal with our saturation data, and they are also discussed below.

1. PBSQ

As noted, the coupled relaxation problem for PBSQ was computerized based on the general saturation theory [e.g., Eqs. (2.20)–(2.22) of Paper V].[11] This program was, however, written for completely-equivalent nuclei, because of the considerable added complexities introduced for non-completely-equivalent nuclei. We have, however, shown in Paper V that in the limit $b = W_n/W_e \ll 1$ when an "average ESR saturation" is obtained, that such a procedure is completely justified. The case for $b \sim 1$ has not been rigorously studied. (In our studies, b varies from 0.06 to 0.7 for DME solvent and 0.07 to 1 for EtOH.) The experimental input parameters A and $j_{aa}^D(0)\Gamma_{ab} = 3/8C$ were those of Figs. 7 and 8. We used $\Gamma_{ab} = 0.422$ from the theoretical estimates in order to obtain W_n from Eq. (4.12), but then considered the effect of other choices. The method then involves a trial-and-error procedure of first estimating W_e, then predicting T_1 by computer simulation to compare with the experimental T_1 of Figs. 19 and 20. This is repeated until the predicted and experimental T_1's agree. Our results for W_e are shown in Figs. 23 and 24. They demonstrate good linear dependence with T/η as expected for a spin–rotational mechanism [cf. Eq. (4.8)].

These studies, because they involve values of $b \gg 0.03$, are not candidates for the averaging theory given in Paper V based on very small values of b. However, another form of averaging may be considered because in

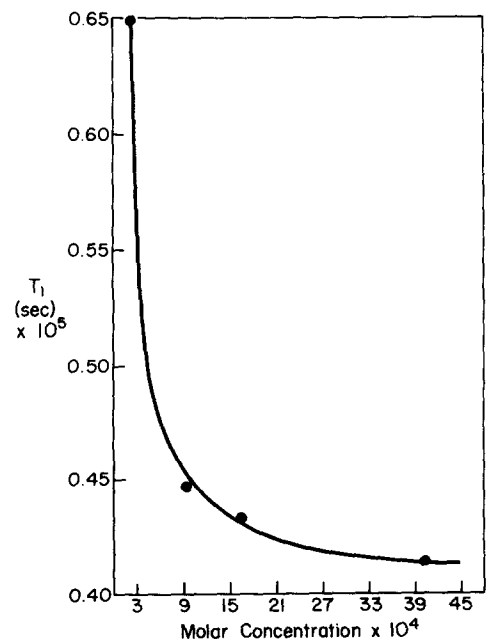

FIG. 21. T_1 for PBSQ in EtOH at $T = -50$ °C plotted as a function of concentration.

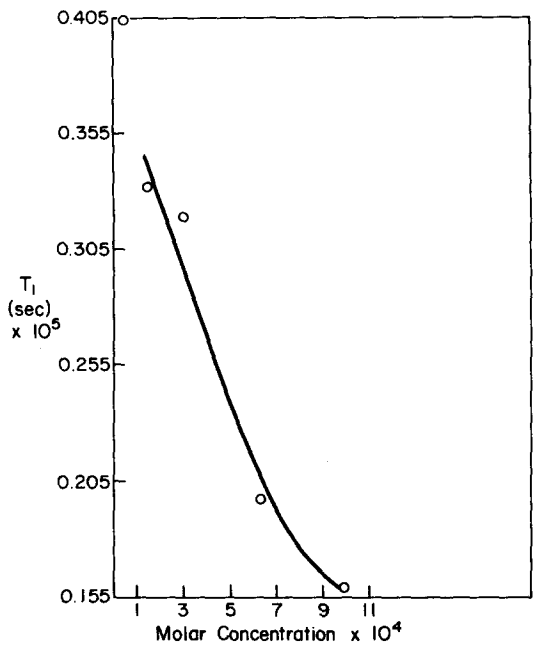

FIG. 22. T_1 for DSQ in DME at $T=-40\,°C$ plotted as a function of concentration.

our saturation technique, the ESR spectrum is only very mildly saturated ($\gamma_e^2 B_1 T_1 T_2 \leq 0.5$). One readily shows [cf. Eqs. (2.21) and (2.33) of Paper V] that if the T_2's for the different components of the ESR line are nearly equal, and if the saturation factor $Z_\lambda \equiv [1+\gamma_e^2 B_1^2 T_{1,\lambda} T_{2,\lambda}]^{-1/2}$ does not vary much among the components (either because the $T_{1,\lambda}$'s are nearly the same, or B_1^2 is small, or some combination of these two), then one may use the average $\overline{T}_1 = \sum_\lambda D(\lambda) T_{1,\lambda} / \sum_\lambda D(\lambda)$ as the correct T_1 for a

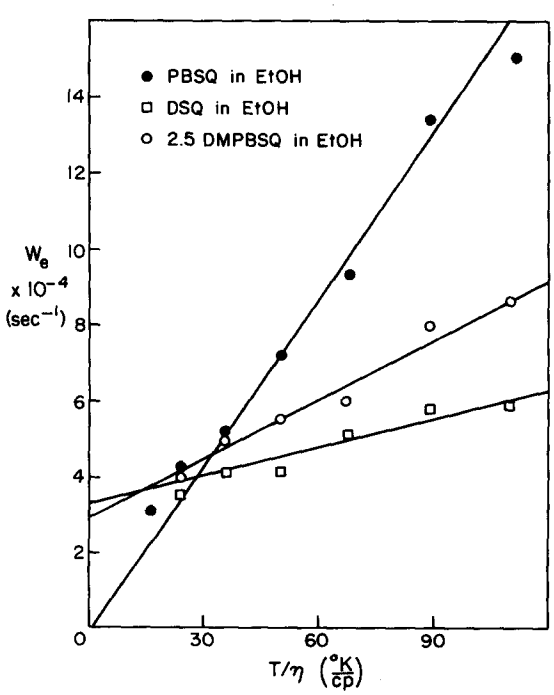

FIG. 23. W_e as a function of T/η for solutions of PBSQ, DSQ, and 2,5-DMPBSQ in EtOH.

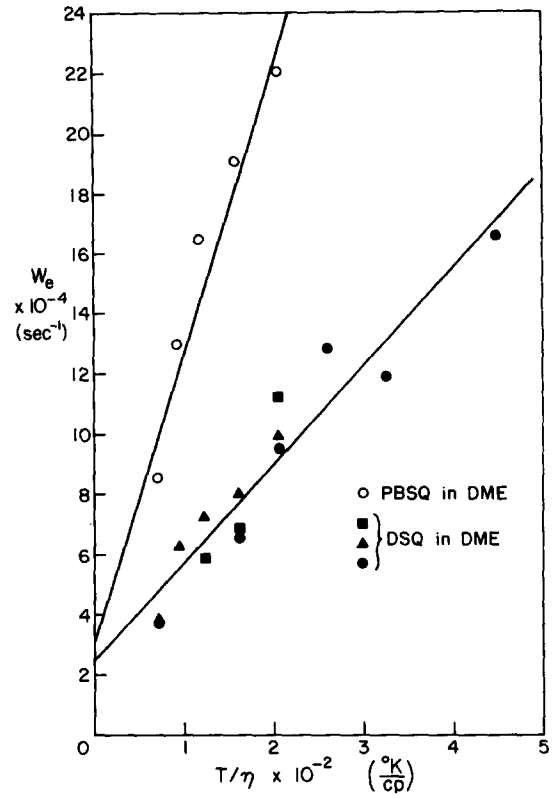

FIG. 24. W_e as a function of T/η for solutions of PBSQ and DSQ in DME.

simple average saturated Lorentzian. The proper $\overline{T}_1$ for dilute solutions of PBSQ (four completely equivalent protons) may be obtained from the entries in Table I of Paper I. One has

$$\overline{T}_1 \cong (12 W_e)^{-1}\left[2+\frac{3(1+2b+b^2)}{(1+4b+3b^2)} + \frac{(1+14b+61b^2+84b^3+36b^4)}{(1+20b+127b^2+288b^2+180b^4)}\right]. \tag{4.20}$$

We have checked the applicability of Eq. (4.20) to the present case, and we have found that it is in very good agreement with the results of the rigorous computer simulations. (The deviations range from virtually 0 to 5% over the range studied.)

The analytic equation equivalent to Eq. (4.3), but for not-completely-equivalent nuclei, has not yet been derived because of the complications of calculating the (coupled) $T_{1,\lambda}$'s. However, we note that when $j^D_{ab}(0) \approx 0$ (uncorrelated nuclei), the effectiveness of nuclear-spin transitions is reduced.

Thus, we can roughly approximate this effect by utilizing a W_n of reduced magnitude in Eq. (4.20). We have done this for typical values of b, reducing W_n by as much as a factor of 2. At most (for $b \lesssim 1$) it leads to an increase in W_e by about 10%. [Note also that if we were to use a $\Gamma_{ab}=1$ corresponding to complete correlation instead of $\Gamma_{ab}=0.422$, this would result in values of W_n, estimated from Eq. (4.2c), which would be about half those we have used.]

Thus, the nature of the correlation affects (a) our esti-

mates of W_n from Eq. (4.2c), and ultimately (b) our usage of W_n in the complete transition-probability matrix, but in such a way that any errors from (a) and (b) resulting from our uncertainty in the correlation tend to offset each other at least in part.

To summarize, then: (1) the results for W_e shown in Figs. 23 and 24 are rather insensitive to the uncertainties in the analysis from which they are obtained; and (2) an averaging formula such as Eq. (4.20) appears to be quite applicable to the kind of saturation measurements we have utilized.

2. DSQ

The analysis of the saturation data for DSQ is, in principle, much more complex than that for PBSQ because of the large number of hyperfine lines and degeneracies. We have therefore not attempted a completely rigorous analysis of this case. However, we are aided by the fact, noted in Sec. IV. A, that the values for $j^D_{aa}(0)$(DSQ) are about an order of magnitude smaller (judging from the parameters of Sec. IV. A) than for PBSQ. Thus, we may attempt to use the simple averaging expression for the center line to obtain W_e:

$$\langle T_1(0)\rangle = \tfrac{1}{4}\langle \Omega_e(0)\rangle$$

$$\cong \left[2W_e\left(1+\frac{\omega_{HE}}{2W_e}\right)\right]^{-1}\left[1-6b\Big/\left(1+\frac{\omega_{HE}}{2}\right)+\frac{D(0)}{N}\,\frac{\omega_{HE}}{W_e}\right], \tag{4.21}$$

where $\frac{1}{2}N=\sum_\lambda D(\lambda)$. Note that in the limit $\omega_{HE}/W_e \gg 1$, Eq. (4.21) has the asymptotic value

$$T_1(0) \sim \frac{1}{2W_e}\,(D(0)/\tfrac{1}{2}N)\,, \tag{4.22}$$

which represents strongly coupled relaxation of all the hyperfine lines due to the exchange.[6] We have utilized Eq. (4.21) (to zero order in b'') for our dilute solution ($0.5\times10^{-4}M$ in DME and $2\times10^{-4}M$ in EtOH) data, where HE effects are unimportant (see Sec. IV. C), while we have used the asymptotic form, Eq. (4.22), for our very concentrated data (6.3×10^{-4} and $9.9\times10^{-4}M$ in DME). One sees from Fig. 24 that the two different approximate forms of estimating W_e give very much the same results, which is encouraging. One sees that W_e for DSQ is roughly a factor of 2 smaller for DSQ than for PBSQ in the same solvent and for the same T/η, as we have already noted.

3. 2, 5-DMPBSQ

In the case of 2, 5-DMPBSQ, we have analyzed for W_e using a combination of the type of averaging of Eq. (4.20) for the two ring protons and Eq. (4.21) for the six methyl protons to yield

$$\langle T_1(0)\rangle \cong (4W_e)^{-1}\left[1+\frac{1+2b_R+b_R^2}{1+4b_R+3b_R^2}\right][1-3b_M]\,, \tag{4.23}$$

with $b_R \cong W_{n,R}/W_e$ and $b_M = W_{n,M}/W_e$ and $W_{n,R}$ and $W_{n,M}$ obtained as described in Sec. IV. A. The results for W_e are shown in Fig. 23. Again, for a given temperature, they lie intermediate between the results for DSQ and PBSQ, as anticipated.

C. ENDOR

It has already been noted the the ENDOR line shape, in the absence of coherence effects, is very nearly Lorentzian. This result is suggestive of the applicability of an "average ENDOR" line, which is some simple average over all the six types of allowed ENDOR transitions. One must, however, recognize that superpositions of Lorentzians can deceptively appear to be a simple Lorentzian.[20] One type of average ENDOR has been discussed in Paper V. It is based upon $b \ll 1$, and it yields an expression for the derivative ENDOR enhancement of

$$\tfrac{1}{2}E_{(\text{deriv})} \cong E = \frac{\langle J^2\rangle d_n^2\,\Omega_{e,n}^2\,T_{2,n}\,\bar{\Omega}_e^{-1}}{1+(\Delta\omega_n^2\,T_{2,n})^2+\langle J^2\rangle d_n^2\,T_{2,n}(\Omega_n-\Omega_{e,n}^2/\bar{\Omega}_e)}\,, \tag{4.24}$$

where

$$d_n = \tfrac{1}{2}\gamma_n(1+\tfrac{1}{10}a)\,B_n\,, \tag{4.25}$$

$$\bar{\Omega}_e \equiv \Omega_e + (1+\Delta\omega_e^2\,T_{2,e}^2)/T_{2,e}\,d_e^2\,. \tag{4.26}$$

Here the T_2's and $\Omega_{i,j}$'s are all average values for which detailed expressions are given in V. [Actually it is the products $\langle J^2\rangle\Omega_n$ and $\langle J^2\rangle^{1/2}\Omega_{e,n}$ which are given, but it is convenient, for equivalent protons, to set $\langle J^2\rangle \equiv n$ (since the "average" transition moment is approximated by nd_n^2).] It then follows from Eq. (4.24) that (cf. also Sec. II. D. 2)

$$E^{-1} = k + l d_n^{-2}\,, \tag{4.27}$$

where

$$k = [-1+\langle J^2\rangle\Omega_n\bar{\Omega}_e/\langle J^2\rangle\Omega_{e,n}^2]\,, \tag{4.28a}$$

$$l = \bar{\Omega}_e/\langle J^2\rangle\Omega_{e,n}^2\,T_{2,n} \tag{4.28b}$$

when $\Delta\omega_n = 0$. It also follows from Eq. (4.24) that the ENDOR line shape is that of a saturated Lorentzian of width $T_{2,n}^{-1}$ and a modified saturation parameter

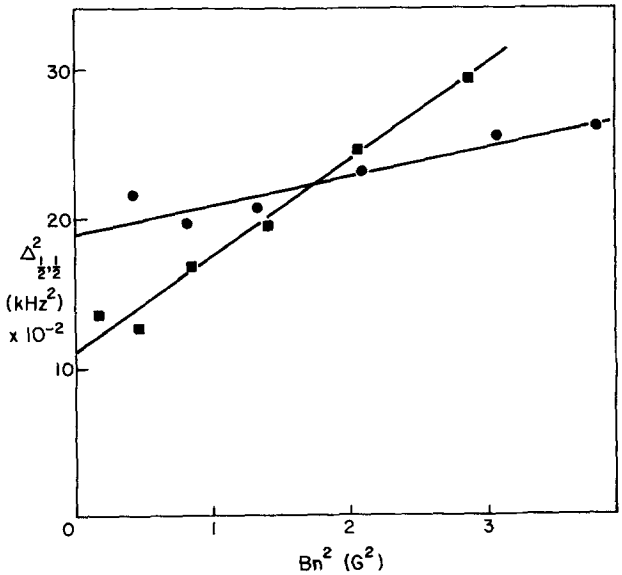

FIG. 25. Plots of $\Delta^2_{1/2,1/2}$ as a function of B_n^2 (as determined by the rf coherence effect) for PBSQ (•) and DSQ (■) in EtOH at $T = -30\,^\circ$C.

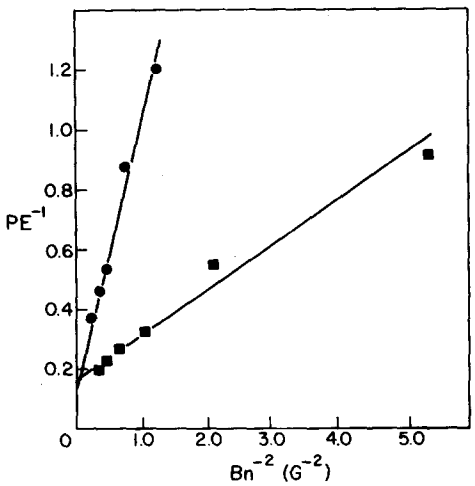

FIG. 26. Plot of PE^{-1} as a function of B_n^{-2} (as determined by the rf coherence effect) for PBSQ (•) and DSQ (■) in EtOH at $T = -30\,°C$.

$$\langle J^2\rangle \Omega_n' \equiv \langle J^2\rangle (\Omega_n - \Omega_{e,n}^2 \bar{\Omega}_e^{-1}) \,. \tag{4.29}$$

Thus, one has for the $\frac{1}{2} - \frac{1}{2}$ width ($\Delta_{1/2,1/2}$) (cf. also Sec. II. D. 2)

$$\Delta_{1/2,1/2}^2 = i + m d_n^2 \,, \tag{4.30}$$

where

$$i = T_{2,n}^{-2} \tag{4.31a}$$

$$m = \langle J^2\rangle \Omega_n' T_{2,n}^{-1} \,. \tag{4.31b}$$

We have found the expressions Eqs. (4.27) and (4.30) to be generally valid in our studies (providing, as noted in Sec. III, serious distortions from coherence effects are neglected) even when the average ENDOR expressions of V are clearly inapplicable. We show typical experimental results for the dependences of $\Delta_{1/2,1/2}^2$ and E^{-1} on B_n^2 and B_n^{-2}, respectively, as given by Eqs. (4.27) and (4.30) in Figs. 25 and 26. These linear dependences serve as the basis of our comparison between predicted and experimental ENDOR signals. That is, from both the experimental and computer-simulated spectra, the parameters i, m, k, and l are determined, and we let

$$T_{2,n}^{-1} \equiv i^{1/2} \,, \tag{4.32a}$$

$$\langle J^2\rangle \Omega_n' \equiv m T_{2,n} \,, \tag{4.32b}$$

with $\langle J^2\rangle \Omega_n'$ following from Eq. (4.29) (the difference between Ω_n and Ω_n' generally being very small). Then we obtain

$$\langle J^2\rangle \Omega_{e,n}^2(k) \equiv [\langle J^2\rangle \Omega_n \bar{\Omega}_e]/(k+1) \tag{4.33a}$$

and by

$$\langle J^2\rangle \Omega_{e,n}^2(l) \equiv \bar{\Omega}_e / T_{2,n} l \,. \tag{4.33b}$$

Only when the average ENDOR theory is truly applicable should $\Omega_{e,n}(k) = \Omega_{e,n}(l)$. Thus, the extent to which they are unequal becomes one measure of the inapplicability of average ENDOR.

Actually, because in many cases the saturation of the ENDOR transitions was not very appreciable, it was found useful to plot E of Eq. (4.24) vs d_n^2 with the lowest order term in a power series expansion in d_n^2 going as $\langle J^2\rangle d_n^2 \Omega_{e,n}^2 T_{2,n} \Omega_e'^{-1}$ (when $\Delta\omega_n = 0$). This permitted another determination of $\langle J^2\rangle \Omega_{e,n}^2$.

Typical experimental results on $\Delta_{1/2,1/2}$ and E (PE is percent enhancement) are shown in Figs. 27 and 28, re-

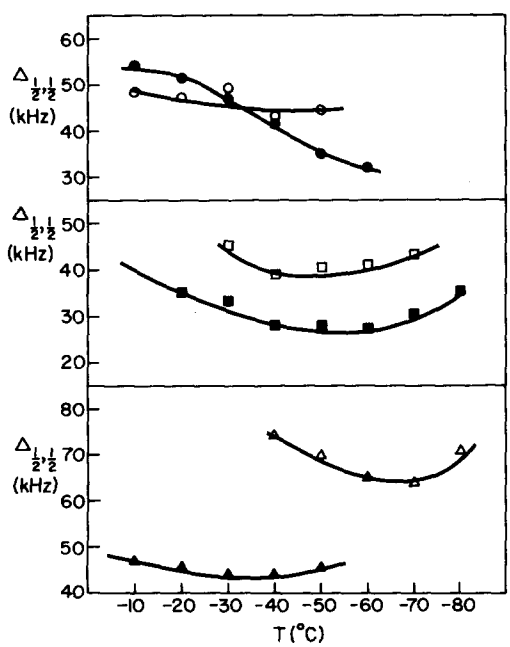

FIG. 27. Unsaturated ENDOR linewidth as a function of temperature for dilute solutions of semiquinones. Δ = PBSQ in DME; ▲ = PBSQ in EtOH; □ = DSQ in DME; ■ = DSQ in EtOH; ○ = 2,5-DMPBSQ in EtOH ring proton; • = 2,5-DMPBSQ in EtOH methyl proton.

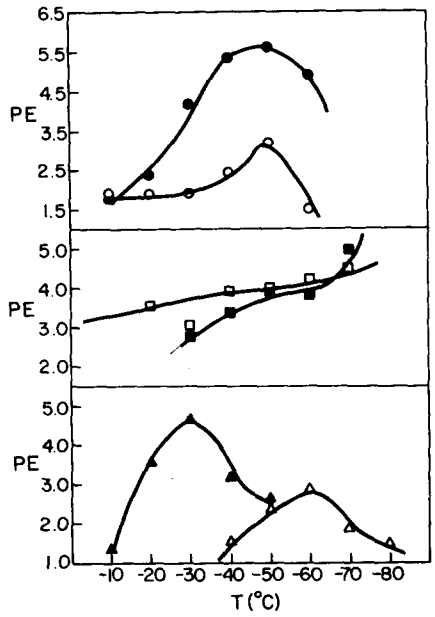

FIG. 28. The percent enhancement at infinite rf power as a function of temperature for dilute solutions of semiquinones: Δ = PBSQ in DME; ▲ = PBSQ in EtOH; □ = DSQ in DME; ■ = DSQ in EtOH; ○ = 2,5-DMPBSQ in EtOH ring proton; • = 2,5-DMPBSQ in EtOH methyl proton.

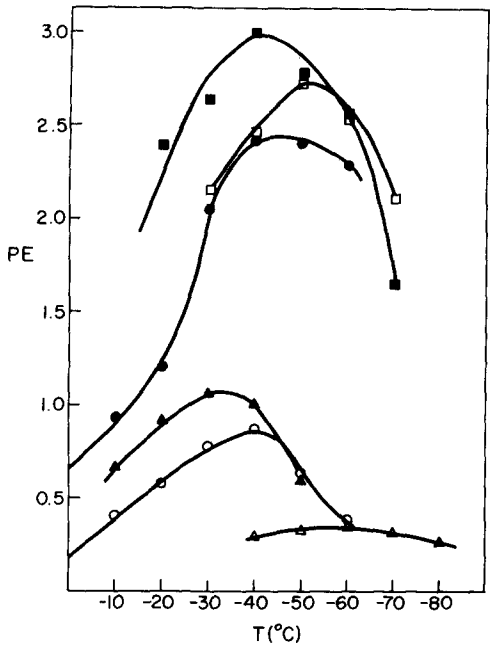

FIG. 29. ENDOR percent enhancement for rf (Varian probe) = 2.2 V as a function of temperature for solutions of semiquinones. Δ = PBSQ in DME; ▲ = PBSQ in EtOH; □ = DSQ in DME; ■ = DSQ in EtOH; • = 2,5-DMPBSQ in EtOH methyl proton; ○ = 2,5-DMPBSQ in EtOH ring proton.

spectively, as a function of temperature for the different systems studied. These results are extrapolated to $d_n^2 = 0$ and $d_n^2 \to \infty$, respectively. Enhancements obtained at typical finite values of d_n^2 are shown in Fig. 29. One immediately notes that while the extrapolated values of E are comparable for PBSQ and DSQ, the latter are considerably greater (by about a factor of 3) at lower rf powers.

1. PBSQ

In order to compare our experimental ENDOR results with the theory of Freed, it was necessary to calculate ENDOR spectra utilizing the computer program described in Leniart's thesis.[11]

This program can calculate either ESR spectra as a function of microwave power or ENDOR spectra as a function of nuclear rf power. The input data for the program are d_e, d_n, W_e, $W_n = \frac{1}{2} j_{aa}^D(0)$, ω_{HE}/N, and A', where the first five parameters are as defined previously and the sixth is A minus the dipolar and W_e contributions.

The ESR version of the program was used to calculate the values of W_e and A' from the experimentally determined T_1's, T_2's, and W_n's as already noted. The input values of W_e and A' were varied until the values of T_1/T_2 and T_2 obtained from the analysis of the microwave power dependence of the calculated spectra were the same as the experimental values.

The values of W_e and A' obtained from the saturation experiments and the values of W_n, ω_{HE} obtained from the width measurement as well as the measured values of d_e and d_n were used to calculate the ENDOR spectra. See Table III.

The program was written for a system containing four completely equivalent protons, whereas the four protons in PBSQ are two equivalent sets of two completely equiv-

TABLE III. Computer inputs for the calculation of the ENDOR parameters for solutions of PBSQ.

PBSQ in DME

Temp. (°C)	b	b'' dilute[a]	b'' conc.	W_e^*(sec^{-1}) $\times 10^{-4}$	A'	d_e (dilute) (sec$^{-1}\times 10^{-5}$)	d_e (conc.) (sec$^{-1}\times 10^{-5}$)
−40	0.0586	0.013	0.2183	22.0	3.91	4.86	11.03
−50	0.093	0.013	0.197	19.0	4.84	4.76	9.77
−60	0.150	0.013	0.176	16.5	6.63	4.77	8.52
−70	0.282	0.013	0.170	13.0	10.76	4.74	7.39
−80	0.713	0.013	0.192	8.5	21.50	5.10	6.35

PBSQ in EtOH

Temp. (°C)	b	b'' dilute	b'' conc. I[b]	b'' conc. II[c]	W_e^*(sec^{-1}) $\times 10^{-4}$	R_{temp}
−20	0.0743	0.005	0.023	0.046	13.4	7.19
−30	0.149	0.005	0.041	0.122	9.4	10.15
−40	0.329	0.010	0.127	0.244	7.2	15.04
−50	0.644	0.020	0.220	0.469	5.2	23.50

Temp. (°C)	d_e (dilute) (sec$^{-1}\times 10^{-5}$)	d_e (conc. I) (sec$^{-1}\times 10^{-5}$)	d_e (conc. II) (sec$^{-1}\times 10^{-5}$)
−20	2.32	3.48	4.13
−30	2.32	2.92	3.89
−40	2.32	3.09	3.89
−50	2.46	2.92	3.68

[a]Dilute = $< 10^{-5}$ m. [b]Conc. I = $1.0\times 10^{-4} M$. [c]Conc. II = $1.2\times 10^{-3} M$.

TABLE IV. PBSQ in DME[a] experimental and theoretical ENDOR relaxation parameters.[b] (All values given in seconds.)

Temp. (°C)	$T_n\times10^5$	$\bar{\Omega}_e\times10^5$[c]	$\langle J^2\rangle\Omega_n\times10^5$	$\langle J^2\rangle^{1/2}\Omega_{e,n}\times10^5$[d]	$\langle J^2\rangle^{1/2}\Omega_{e,n}\times10^5$[e]	$\langle J^2\rangle^{1/2}\Omega_{e,n}\times10^5$[f]
−40	0.212(0.236, 0.262)	1.71(1.43, 1.71)	8.59(12.75, 12.78)	0.485(0.712, 0.735)	0.608(0.623, 0.632)	0.531(0.504, 0.588)
−50	0.227(0.239, 0.266)	1.94(1.62, 1.94)	9.39(10.14, 10.18)	0.652(0.763, 0.788)	0.666(0.655, 0.669)	0.585(0.540, 0.634)
−60	0.224(0.235, 0.259)	2.18(1.82, 2.18)	12.8(7.97, 8.00)	0.887(0.773, 0.803)	0.674(0.660, 0.668)	0.631(0.549, 0.642)
−70	0.247(0.226, 0.242)	2.79(2.33, 2.79)	20.0(6.30, 6.36)	1.02(0.840, 0.825)	0.748(0.686, 0.687)	0.647(0.583, 0.662)
−80	0.221(0.196, 0.206)	3.78(3.15, 3.78)	12.6(4.77, 4.83)	0.837(0.845, 0.803)	0.824(0.688, 0.668)	0.679(0.581, 0.649)

[a]Concentration of solution, $1\times10^{-4}M$ rf field calibrated by coherence effect; to convert to probe results divide Ω_n by 2.29 and $\Omega_{e,n}$ by 1.51.
[b]The first values in the parentheses are theoretical results calculated with values of W_e 20% higher than those obtained experimentally. The second values in the parentheses are theoretical results calculated with the experimentally determined W_e.
[c]$\bar{\Omega}_e=\Omega_e+\{1+[\Delta\omega_e T_{2,e}]^2\}/T_{2,e}d_e^2$.
[d]Determined from the intercept of the PE^{-1} vs d_n^{-2} plot.
[e]Determined from the slope of the PE^{-1} vs d_n^{-2} plot.
[f]Determined from the slope of the PE vs d_n^{-2} plot.

alent protons, because a proper inclusion of the latter would greatly increase the complexity of the program. We discuss below simple attempts to adjust for this discrepancy.

A complete summary of all the relevant experimental and theoretical results appears in Connor's[12] and Leniart's[11] theses. We give here only the final results for the parameters defined by Eqs. (4.32) and (4.33). These are summarized in Tables IV, V, and VI for dilute solutions of PBSQ. Tables IV and V include a comparison between the experimental ENDOR results and those obtained by the computer simulations. Considering the inherent uncertainties in the estimation of the relevant relaxation parameters from the ESR studies described above, and the great difficulties in the ENDOR relaxation studies themselves, the agreement is seen to be generally quite satisfactory.

One may note, first of all, that the $T_{2,n}$ are found to range from about twice as long as $T_{2,n}$ at the higher temperatures to about 5 times as long at the lower temperatures. This large difference is directly attributable to the fact that the secular g-tensor broadening is the dominant contribution to $T_{2,e}$ and its role increases at lower temperatures (cf. Sec. IV. A). However, it makes *no* contributions to the ENDOR linewidth. The net result of having a significantly narrow ENDOR width is that it is more sensitive to small errors in the relaxation parameters affecting it, and/or to weaker contributions which may be obscured in the case of the broader ESR lines.

The predicted values of $T_{2,n}$ are seen to be about 24% too large at the higher temperatures, but in better agreement at the lower temperatures. One might therefore assume that a relaxation process which decreases in importance with decreasing temperature is not adequately included in the theoretical simulations. Such processes include W_e and ω_{HE}. We include in Tables IV and V the results when W_e is increased by 20%. This represents the uncertainty in the saturation measurements, and previous results from this laboratory for the solvents used here suggest the possibility of a small systematic experimental error of this order.[26,27] This adjustment does, of course, reduce the discrepancy in $T_{2,n}$ appreciably. The other predicted ENDOR parameters are not affected very significantly, although the $\Omega_{e,n}$ values tend to deviate somewhat more from experiment. Small increases in ω_{HE} (discussed below) could improve the agreement in $T_{2,n}$ with less change in $\Omega_{e,n}$.

As we have discussed in Sec. IV. B, we can try to roughly approximate the reduced effectiveness of nuclear-spin transitions due to the lack of complete equivalence of the nuclear spins by using W_n of reduced magnitude. Typical results of such calculations are shown in Table V. As already noted, the analysis for W_e is

TABLE V. Theoretical ENDOR relaxation parameters calculated with different values of W_n for a $1\times10^{-4}M$ solution of PBSQ in DME. (All values given in seconds.)

Temp. (°C)	W_n	$T_n\times10^5$	$\bar{\Omega}_e\times10^5$[a]	$\langle J^2\rangle\Omega_n\times10^5$	$\langle J^2\rangle^{1/2}\Omega_{e,n}\times10^5$[b]	$\langle J^2\rangle^{1/2}\Omega_{e,n}\times10^5$[c]	$\langle J^2\rangle^{1/2}\Omega_{e,n}\times10^5$[d]
−40	W_n	0.262	1.71	12.78	0.735	0.632	0.588
−80	W_n	0.206	3.78	4.79	0.803	0.668	0.649
−40	$3W_n/4$	0.279	1.71	16.1	0.753	0.663	0.570
−80	$3W_n/4$	0.249	3.78	6.14	0.966	0.789	0.591
−40	$W_n/2$	0.302	1.71	22.00	1.02	0.697	0.548
−80	$W_n/2$	0.322	3.78	8.40	1.15	0.977	0.520

[a]$\bar{\Omega}_e=\Omega_e+\{1+[\Delta\omega_e T_{2,e}]^2\}/T_{2,e}d_e^2$.
[b]Determined from the intercept of the PE^{-1} vs d_n^{-2} plot.
[c]Determined from the slope of the PE^{-1} vs d_n^{-2} plot.
[d]Determined from the slope of the PE vs d_n^2 plot.

TABLE VI. PBSQ in EtOH[a] experimental and theoretical ENDOR relaxation parameters.[b] (All values given in seconds).

Temp. (°C)	$T_n\times10^5$	$\bar{\Omega}_e\times10^5$[c]	$\langle J^2\rangle\,\Omega_n\times10^5$	$\langle J^2\rangle^{1/2}\Omega_{e,n}\times10^5$[d]	$\langle J^2\rangle^{1/2}\Omega_{e,n}\times10^5$[e]	$\langle J^2\rangle^{1/2}\Omega_{e,n}\times10^5$[f]
−10	0.338	3.27	11.8	0.743	1.34	1.18
−20	0.350(0.390, 0.435)	3.31(2.76, 3.31)	7.36(17.9, 18.4)	0.929(1.00, 1.04)	1.27(0.852, 0.902)	0.859(0.641, 0.771)
−30	0.362(0.440, 0.481)	4.06(3.38, 4.06)	9.44(14.8, 15.4)	1.32(1.27, 1.32)	1.47(1.06, 1.10)	1.38(0.813, 0.964)
−40	0.363(0.394, 0.407)	5.15(4.29, 5.15)	9.60(10.3, 10.7)	1.25(1.28, 1.26)	1.62(1.07, 1.46)	1.30(0.861, 0.955)
−50	0.350(0.352, 0.362)	6.55(5.46, 6.55)	7.42(8.27, 8.30)	1.13(1.35, 1.27)	1.32(1.12, 1.55)	1.14(0.916, 0.998)

[a]Concentration of solution; $2\times10^{-4}M$; rf field calibrated by coherence effect; to convert to probe results divide Ω_n by 2.29 and $\Omega_{e,n}$ by 1.51.

[b]The first values in the parentheses are theoretical results calculated with values of W_e 20% higher than those obtained experimentally. The second values in the parentheses are theoretical results calculated with the experimentally determined W_e.

[c]$\bar{\Omega}_e=\Omega_e+\{1+[\Delta\omega_e T_{2,e}]^2\}/T_{2,e}d_e^2$.

[d]Determined from the intercept of the PE^{-1} vs d_n^2 plot.

[e]Determined from the slope of the PE^{-1} vs d_n^2 plot.

[f]Determined from the slope of the PE vs d_n^2 plot.

hardly affected (but $\bar{\Omega}_e$ has been adjusted accordingly). In general, a reduction in b tends to lead to less satisfactory agreement with experiments, with the worst discrepancies for $T_{2,n}$ and Ω_n. We note, however, that a proper analysis of incomplete equivalence for the simpler case of average ENDOR from two protons[5] indicates that Ω_n and $T_{2,n}$ are hardly affected by the incomplete equivalence, because they are rather insensitive to the value of $j_{ab}^D(0)/j_{aa}^D(0)$. This suggests that the rough approximations of Table V are probably too drastic to be applicable to these parameters.

The parameter for which the agreement is least satisfactory is Ω_n, the NMR saturation parameter. One should first note that Ω_n is obtained from a progressive rf saturation ENDOR experiment in the same manner that Ω_e is obtained from a progressive microwave saturation ESR experiment. Thus, this measurement would suffer from any uncertainties in the determination of B_n, as already discussed. Probably the most serious problem we encountered with these measurements was the very weak sensitivity of the ENDOR $\Delta_{1/2,1/2}$ to B_n for PBSQ over the range of B_n available. This is illustrated in Fig. 25. That is, the value of $\Omega_n' T_{2,n}$ of Eq. (4.31b) for PBSQ is small enough that we could not very appreciably saturate the NMR transitions. In fact, the standard deviations on the ENDOR widths at a given temperature (for the 6 or 7 rf power levels used) introduced an uncertainty in the value of Ω_n greater than the variation of Ω_n with a temperature change of the order of 10 °C. [The accuracy of the measurements of $T_{2,n}$ is, of course, not affected by the fact that only marginal degrees of saturation could be achieved. Note also from Fig. 26 and Eqs. (4.27) and (4.28) that the measurements of E are still adequately sensitive to the values of B_n used.] All in all, however, reasonable agreement is achieved for PBSQ in EtOH at the lower temperatures and for PBSQ in DME at the higher temperatures.

In general, our results show better agreement between experimental and simulated values for EtOH solvent at the lower temperatures (−40 and −50 °C) and for DME solvent at the higher temperatures (−40 to −60 °C). This may, at least in part, be due to the fact that for PBSQ in EtOH, (1) at the lower temperatures used there was no decomposition of sample, although some occurred at the higher temperatures, and (2) because the broader ESR line at the lower temperatures resulted in better S/N with respect to the F/F lock oscillation about the ESR peak maximum. For DME solvent, precipitation of the supporting electrolyte became a problem at the lower temperatures, while the stability of the radical was not a factor over the temperature range studied.

Note, however, that with $\langle J^2\rangle=n=4$ we obtain values of Ω_n which are substantially longer than $T_{2,n}$. Thus, the estimates of Ω_n should be even more seriously affected by uncertainties in, e.g., b (cf. Table V) or other mechanisms that hardly affect the ESR relaxation parameters.

In view of (1) the complexities of computer simulating the ENDOR spectrum; (2) the appearance of the ENDOR spectrum as a single average Lorentzian; (3) the success of a modified average method for dealing with the saturation behavior of PBSQ largely because B_1^2 is never very large (cf. Sec. IV. B), and the fact that the NMR transitions for PBSQ are only marginally saturated, we have studied the validity of applying a modified averaging method to predict the PBSQ ENDOR observations.

If one first uses the analysis suggested above for the modified average ESR saturation and then the fact discussed in Paper V [cf. V, Eqs. (2.37) and (2.38)] that an average ENDOR line arises when the NMR transitions are only weakly saturated, then one may almost justify the use of such a modified average technique even when b is not small. The only possible difficulty is the fact that one must take the matrix of nuclear T_{2,n_i}^{-1} to be nearly diagonal, and this need not be so (cf. Paper I) for nonnegligible b. If we neglect this last problem for the moment, then Eq. (4.24) is again applicable with Ω_e given by Eq. (4.27) for PBSQ. The other needed parameters may be calculated from the definitions of Eq. (2.45) of V and Appendix A of V as well as the results in I. One obtains for dilute solutions (i.e., $b'\approx0$)

$$\langle J_-^2\rangle\,\Omega_{e,n}^2=\frac{2}{W_e^2}\left(\frac{2}{3D^2}\,(3b+16b^2+18b^3)^2 + D^{-2}(1+11b+39b^2+24b^3)^2+(1+3b)^{-2}\right), \quad (4.34)$$

where

$$D = 1 + 20b + 127b^2 + 288b^3 + 180b^4 , \tag{4.34'}$$

and

$$\langle J_-^2\rangle^2 \Omega_n \Omega_{e,n}^2 = \frac{2}{W_e^2}\left(\frac{2S_{44}}{3D^2 d_n^2}\,(3b + 16b^2 + 18b^3) + \frac{S_{55}}{D^2 d_n^2}\,(1 + 11b + 39b^2 + 24b^3) + \frac{(1 + 6b + 6b^2)}{W_e b(1+3b)^3(1+b)} \right) , \tag{4.35}$$

where

$$S_{44}/d_n^2 = \frac{2}{W_e}\left[(2b)^{-1} + (2 + 29b + 135b^2 + 90b^3)/D\right] \tag{4.36a}$$

and

$$S_{55}/d_n^2 = \frac{2}{W_e}\left[(3b)^{-1} + (2 + 23b + 82b^2 + 60b^3)/D\right] . \tag{4.36b}$$

For the case of average $T_{2,n}^{-1}$, we have neglected the off-diagonal elements [cf. Eq. (B4) of Paper I] and have used

$$T_{2,n}^{-1}\langle J_-^2\rangle \Omega_{e,n}^2 = \frac{2}{W_e}\left\{ \frac{2}{3D^2}\,(3b + 16b^2 + 18b^3)(1 + \tfrac{25}{3}b) + D^{-2}(1 + 11b + 39b^2 + 24b^3)^2 + (1 + \tfrac{37}{3}b) + (1+3b)^{-2}(1 + \tfrac{13}{3}b) \right\} , \tag{4.37a}$$

which is a direct application of Eq. (2.45) of V (but written as the more appropriate average of $T_{2,n}^{-1}$ instead of an average of $T_{2,n}$) and of Eqs. (B1)–(B3) of I [note that the 3/8 in Eq. (B1) should be inverted to read 8/3].

We have in Eqs. (4.34)–(4.37) neglected any contributions from b''. They would complicate the calculation of the saturation parameters for the modified average approach except in the limit when the simple average theory of V applies (i.e., $b \ll 1$). However, the effect of b'' on the NMR widths is a simple one (cf. Paper II). One need only add

$$T_{2,n}^{-1EX} \approx \frac{N}{2}\, b''\, W_e = \omega_{HE}/2 \tag{4.37b}$$

to the rhs of Eq. (4.37a) to get the direct contribution of exchange [we are neglecting the indirect effect exchange has on the averaging process of the terms in Eq. (4.37a)].

We compare in Table VII modified average calculations based on Eqs. (4.34)–(4.37) with the results of the complete computer simulations already given in Tables IV and VI. In general, the agreement is quite good. Note that the modified average results for $T_{2,n}$ are improved by including (4.37b) into Eq. (4.37a). The least satisfactory agreement is for Ω_n, where the two methods tend to disagree by as much as almost a factor of 2. We have examined this matter in more detail and have found that this discrepancy is at least partly attributable to an incipient rf coherence effect (the same as that utilized to calibrate the rf probe), which is automatically included in the computer simulations but not in any of the average methods. The results on $\Omega_{e,n}$ are somewhat affected by this, but the analysis given in Tables IV and VI show that the true ENDOR line for the PBSQ systems is not given by a simple single $\Omega_{e,n}$.

At any rate, the approximate agreement of the modi-

TABLE VII. ENDOR relaxation parameters.[a]

Temp. (°C)	W_n $\times 10^{-4}$	W_e $\times 10^{-4}$	$T_n \times 10^5$ (sec) Comp.	$T_n \times 10^5$ (sec) Mod. ave.[b]	$\Omega_e \times 10^5$ (sec) Comp.[c]	$\Omega_e \times 10^5$ (sec) Mod. ave.	$\langle J^1\rangle\,\Omega_e \times 10^5$ (sec) Comp.	$\langle J^1\rangle\,\Omega_e \times 10^5$ (sec) Mod. ave.	$\langle J^2\rangle^{1/2}\Omega_{e,n} \times 10^5$ (sec) Comp.[d]	$\langle J^2\rangle^{1/2}\Omega_{e,n} \times 10^5$ (sec) Mod. ave.
					PBSQ in DME					
−40	1.29	22.0	0.262	0.317 (0.277)	1.71	1.71	12.78	8.95	0.632	0.697
−50	1.77	19.0	0.266	0.288 (0.259)	1.94	1.94	10.18	6.74	0.669	0.647
−60	2.48	16.5	0.259	0.277 (0.253)	2.18	2.18	8.00	5.09	0.668	0.650
−70	3.67	13.0	0.242	0.274 (0.255)	2.79	2.79	6.36	3.82	0.687	0.689
−80	6.06	8.5	0.206	0.222 (0.214)	3.78	3.78	4.83	2.63	0.668	0.603
					PBSQ in EtOH					
−10	0.962	15.0		0.453	3.27			12.1		1.00
−20	0.996	13.4	0.435	0.485 (0.461)	3.31	3.31	18.4	11.9	0.902	1.08
−30	1.40	9.4	0.481	0.529 (0.509)	4.06	4.06	15.4	9.2	1.10	1.25
−40	2.37	7.2	0.407	0.450 (0.428)	5.15	5.15	10.7	6.0	1.46	1.15
−50	3.35	5.2	0.362	0.391 (0.367)	6.55	6.55	8.3	4.7	1.55	1.06
−60	5.67	4.3		0.266				3.0		0.75
−70	6.77	3.2		0.236				2.66		0.67

[a] Comparison of the ENDOR relaxation obtained from the complete computer calculation (Comp.) with those obtained from an average theory calculation (Mod. ave.).
[b] The results in parenthesis include $(N/2)b''W_e$.
[c] These are the experimentally determined Ω_e's. In some cases they are used to calculate W_e, in other cases Ω_e is calculated from W_e.
[d] $\Omega_{e,n}$ values as determined from the slope of the PE^{-1} vs d_n^{-2} computer calculated results.

TABLE VIII. A comparison of the theoretical and experimental ENDOR relaxation parameters for DSQ in DME.[a]

Temp. (°C)	Conc. $\times 10^4$(m)	$T_n \times 10^5$ (sec)		$\langle J^2 \rangle \Omega_n \times 10^5$ (sec)		$\langle J^2 \rangle^{1/2} \Omega_{e,n} \times 10^5$ (sec)[b]	
−40	9.9	0.190	(0.163)	23.6	(66.3)	0.331	(0.577)
−50	9.9	0.199	(0.156)	21.7	(56.8)	0.551	(0.552)
−60	9.9	0.218	(0.189)	31.3	(48.9)	0.731	(0.674)
−40	6.3	0.198	(0.176)	28.6	(66.4)	0.544	(0.620)
−50	6.3	0.218	(0.180)	37.7	(57.2)	0.825	(0.637)
−60	6.3	0.248	(0.250)	39.6	(51.4)	1.09	(0.898)
−40	3.0	0.243	(0.261)	34.6	(67.7)	0.863	(0.932)
−50	3.0	0.256	(0.236)	33.5	(58.0)	0.934	(0.841)
−60	3.0	0.288	(0.328)	38.5	(51.1)	1.33	(1.20)

[a]The values in parentheses are theoretical results.
[b]Experimental values determined from the intercept of the PE^{-1} vs d_n^{-2} plot with the rf field calibrated via the coherence effect.

fied average method with the computer simulations suggests it could be useful for approximate analyses.

In summary, we note that the results and analysis of ENDOR relaxation parameters for PBSQ has shown that $T_{2,n}$ is the most accurately measured, as well as the one which tends to show the best agreement with predictions. In general, the errors associated with the percent enhancement measurements tend to be greater than those associated with the corresponding width measurements.

2. DSQ

A rigorous theoretical analysis of DSQ with 12 equivalent methyl protons in an enormous task, even for computer simulations. Even the modified averaging approach discussed for PBSQ would involve the average parameters for degenerate ESR transitions for the center hyperfine line, and 42 degenerate NMR transitions with the associated $\Omega_{i,j}$'s calculated from 49×49-fold reduced transition probability matrices (cf. Paper V). However, one may immediately write down the resulting expressions when the simple averaging approach of V is appropriate, as we have already done for the case of saturation, cf. Eq. (4.4) of that paper, for $\langle \Omega_e(0) \rangle$. Thus we have

$$\langle J_-^2 \rangle \langle \Omega_{e,n}^{s\,2} \rangle \approx n(W_e h)^{-2}[1 - 3nb/h] \cong n(W_e h)^{-2}(1 + 3nb/h)^{-1} , \tag{4.38}$$

$$\langle J_-^2 \rangle \langle \Omega_n^s \rangle \approx (bW_e)^{-1}(1 + nb/h) , \tag{4.39}$$

$$\langle T_{2,n}^{-1} \rangle \approx W_e h(1 + [2n + \tfrac{1}{3}]\, b/h) , \tag{4.40}$$

with

$$h = 1 + \omega_{HE}/2W_e \tag{4.41}$$

and

$$n = 12 .$$

Equation (4.38) as written in its last form has somewhat better convergence properties when the reqiurement for validity of these expressions,

$$3nb/h \ll 1 , \tag{4.42}$$

is not rigorously met. We have only been able to apply Eqs. (4.38)–(4.41) to some of our more concentrated samples, where (4.42) is reasonably fulfilled. We summarize in Table VIII these results. (Note that W_e is obtained from Figs. 23 and 24, while W_n is from the C terms in Figs. 10 and 11, and [with Eqs. (4.2c) and (4.3b) as well as a value of $\Gamma_{ab} = 0.82$], ω_{HE} is from Fig. 16). One finds generally reasonable agreement between the experiments and the simple theory, especially considering the limited validity of the latter and our uncertainty in estimating W_n (cf. Sec. IV. A).

It is, however, not unreasonable to employ the expression Eq. (4.40) for $T_{2,n}^{-1}$ even when the averaging theory

TABLE IX. DSQ in DME[a] experimental ENDOR relaxation parameters.

Temp. (°C)	Conc. $\times 10^4(M)$	$T_n \times 10^5$ $\times 10^5$ (sec)	$\bar{\Omega}_e \times 10^5$ (sec)[b]	$\langle J^2 \rangle \Omega_n$ $\times 10^5$ (sec)	$\langle J^2 \rangle \Omega_{e,n}$ $\times 10^5$ (sec)[c]	$\langle J^2 \rangle^{1/2} \Omega_{e,n}$ $\times 10^5$ (sec)[d]
−30	0.5	0.355 (0.686)	4.20	22.0	1.59	3.62
−40	0.5	0.408 (0.752)	4.91	34.73	2.40	4.06
−50	0.5	0.397 (0.803)	6.40	33.13	2.86	4.56
−60	0.5	0.387 (0.851)	8.03	32.75	3.16	4.78
−70	0.5	0.370 (1.22)	8.19	28.76	3.31	3.49

[a]rf field calibrated by coherence effect; to convert to probe results, divide Ω_n by 2.29 and $\Omega_{e,n}$ by 1.51. Results in parentheses calculated using Eq. (4.40).
[b]$\bar{\Omega}_e = \Omega_e + \{1 + [\Delta\omega_e T_{2,e}]^2\}/T_{2,e} d_e^2$.
[c]Determined from the intercept of the PE^{-1} vs d_n^{-2} plot.
[d]Determined from the slope of the PE^{-1} vs d_n^{-2} plot.

TABLE X. DSQ in EtOH experimental ENDOR relaxation parameters.[a]

Temp. (°C)	Conc. $\times 10^4$ (M)	$T_n \times 10^5$ (sec)	$\bar{\Omega}_e \times 10^5$ (sec)[b]	$\langle J^2 \rangle \Omega_n$ $\times 10^5$ (sec)	$\langle J^2 \rangle^{1/2} \Omega_{e,n}$ $\times 10^5$ (sec)[c]	$\langle J^2 \rangle^{1/2} \Omega_{e,n}$ $\times 10^5$ (sec)[d]
−20	2	0.446 (1.13)	7.85	50.90	3.76	4.20
−30	2	0.479 (1.01)	9.83	42.23	3.53	5.23
−40	2	0.559 (1.03)	11.39	44.37	4.45	5.12
−50	2	0.563 (0.959)	11.24	54.5	4.52	4.51
−60	2	0.588 (0.899)	11.05	47.02	4.68	3.89
−70	2	0.526 (0.442)	11.44	25.71	3.69	3.02

[a] rf field calibrated by coherence effect; to convert to probe results divide Ω_n by 2.29 and $\Omega_{e,n}$ by 1.51. Results in parentheses calculated using Eq. (4.40).
[b] $\bar{\Omega}_e = \Omega_e + \{1 + [\Delta\omega_e T_{2,e}]^2\}/T_{2,e} d_e^2$.
[c] Determined from the intercept of the PE^{-1} vs d_n^{-2} plot.
[d] Determined from the slope of the PE^{-1} vs d_n^{-2} plot.

does not apply. As we have already noted, it only neglects off-diagonal elements in the proper matrix for the inverse widths.[1] These results are given in Tables IX and X. One obtains rather good agreement between the experimental and estimated results, especially for EtOH solvent at the lower temperatures where the END terms (proportional to b) predominate. However, the predicted values of $T_{2,n}^{-1}$ at the higher temperatures are only about half the experimental values. It is most likely that the extra contribution is largely due to a combination of Heisenberg and chemical exchange. That is, we estimate that at −20 °C a $1\times10^{-4}M$ solution of DSQ anion (and residual DSQ) would exhibit about 4 mG of exchange broadening for the $M_I = 0$ ESR line. This nearly negligible ESR contribution is equivalent to a $T_{2,n}^{-1}$ contribution [from Eq. (4.27a)] of 0.6×10^5 sec^{-1}, or almost sufficient to explain the discrepancy.

It is, of course, instructive to compare the experimental results for the relaxation parameters for DSQ and PBSQ for the same solvent at the same temperature. Thus, we compare Tables IX and IV and Tables X and VI. The DSQ $T_{2,n}^{-1}$ values are consistently narrower, since DSQ has smaller values both for W_e and W_n.

The most striking differences in such a comparison are the values of $\langle J_-^2 \rangle \Omega_n$. Thus for DSQ in EtOH vs PBSQ in EtOH, the $\langle J_-^2 \rangle \Omega_n$ are 5–7 times greater, with only a slightly smaller difference in DME (neglecting the lowest temperature DME results which are uncertain, see above). This is most certainly due to the much smaller value of W_n (or b) for DSQ, which has already been demonstrated from the discussion of the linewidth parameter C, cf. Sec. IV. A. It is seen from Eq. (4.39) that the leading term for $\langle J_-^2 \rangle \langle \Omega_n^s \rangle$ goes as b^{-1}, for small b. [Even in the limit of large b, each NMR transition, n_j, would have a $\Omega_{n_j} \cong 2(W_e b)^{-1}$.][1] Thus, these large differences are of the correct order as expected from our earlier comparison of the parameter C that was calculated from the ESR terms. It is the larger values of the (experimentally measured) $\langle J_-^2 \rangle \langle \Omega_n^S \rangle$ for DSQ vs PBSQ that explain why it is much easier to saturate the ENDOR transitions for the former (cf. Fig. 26).

The quantity $\langle J_-^2 \rangle \Omega_{e,n}^2$ plays a dominant role in determining the ENDOR enhancements as may be seen from Eqs. (4.24)–(4.33). The significantly greater dependence of PE^{-1} on B_n^{-2} for PBSQ vs DSQ (cf. Fig. 26) is seen to arise because l of Eq. (4.28b) is proportional to $[\langle J^2 \rangle \Omega_{e,n}^2]$, and $\langle J_-^2 \rangle \Omega_{e,n}^2$ is consistently about an order of magnitude smaller for PBSQ. [At the same time, the quantity $\bar{\Omega}_e / T_{2,n}$ needed in (4.28b) is seen to be almost comparable for the two radicals.] It is again possible to "explain" this order of magnitude difference in terms of the simple expression of Eq. (4.38). The leading term for $\langle J_-^2 \rangle \langle \Omega_{e,n}^{s\,2} \rangle$ is given by n/W_e^2 (in the absence of exchange) and $n_{PBSQ}/n_{DSQ} = \frac{1}{3}$, while $(W_{e(DSQ)}/W_{e(PBSQ)})^2 \approx \frac{1}{4}$ (cf. Sec. IV. B).

It also follows from the above discussion and Eq. (4.28a) (as well as the fact that $\bar{\Omega}_{e(DSQ)}/\bar{\Omega}_{e(PBSQ)} \approx 1.5$ to 2) that the limiting values of E for large B_n^2 should be roughly comparable for both radicals at the same temperature and in the same solvent.

One may summarize these points by noting that to lowest order in b,

$$\tfrac{1}{2} E_{(\text{deriv})} = E \approx \frac{\delta_e}{\bar{\Omega}_e (d_{e,M}^{-1})} \approx \left(\frac{1}{2.33}\right) \frac{n(d_n^2/hW_e)^2}{1 + (d_n/hW_e)^2 hb^{-1}} \,. \tag{4.43}$$

Thus, for small d_n^2, one has E simply dependent on $n/(hW_e)^2$, while for large d_n^2 it goes as nb/h, and this is the characteristic behavior seen in our comparison of PBSQ and DSQ even though Eq. (4.43) is not strictly valid. That is, at normal rf powers (cf. Fig. 29), PE for DSQ is about 3 times larger than for PBSQ, while the values for both are comparable when extrapolated to infinite rf power (cf. Fig. 26).

3. 2, 5-DMPBSQ

The ENDOR studies on 2, 5-DMPBSQ in EtOH supply further information about the comparative differences in the ENDOR behavior of ring and methyl protons. In general, one finds that the results for the ring protons of 2, 5-DMPBSQ are similar to those for PBSQ in EtOH, while those for the methyl protons are similar to those for DSQ in EtOH. This is particularly evident in Fig. 29, showing typical ENDOR enhancements. (Note, however, the small values of the ring proton PE. This, along with the reduced statistical factor of the ESR line, resulted in a low S/N of the ENDOR line, rendering the measurement of enhancement somewhat uncertain in this case.)

TABLE XI. 2,5-DMPBSQ in EtOH experimental ENDOR relaxation parameters.

Type[a]	Temp.	$T_n\times10^5$[b] (sec)	$\bar{\Omega}_e\times10^5$ (sec)	$\langle J^2\rangle\Omega_n$ $\times10^5$ (sec)	$\langle J_2\rangle^{1/2}\,\Omega_{e,n}$[c] $\times10^5$ (sec)	$\langle J_2\rangle^{1/2}\,\Omega_{e,n}$[d] $\times10^5$ (sec)
R	−10	0.328 (1.00)	3.98	22.88 (43.7)	1.29 (1.49)	1.04
R	−20	0.334 (1.06)	4.06	18.55 (35.1)	1.19 (1.60)	1.24
R	−30	0.322 (1.13)	4.59	15.71 (19.5)	1.16 (1.79)	1.71
R	−40	0.381 (1.05)	5.03	18.06 (15.7)	1.50 (1.70)	1.61
R	−50	0.355 (1.12)	7.28	9.45 (16.0)	1.48 (1.81)	1.52
s.d. (*R*)		3%	6%	20%	14%	4%
M	−10	0.296 (1.02)	3.98	20.43 (263.7)	1.21 (1.54)	1.93
M	−20	0.312 (1.10)	4.06	21.01 (110.1)	1.41 (1.63)	2.27
M	−30	0.343 (1.26)	4.59	24.67 (202.5)	2.17 (1.97)	2.75
M	−40	0.370 (1.05)	5.03	22.69 (133.6)	2.47 (1.84)	2.91
M	−50	0.462 (1.25)	7.28	21.79 (109.3)	2.97 (1.83)	3.09
M	−60	0.498 (0.996)	8.76	19.47 (57.4)	2.86 •••	3.10
s.d. (*M*)		2%	6%	10%	7%	3%

[a] *R* = ring proton, *M* = methyl proton; results in parentheses calculated using Eqs. (4.44)–(4.46). s.d. = standard deviation.
[b] See Table IV, footnote c.
[c] See Table IV, footnote d.
[d] See Table IV, footnote e.

The experimental ENDOR relaxation parameters for 2, 5-DMPBSQ are given in Table XI. Note that at higher temperatures $T_{2,n}(R)\approx T_{2,n}(M)$ as the nuclear widths are dominated by W_e, but at the low temperatures $T_{2,n}(R) < T_{2,n}(M)$ as expected. Also, $T_{2,n}(R)$ is very close to the values for PBSQ. One is surprised by the rather large values of $\Omega_n(R)$ [almost as large as the $\Omega_n(M)$], but this result is seriously affected by the *S/N* problem already mentioned.

One may attempt to analyze these results in terms of a combined averaging of the ring protons [cf. Eqs. (4.33) and (4.34) for PBSQ] and simple averaging of the methyl protons [cf. Eqs. (4.38)–(4.42)] as was done for the saturation of analysis of 2, 5-DMPBSQ [cf. Eq. (4.6)]. One obtains for ENDOR of the ring protons:

$$\langle J_-^2\rangle\,\Omega_{e,n_R}^2 \cong \frac{2}{W_e^2}\left(\frac{1}{1+3b_R}\right)^2(1-6b_M)\,, \tag{4.44}$$

$$\langle J_-^2\rangle\,\Omega_{n_R} \cong \frac{1}{W_e\,b_R}\left(\frac{1+6b_R+6b_R^2}{1+4b_R+3b_R^2}\right), \tag{4.45}$$

$$\langle T_{2,n_R}^{-1}\rangle \cong W_e\left[1+\tfrac{13}{3}\,b_R+6b_M\right]; \tag{4.46}$$

while for the methyl protons one has

$$\langle J_-^2\rangle\,\Omega_{e,n_M}^2 \approx \frac{2}{W_e'^2}\left[1-18b_M\right], \tag{4.47}$$

$$\langle J_-^2\rangle\Omega_{n_M} \cong (W_e\,b_M)^{-1}\left[\frac{1}{2}\left(1+\frac{1+2b_R/6b_M+(b_R/6b_M)^2}{1+4b_R/6b_M+3(b_R/6b_M)^2}\right)\right]^{-1}, \tag{4.48}$$

$$\langle T_{2,n_M}^{-1}\rangle \cong W_e\left[1+12\tfrac{1}{3}\,b_M+2b_R\right], \tag{4.49}$$

where

$$W_e' = 2W_e\left(1+\frac{1+2b_R+b_R^2}{1+4b_R+3b_R^2}\right)^{-1}. \tag{4.50}$$

W_e' has been introduced in Eq. (4.47) to correct for the improved effectiveness of the $T_{1,e}$-type process due to b_R being reasonably substantial. It is an approximate form, justified in part by the expression for $\Omega_{e,n}$ of Eq. (A5) of Paper V. Equation (4.48) follows from simple considerations of the manner in which the W_{n_R} can enhance the relaxation of the methyl proton spins by providing alternate relaxation paths.[28b]

The over-all agreement between the experimental and theoretical results of Table XI is rather poor and this discrepancy is most likely attributed to (i) low values of the input parameters W_e and W_n and (ii) neglect of exchange contributions. Using Eqs. (4.44)–(4.46) and changing the input parameters by increasing W_e (cf. discussion of PBSQ) as well as assuming a small exchange contribution (cf. discussion of DSQ) would improve the agreement of the T_n's dramatically. In addition, the complexity of the ESR linewidth expression, Eq. (4.5), and the relatively small magnitude of the terms involving $j_{MM}^D(0)$ and $j_{RR}^D(0)$ has resulted in values of W_n which are much smaller than those of DSQ and PBSQ. An increase in the values of W_n for 2, 5-DMSQ would significantly improve the agreement between the experimental and theoretical Ω_n's.

4. *Heisenberg exchange-ENDOR*

The ENDOR experiments on PBSQ, DSQ, and 2, 5-DMPBSQ described in the preceding paragraphs of this section for dilute radical solutions were repeated for concentrated solutions in which exchange was playing a prominent role in the relaxation.

We show in Fig. 30 results for the limiting enhancement PE (i.e., extrapolated to $d_n^2\to\infty$) for the stable and well-behaved system of DSQ in DME. These results clearly demonstrate the general prediction of the ENDOR theory (cf. Papers II–V) that exchange acts to reduce ENDOR enhancements [cf. Eq. (4.28a) and Eqs. (4.38)–(4.41) or Eq. (4.43) for the effects of exchange when the average ENDOR theory applies]. Thus, either increasing the radical concentration or increasing T/η

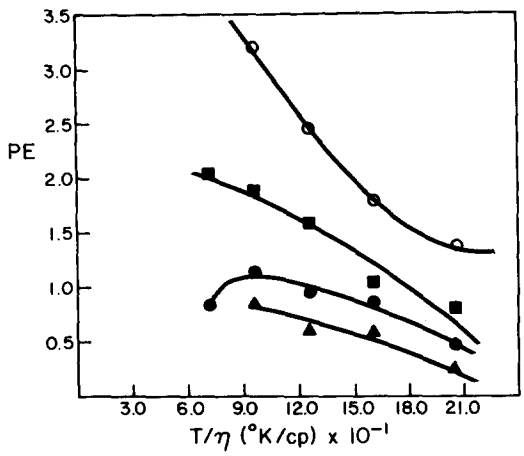

FIG. 30. The percent enhancement at infinite rf power as a function of T/η for solutions of DME. ▲ = Concentration of $9.9\times10^{-4}M$; • = concentration of $6.3\times10^{-4}M$; ■ = concentration of $3.0\times10^{-4}M$; ○ = concentration of $1.5\times10^{-4}M$.

[cf. Eqs. (4.15) and (5.17)] decreases E.

As we have already noted, the ENDOR relaxation parameter $T_{2,n}$ is the most convenient both to obtain experimentally and to predict theoretically. And in the case of the dilute solutions, $T_{2,n}$ showed reasonably good agreement between the experimental and predicted values. One may attempt then to use Eq. (4.37b) to interpret the differences $[T_{2,n}^{-1}(\text{conc.}) - T_{2,n}^{-1}(\text{zero conc.})]$ as the exchange contribution to the ENDOR widths. We have checked the validity of this simple approach by comparing this difference from our computer simulations with the actual value of $\omega_{HE}/2$ used. The agreement was generally good ranging from deviations ~1%–2% for small b ($b<0.1$ where average ENDOR formulas are more applicable), to as much as ~10% for large b ($b>0.2$). The value obtained by the simple subtraction method is consistently slightly greater than the true value and some adjustment is made for this in the results shown below. We show in Figs. 31 and 32 the exchange contributions to the ENDOR linewidth as obtained by this subtraction method, respectively, for PBSQ and DSQ in DME. One notices the linear dependences of the ENDOR width contributions with T/η. These exchange results, utilizing Eq. (4.37a), may then be compared to the results summarized in Figs. 16 and 17 for the exchange contribution to the ESR widths, which also show the expected T/η dependence. It emerges from such a comparison that, although ω_{HE} determined both by ESR and ENDOR widths show the proper T/η and $\mathfrak{N}$ dependences, the values of ω_{HE} from the ESR widths are typically larger by factors of 1.52 ± 0.17 for PBSQ in DME and 1.58 ± 0.39 for DSQ in DME. We have no obvious explanation for this discrepancy, but we wish to point out some experimental problems which could have influenced this comparison.

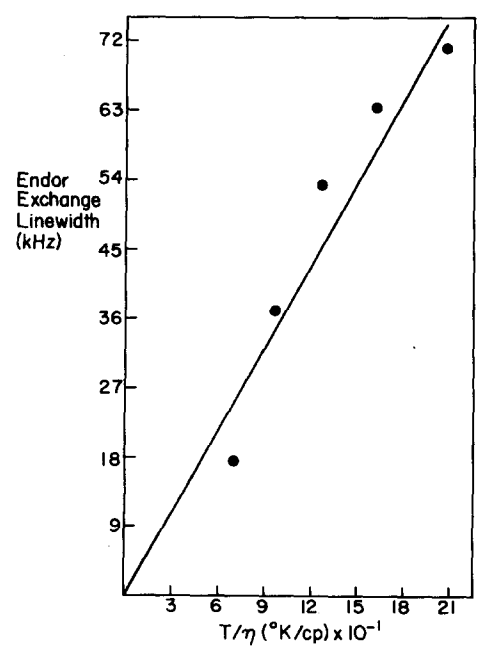

FIG. 31. The exchange contribution to the ENDOR linewidth as a function of T/η for a $1.2\times10^{-3}M$ solution of PBSQ in DME.

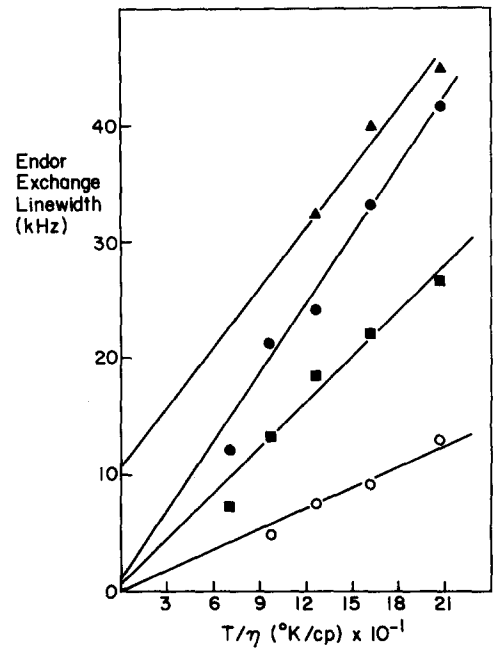

FIG. 32. The exchange contribution to the ENDOR linewidth as a function of T/η for solutions of DSQ in DME. ▲ = $9.9\times10^{-4}M$; • = $6.3\times10^{-4}M$; ■ = $3.0\times10^{-4}M$; ○ = $1.5\times10^{-4}M$.

(1) The large effects of exchange on E [cf. Fig. 30 and Eq. (4.43)] made it necessary to carry out the ENDOR studies under conditions such that the ESR exchange broadening was no greater than 1/3 the dilute solution $T_{2,e}^{-1}$. However, the ENDOR widths are unaffected by (i) the large g-tensor contributions and (ii) the (presumably related) extra broadening due to the supporting electrolyte (TBAP), so the exchange contribution represents a more significant component of the $T_{2,n}^{-1}$ than the $T_{2,e}^{-1}$.

(2) The difficulties caused by the effects of TBAP on the ESR linewidths below −50 °C may well have caused inaccuracies in the values of ω_{HE} obtained from $T_{2,e}^{-1}$,

TABLE XII. Concentrated solutions of PBSQ in DME experimental ENDOR relaxation parameters.[a]

Temp. (°C)	$T_n \times 10^5$ (sec)		$\bar{\Omega}_e \times 10^5$ (sec)[b]	$\langle J^2 \rangle \Omega_n \times 10^5$ (sec)[c]			$\langle J^2 \rangle^{1/2} \Omega_{e,n} \times 10^5$ (sec)[c]		$\langle J^2 \rangle^{1/2} \Omega_{e,n} \times 10^5$ (sec)[d]	
−40	0.110	(0.089)	1.104	27.0	61.72	(9.19)	0.288	(0.228)	0.229	(0.226)
−50	0.119	(0.103)	1.282	13.7	31.44	(7.99)	0.266	(0.282)	0.272	(0.274)
−60	0.133	(0.118)	1.761	7.34	16.74	(8.43)	0.330	(0.372)	0.405	(0.350)
−70	0.156	(0.128)	2.233	8.44	19.21	(7.12)	0.448	(0.440)	0.480	(0.406)
−80	0.182	(0.136)	3.360	7.27	16.47	(7.26)	0.676	(0.458)	0.530	(0.470)

[a]See Table IV, except concentration is $1.2 \times 10^{-3} M$. Also, values in parentheses are theoretical predictions.
[b]See Table IV, footnote c.
[c]See Table IV, footnote d.
[d]See Table IV, footnote e.

but they did not appreciably affect the $T_{2,n}^{-1}$, as already noted. In particular, in those cases where ω_{HE} was estimated from extrapolating the ESR results for large T/η (cf. Sec. IV. A), we may well have been overestimating the ESR values of ω_{HE} if, as we have suggested, the effect of the increased TBAP concentration is to increase the effective $\mathfrak{N}$.

It is for these two reasons that the values of ω_{HE} obtained from the ENDOR may well be the more accurate. However, we do not feel they are sufficient reasons for adequately accounting for the observed systematic discrepancies.

The situation for PBSQ in EtOH is, however, quite different. The ω_{HE} obtained from $T_{2,e}^{-1}$ were found to be linear in η/T (cf. Fig. 18), but the results from $T_{2,n}^{-1}$ show instead a weak decrease with decreasing temperature, or a trend in the ipposite direction! These results are discussed below in terms of the combined effects of exchange and intermolecular electron spin–electron spin dipolar interactions.

The experimental ENDOR relaxation parameters for the concentrated solutions are summarized in Tables XII–XIV. Also shown in Table XII and XIII for the solutions of PBSQ in DME and EtOH are the results from the computer simulations based on the data of Fig. 20. The generally small predicted values for $T_{2,n}$ in Table XII and the discrepancies between prediction and experiment for $T_{2,n}$ in Table XIII have already been discussed. Despite the small discrepancy in estimating ω_{HE} for PBSQ in DME, the agreement between experiment and prediction for $\Omega_{e,n}$ is quite reasonable. There is somewhat poorer agreement in Table XIII for $\Omega_{e,n}$, and this may be due to the greater uncertainties in the concentration-dependent relaxation mechanisms. The experimentally measured $\Omega_n \langle J_-^2 \rangle$ for PBSQ in DME (Table XII) are surprisingly large, larger in fact than the results for dilute solutions (cf. Table IV). We have already noted the considerable difficulties in measuring Ω_n for PBSQ samples. There is increased difficulty for the more concentrated samples because (1) PE is reduced so the S/N is worse; (2) the ENDOR widths are significantly greater, tending to mask any saturating effects of the rf field; and most important (3) the rf saturation parameters $\langle J^2 \rangle d_n^2 T_{2,n}^{-1} \Omega_n$ are themselves reduced because $T_{2,n}^{-1}$ is increased, so that only marginal changes in $\Delta_{1/2,1/2}$ width d_n^2 could be achieved. For these reasons, we believe the Ω_n results in Table XII are the most questionable.

The results in Table XIV for different concentrations of solutions of DSQ in DME have not been compared with theory. These data are presented to show the trends of various experimental ENDOR parameters as a function of both temperature and concentration. A comparison

TABLE XIII. Concentrated solutions of PBSQ in EtOH experimental ENDOR relaxation parameters.[a]

Temp. (°C)	Conc. $\times 10^4 (M)$	$T_n \times 10^5$ (sec)		$\bar{\Omega}_n \times 10^5$ (sec)[b]	$\langle J^2 \rangle \Omega_n \times 10^5$ (sec)		$\langle J^2 \rangle^{1/2} \Omega_{e,n} \times 10^5$ (sec)[c]		$\langle J^2 \rangle^{1/2} \Omega_{e,n} \times 10^5$ (sec)[d]	
−20	12.0	0.258	(0.368)	2.218	6.63	(17.7)	0.801	(0.892)	0.808	(1.55)
−30	12.0	0.276	(0.366)	3.160	4.87	(17.6)	0.622	(0.864)	0.929	(1.55)
−40	20.0	0.272	(0.254)	4.207	6.66	(9.10)	0.555	(0.656)	1.25	(1.86)
−50	20.0	0.280	(0.216)	5.075	5.19	(7.12)	0.620	(0.568)	1.19	(1.98)
−10	18.0	0.214	•••	1.730	5.70	•••	0.272	•••	0.595	•••
−20	28.0	0.244	(0.308)	2.152	7.17	(21.1)	0.417	(0.778)	0.688	(0.686)
−30	27.0	0.222	(0.250)	2.694	6.94	(20.9)	0.396	(0.612)	0.791	(0.564)
−40	39.0	0.222	(0.182)	3.356	6.37	(6.49)	0.328	(0.440)	0.697	(0.416)
−50	41.0	0.226	(0.147)	4.354	8.27	(8.22)	0.460	(0.488)	0.701	(0.304)

[a]The standard deviations are T_n (3%), $\bar{\Omega}_e$ (8%), Ω_n (75%), $\Omega_{e,n}$[c] (43%), $\Omega_{e,n}$[d] (7%). Also, the values in parentheses are theoretical predictions.
[b]See Table IV, footnote c.
[c]See Table IV, footnote d.
[d]See Table IV, footnote e.

TABLE XIV. DSQ in DME experimental ENDOR relaxation parameters.[a]

Temp. (°C)	Conc. $\times 10^4(M)$	$T_n \times 10^5$ (sec)	$\bar{\Omega}_e \times 10^5$ (sec)[b]	$\langle J^2\rangle \Omega_n$ $\times 10^5$(sec)	$\langle J^2\rangle^{1/2}\Omega_{e,n}$ $\times 10^5$(sec)[c]	$\langle J^2\rangle^{1/2}\Omega_{e,n}$ $\times 10^5$(sec)[d]
−40	1.5	0.307	1.960	19.23	0.722	1.37
−40	3.0	0.243	1.830	34.61	0.720	1.06
−40	6.3	0.198	1.185	28.56	0.403	0.603
−40	9.9	0.190	0.978	23.64	0.244	0.445
−50	1.5	0.322	2.318	32.03	1.152	1.151
−50	3.0	0.256	1.541	33.47	0.716	1.03
−50	6.3	0.218	1.429	37.73	0.625	0.741
−50	9.9	0.199	0.978	21.67	0.352	0.428
−60	1.5	0.327	2.965	23.71	1.33	1.96
−60	3.0	0.288	1.764	34.86	0.978	1.10
−60	6.3	0.248	1.739	39.61	0.823	0.787
−60	9.9	0.218	1.735	31.31	0.569	0.649
−70	1.5	0.333	3.863	23.64	1.71	2.14
−70	3.0	0.283	2.998	28.17	1.26	1.40
−70	6.3	0.243	2.063	32.93	0.869	0.848
−70	9.9	0.173	2.810	32.92	0.895	0.874
−80	3.0	0.306	3.501	29.30	1.45	1.222
−80	6.3	0.283	2.996	47.50	1.09	1.08
s.d.		3.5%	9%	18%	8%	8%

[a]The standard deviations given above are for the more concentrated solutions; those for the dilute solutions are reduced by approximately a factor of 2.
[b]See Table IV, footnote c.
[c]See Table IV, footnote d.
[d]See Table IV, footnote e.

of the experimental and theoretical ENDOR relaxation parameters for DSQ in DME may be found in Table VIII, and the reasonable agreement shown here lends credence to the experimental trends indicated in Table XIV.

V. FURTHER ANALYSIS AND DISCUSSION

A. Rotational diffusion and ESR results

It is of some interest to analyze the values of τ_R obtained from the linewidth analyses of Sec. IV. If one employs the Stokes–Einstein relation of Eq. (4.8′) (and if we let $\kappa^{1/3}a \to a$, a microscopic radius including κ), then the results for the different radicals and solvents appear in Table XV. We also include mean radii estimated from molecular dimensions and van der Waals radii. In each solvent, the trends are as expected. That is $a_{\text{PBSQ}} < a_{2,5\text{-DMSQ}} < a_{\text{DSQ}}$. The experimental effective radii are found to be larger than those estimated from molecular dimensions. This most likely reflects solvation and counterion effects on the radical anions. We have already seen, from the Heisenberg spin-exchange studies, that PBSQ and DSQ are most likely strongly interacting with their respective TBAP counterions, while PBSQ in EtOH is most likely dissociated. The substantially larger values of a for DME solvent given in Table XV are fully consistent with this picture.

We have also seen that the values of W_e obtained from saturation studies are all linear T/η (cf. Figs. 23 and 24), as predicted for a Stokes–Einstein model by Eqs. (4.8) and (4.8′). It follows from (4.8) that

$$W_e^{SR} \cong \sum_i (g_i - g_e)^2/18\tau_R \,, \tag{5.1}$$

while for the g-tensor contribution, when $\omega_e^2\tau_R^2 \gg 1$,

$$W_e^G \cong \sum_i (g_i - g_s)^2/40\tau_R \,; \tag{5.2}$$

then for the g values of Eq. (4.10), one obtains

$$W_e^T \equiv W_e^{SR} + W_e^G \cong 1.906\times 10^{-6}/\tau_R \tag{5.3}$$

with τ_R in seconds. One may use Eq. (5.3) with the values of τ_R from Figs. 7–12 to estimate W_e^T and compare with the values in Figs. 23 and 24. When this is done, it is found that the estimated W_e^T are systematically about 12 times *smaller* than the experimental results for the three radicals in EtOH solvent and about 25 times *smaller* in DME solvent. (There is some deviation at the lower T/η values because the intercepts in Figs. 23 and 24 are not zero in most cases; see below.) In other words, the relation

$$\tau_R \tau_J = I/6KT \,, \tag{5.4}$$

where τ_J is the spin–rotational relaxation time, which follows from Brownian motion theory[29] upon which Eq.

TABLE XV. Effective rotational radii of radical anion solutes.[a]

	Solvent		
	EtOH	DME	Calculated average[b]
PBSQ	3.80±0.16	5.36±0.22	3.13
2,5-DMSQ	4.51±0.09	• • •	3.53
DSQ	4.91±0.07	7.10±0.07	3.89

[a]The experimental results are from Eq. (4.8b) (with $\kappa = 1$) and the values of τ_R given in Figs. 7–12. Values are in Å.
[b]Based on the oxygen to oxygen distance of 4.16 Å, the half-thickness of the *pi* bonds of 1.7 Å (or the radius of a methyl group of 2.0 Å) and third dimension of 3.52 Å for PBSQ, 4.58 for 2,5-DMSQ, and 5.51 for DSQ.

TABLE XVI. Heisenberg exchange frequencies for a $4.27 \times 10^{-3}M$ solution of PBSQ in EtOH.

Temp. (°C)	η/T (cp/°K)$\times 10^2$	ω_{HE}(expt.) (sec^{-1})$\times 10^{-5}$	ω_{HE}(DME)[a] (sec^{-1})$\times 10^{-5}$	ω_{HE}(ENDOR)[b] (sec^{-1})$\times 10^{-5}$
−20	1.15	3.41	13.75	3.20
−30	1.45	4.15	10.71	3.48
−40	2.05	5.37	7.43	3.48
−50	2.93	7.80	5.43	3.14
−60	4.13	10.97	3.85	
−70	6.23	16.58	2.55	

[a]Determined by multiplying ω_{HE} at 15 °C for PBSQ in DME by $[(\eta/T)$ DME$/(\eta/T$ EtOH$]$ at 15 °C.

[b]Concentration for this data not $4.27\times 10^{-3}M$, but rather $2.8 \times 10^{-3}M$ at $T=-20°$, $2.7\times 10^{-3}M$ at $T=-30°$, $3.8\times 10^{-3}M$ at $T=-40°$, and $4.1\times 10^{-3}M$ at $T=-50°$.

(4.8) is based, is not an adequate description even though it gives the correct linear dependence upon T/η. The values of τ_J are significantly longer than predicted by Eq. (5.4).

One way to rationalize such results is to recognize that for small molecules in liquids, a Brownian model of reorientation by infinitesimal jumps need not be satisfactory. Thus, in recent ESR experiments in the slow tumbling region, it was found that comparable size molecules may be better described as engaging in jumps of moderate angle (~1 rad). In these cases, one must rewrite Eq. (4.8′) as

$$\tau_R = (6B_2R)^{-1}\,, \tag{5.5}$$

where $B_2 \leq 1$ is a "model parameter" discussed extensively by Goldman *et al.*[30] (for Brownian motion $B_2 = 1$). One may then relate, by a simple analysis, the Brown *et al.*[31] model for spin–rotational relaxation to Eq. (5.5) to obtain

$$\tau_R \tau_J = I/6kTB_2\,. \tag{5.6}$$

Our experimental results would then be consistent with $B_2 \lesssim 0.1$. An examination of typical jump models indicates that this value is near the lower limit one may expect, i.e., for jumps with a random distribution [i.e., $W(\epsilon) = 1/\pi$, where $W(\epsilon)$ is the probability of jump by angle ϵ], then $B_2 = 12/5\pi^2 = 0.243$, while for a large jump model [e.g., $W(\epsilon) \cong \delta(\epsilon - \pi)$] one gets $B_2 \cong 4/5\pi^2$. Thus, it is not unreasonable to suppose that the explanation may lie in terms of such jump models, but further analysis of this matter [including a more rigorous value for W_e^T than Eq. (5.3)] would be called for.[32]

The nonzero intercepts of W_e vs T/η in Figs. 23 and 24 appear to be a common phenomenon, and may result from intramolecular contributions to spin–rotational relaxation.[32]

B. Weak Heisenberg exchange and intermolecular dipolar interactions

We have already noted that concentrated PBSQ solutions in EtOH appear to exhibit weak Heisenberg exchange. There are, however, two difficulties which arise in a detailed effort to explain the ESR and ENDOR results in such terms.

(1) The values of ω_{HE} obtained for $T \lesssim -50$ °C become *greater* than those estimated for strong exchange, i.e., the diffusion controlled limit. These were estimated by taking the results for PBSQ in DME (cf. Sec. IV. A) and correcting for the different η/T values in the two solvents. These results are summarized in Table XVI.

(2) While the ω_{HE} values obtained by ESR (cf. Sec. IV. A) vary significantly with temperature, those obtained from the ENDOR widths do not, cf. Table XVI. The values of ω_{HE} as determined from ESR and ENDOR results for DSQ and PBSQ in DME, while not agreeing exactly in magnitude, show the same temperature dependence.

We now wish to show that a possible explanation for these inconsistencies is that both exchange as well as intermolecular electron–electron dipolar interactions are important.

The role of intermolecular electron–electron dipolar (EED) interactions for free radicals in liquids has been radicals in liquids has been discussed by Eastman *et al.*[33] When the ESR spectrum consists of unoverlapped lines so that it is possible to speak of an interaction between two radicals with differing nuclear configurations as an interaction between two unlike spins, while those between radicals with the same nuclear configuration are considered to be between like spins, then one obtains, from the results summarized by Abragam,[34,6]

$$[T_2(M)]_1^{-1} = [\hbar^2\gamma^4 S(S+1)2/N]\left\{(\tfrac{1}{2}N - D_M)\tfrac{1}{6}J^0(0) + \frac{1}{24}\sum_{M\neq M'} D_{M'}J^{(0)}[a(M-M')]\right\}\,, \tag{5.7}$$

$$[T_2(M)]_2^{-1} = \hbar^2\gamma^4 S(S+1)(2D_M/N)\tfrac{3}{8}J^{(0)}(0)\,, \tag{5.8}$$

where $[T_2(M)]_1^{-1}$ and $[T_2(M)]_2^{-1}$ are the width contributions for interactions between like and unlike nuclei, respectively. We have, in Eqs. (5.7) and (5.8), neglected nonsecular contributions.[6]

When, as is often the case,

$$J^{(0)}[a(M-M')] \sim J(0)(0) \tag{5.9}$$

(i.e., hyperfine frequencies are small compared to inverse correlation times), then one has, from Eqs. (5.7) and (5.8),

$$[T_{2,e}(M)]_{\text{EED}}^{-1} = \hbar^2\gamma^4 S(S+1)\tfrac{1}{24}J^{(0)}[5 + 8D_M/N]\,. \tag{5.10}$$

For a Stokes–Einstein model,

$$J(0) = 32\pi^2\mathfrak{N}\eta/25kT\,, \tag{5.11}$$

and the appropriate correlation time τ for the relative translational diffusion is just $\tau = 3\tau_1$.

The resulting Eqs. (5.7)–(5.10) could have been obtained from a relaxation-matrix approach.[20] The dipolar contribution to $T_{2,n}$ can also readily be obtained from a relaxation-matrix approach. One quickly finds from such an analysis that (when nonsecular terms are negligible)

(1) Only the pseudosecular terms are appropriate (i.e., the $S_{1\pm}S_{2\mp}$ terms), and

(2) No distinction need be made between like and un-

like nuclei.

In both those respects, there is a simple analogy with the exchange contributions to $T_{2,e}^{-1}$ and $T_{2,n}^{-1}$. One then obtains, when Eq. (5.9) is appropriate,

$$[T_{2,n}]_{EED}^{-1} = \tfrac{1}{24} J^{(0)}(0) . \tag{5.12}$$

Thus, for PBSQ,

$$[T_{2,n}]_{EED}^{-1} = \tfrac{2}{13} [T_{2,e}]_{EED}^{-1} . \tag{5.13}$$

It is then possible to write the concentration-dependent (CD) portion of the linewidth as

$$[T_{2,i}]_{CD}^{-1} = [T_{2,i}]_{HE}^{-1} + [T_{2,i}]_{EED}^{-1} \tag{5.14}$$

where $i = e$ or n. One obtains for PBSQ that

$$\omega_{HE} = 2.476 [T_{2,n}]_{CD}^{-1} - 0.38 [T_{2,e}]_{EED}^{-1} \tag{5.15a}$$

and

$$[T_{2,e}]_{EED}^{-1} = ([T_{2,e}]_{CD}^{-1} - \tfrac{5}{4}[T_{2,n}]_{CD}^{-1})/0.808 . \tag{5.15b}$$

It is clear from Eq. (5.13) that the intermolecular dipolar contributions are significantly more important for the ESR widths as compared to the ENDOR widths, and it follows from Eqs. (5.15a) and (5.15b) that when $[T_{2,n}]_{CD}^{-1}$ and $[T_{2,e}]_{CD}^{-1}$ are of comparable order (as is true in this work), that ω_{HE} is mainly determined by $[T_{2,n}]_{CD}^{-1}$, while $[T_{2,e}]_{EED}^{-1}$ may be somewhat uncertain as the small difference between two large numbers (as well as from the apparent discrepancy in the analysis of $[T_{2,i}]_{CD}^{-1}$ $(i = e, n)$ found in the cases of strong exchange).

We give in Table XVII the values of ω_{HE} and $T_{2,e}^{-1}$ (EED) obtained with Eqs. (5.15). It is clear that ω_{HE} is still small compared to the values estimated in Table XVI for simple exchange. Also the values of $[T_{2,e}]_{EED}^{-1}$ are significantly smaller than the theoretical results predicted from Eqs. (5.10) and (5.11) and given in Table XVII.

TABLE XVII. Dipolar and Heisenberg exchange contributions to ENDOR and ESR linewidths.

Temp. (°C)	Conc. $(M)\times 10^4$	T_n^{-1}(ENDOR)[a] $(sec^{-1}\times 10^{-5})$	T_2^{-1}(ESR)[a] $(sec^{-1})\times 10^{-5}$	ω_{HE}[b] $(sec^{-1})\times 10^{-5}$
−20	2.0	2.85	2.83	5.98
−30	2.7	2.86	3.01	5.93
−40	3.8	2.02	3.79	3.56
−50	4.1	1.63	4.97	2.14
Temp. (°C)	Conc. $(M)\times 10^4$	T_2^{-1}(EED)[b] $(sec^{-1})\times 10^{-5}$	ω_{HE}(DME)[c] $(sec^{-1})\times 10^{-5}$	ω_{HE}(DME)$\times f^*$[c] $(sec^{-1}\times 10^{-5}$
−20	2.8	~0	13.75	2.72
−30	2.7	~0	10.71	2.23
−40	3.8	1.27	7.43	1.61
−50	4.1	2.93	5.43	1.23
Temp. (°C)	Conc. $(M)\times 10^4$	T_2^{-1}(EED)[d] $(sec^{-1})\times 10^{-5}$	T_2^{-1}(EED)$\times r$[d] $(sec^{-1})\times 10^{-5}$	
−20	2.8	3.8	1.07	
−30	2.7	4.63	1.33	
−40	3.8	9.2	2.70	
−50	4.1	14.2	4.26	

[a]Concentration dependent component adjusted to a common concentration of $4.3\times 10^{-3} M$.
[b]Calculated from Eq. (5.15). The uncertainty in the value is $\pm 1\times 10^{-5}$ sec^{-1}.
[c]Determined by multiplying ω_{HE} at 15 °C for PBSQ in DME by $|(\eta/T)\text{DME}/(\eta/T)\text{ETOH}|$ at 15 °C.
[d]Calculated from Eqs. (5.10) and (5.11).

The most sensible explanation for this behavior of PBSQ in EtOH is in terms of charge effects. This is borne out by the lack of counterion effects in the ESR spectra of K^+PBSQ^- in EtOH as compared to the spectra of soultions of K^+PBSQ^- in DME, indicating that $PBSQ^-$ probably exists in EtOH as a dissociated singly charged anion. We must thus modify Eqs. (4.15) and (4.16) in the manner of Eastman, Bruno, and Freed[33] following Debye's theory for the reaction rates of charged particles in ionic solutions. Thus,[25a]

$$k = 4\pi d D f^* , \tag{5.16}$$

$$\tau_1^{-1} = (6D/d^2) r , \tag{5.17}$$

where

$$(df^*)^{-1} = \int_d^\infty \exp[U(r')\,kT]\, dr'/r'^2 , \tag{5.18}$$

$$r^{-1} = f^* \exp[U(d)/kT] \tag{5.19}$$

and

$$U(r') = [\exp(\xi d)/(1+\xi d)]\,(Z^2 e^2/\mathcal{S} r')\exp(-\xi r') , \tag{5.20}$$

where

$$\xi^2 = (4\pi e^2/\mathcal{S} kT)\sum_i N_i Z_i^2 . \tag{5.21}$$

Here $\mathcal{S}$ is the dielectric constant of the medium, Z the charge on the radicals, and e the electron charge. Also, N_i is the number density of particles of type i and charge Z_i. The parameter ξ is known as the reciprocal thickness of the ionic layer. One has $f^* < 1$. Values of f^* and r have been obtained by numerical integration for the ionic solutions in this work.

It is also necessary to modify Eq. (5.11) to account for charge effects. Rather than attempt a rigorous analysis of this, we note that Eq. (5.11), first calculated by Torrey,[35] may also be obtained in slightly modified form from a model of turning on and off an r^{-3} perturbation due to jump diffusion, as also shown by Torrey. Thus, the lifetime τ_1 is relevant here. We have already noted that τ, the translational diffusion correlation time neglecting charge, obeys $\tau = 3\tau_1$. Therefore, we modify Eq. (5.11) to

$$J(0) \cong 32\pi^2 \mathfrak{N}\eta r/25kT . \tag{5.22}$$

We give in Table XVII the predicted values of ω_{HE} and $[T_{2,e}]^{-1}$ EED corrected for charge effects according to Eqs. (5.16) and (5.19) [and (5.22)], respectively. (The values of f^* and r were calculated to range from 0.20–0.23 and 0.28–0.30, respectively.) These predictions corrected for charge effects are seen to overcorrect the values of ω_{HE} compared to experimental estimates, and the values of $[T_{2,e}]^{-1}$ EED are nearer the respective experimental estimates. Over all, the agreement appears improved. These estimates emphasize the general fact that at sufficiently large values of $\mathfrak{N}/kT$ the EED contribution can become comparable to the exchange contribution [cf. Eq. (C9) of Ref. 9]. Owing to the considerable uncertainties in the experimental values and the aspects of the analysis already noted, it was not deemed useful to attempt any more detailed an analysis

TABLE XVIII. Heisenberg exchange parameters calculated from experimental results and charge effect calculations.

Temp. (°C)	ω_{HE}(est.) (sec$\times 10^{-5}$)	$(J^{-1}\tau_1^2)_{int}$ [a]	$J\tau_1$	(τ_2^{-1}) [b] (sec$\times 10^{-5}$)	ω_{HE}(calc)[c] (sec$\times 10^{-5}$)	$(J^{-2}\tau_1^2)$ [d] (slope)	ω_{HE}(calc)[e] (sec$\times 10^{-5}$)
−20	3.36 f	0.345	1.71	8.31	6.18	0.278	6.50
−30	3.42	0.407	1.57	6.80	4.84	0.387	4.90
−40	3.24	0.440	1.51	5.04	3.50	0.502	3.36
−50	2.64	0.600	1.29	3.73	2.33	0.552	2.40

Temp. (°C)	$(J\tau_1\gamma)$ [g]	ω_{HE}(theoret)[h] (sec$\times 10^{-5}$)	$(J\tau_1\gamma)^2$ [i]	ω_{HE}(theoret)[j] (sec$\times 10^{-5}$	T_2^{-1}(EED-exptl) (sec$^{-1}\times 10^{-5}$)	T_2^{-1}(EED-theoret) (sec$^{-1}\times 10^{-5} f^*\gamma$)	T_2^{-1}(EED-theoret) (sec$^{-1}\times 10^{-5} f^*$)
−20	1.56	5.06	1.53	5.03	0	0.059	0.75
−30	1.76	4.34	1.79	4.36	0.12	0.079	0.96
−40	2.64	3.66	2.74	3.69	1.48	0.172	2.00
−50	17.98	3.53	16.29	3.51	3.28	0.29	3.21

[a] Determined from the relationship $J^{-2}T_1^{-2} = |(\omega_{HE} - \bar{\omega}_{HE})/(\omega_{HE} + \bar{\omega}_{HE})|$ with ω_{HE} equal to the intercept of the ω_{HE} vs T/η plot.
[b] Calculated from the equation (5.16) $(k = \tau_2^{-1})$.
[c] Obtained from the relationship $\omega_{HE} = \tau_2^{-1}(1.0 + J^{-2}\tau^{-2})^{-1}$ utilizing values of τ_2^{-1} and $(J^{-2}\tau^{-2})$ intercept in this table.
[d] Determined from the equation in a with $\omega_{HE} = (T/\eta)d\omega_{HE}/d(T/\eta)$.
[e] Calculated from the equation in c with values of τ_2^{-1} and $(J^{-2}\tau^{-2})_{slope}$ in this table.
[f] The value of ω_{HE}(est) for this temperature was not included in the ω_{HE} vs T/η least squares analysis (see text).
[g] Determined from the relationship $(J\tau_1\gamma)^2 = (y-y)/(y+y)$ with $y-y$ equal to the intercept of the $\omega_{HE}/f^*\gamma$ vs η/T plot.
[h] Calculated from Eq. (5.17) using values of τ_2^{-1} from b above and $(J\tau_1\gamma)^2$ intercept from this table.
[i] Determined from the relationship in $y = (\eta/\mathrm{Tr}(d\omega_{HE}/(d(\eta\gamma/T))$.
[j] Calculated from Eq. (5.16) using values of τ_2^{-1} from above and $J\tau_1\gamma_{slope}$ in this table.

(e.g., whether the exchange was weak in the sense that $J^2\tau_1^2 \lesssim 1$). Nevertheless, the potential value of ENDOR linewidths (in conjunction with ESR linewidths) as a means to distinguish between the two types of intermolecular relaxation processes should be clear.

C. Methyl groups and internal rotation

There is some question as to the relaxation behavior of the rotating methyl groups. We have in Sec. IV. C analyzed the methyl group ENDOR results in terms of the averaging theory and have found that the observed relative enhancements of methyl and ring protons are fully consistent with an END mechanism being dominant. For the range of experiments studied here, we have $\omega_e^2 T_R^2 \gg 1$, so the pseudosecular terms of the END mechanism which yield the W_n are dominant relative to the cross relaxation W_x type terms. However, a rotating methyl group causes modulation of the isotropic hyperfine interaction $a(t)$, and this can lead to relaxation effects. Such relaxation effects have been treated classically[21] as well as quantum mechanically,[36] and it was shown in Theory I, that when operative, it is the most effective ENDOR enhancement mechanism. That is, one may write $a_i(t) \cong 2\bar{a}\cos^2 Q_i$ for the ith methyl proton, and it is necessary to consider the cross-correlation effects between the equivalent but not completely equivalent nuclei. The effects these have upon the nonsecular $a_i(t) I_\pm S_\mp$ terms (which leads to W_x) have been discussed elsewhere.[21] In the present case, where $a \sim |\mathbf{A} - \bar{a}|$, it would be necessary to include that portion of the methyl proton hyperfine tensor which was calculated in Ref. 25 and averaged over the internal rotation. It is generally true that $\tau_I \ll \tau_R$, where τ_I is the correlation time for the internal rotation (when approximated by a classical model). Thus, the relaxation of these terms is in terms of a reduced $\tau^{-1} = \tau_I^{-1} + \tau_R^{-1} \cong \tau_I^{-1}$, and they could, if $\tau_I^2\omega_e^2 \lesssim 1$, contribute to both types of cross-relaxation terms. It has been shown in Papers I and V, however, that such cross-relaxation effects will lead to predictions on relative enhancements between methyl and ring protons that are different from those predicted when just the W_n are operative; and furthermore the $W_x \propto \tau_I$ vs $W_n \propto \tau_R$ should exhibit rather different temperature dependences, and this does not appear consistent with our results. Our results would thus suggest that the τ_I are too fast for these other terms modulated by the internal methyl-group modulation to make a major contribution to the ENDOR enhancements.

VI. CONCLUSION

The primary objective of this work has been to provide a quantitative test of the theory for ENDOR for free radicals in solution. The approach was to use ESR linewidth and saturation analyses to obtain basic information on the details of the various spin–relaxation processes, and then to use this information to predict the observed ENDOR enhancements and line shapes in terms of the theory. The most extensive study was performed for PBSQ, where the general theory could most readily be applied. Generally, quite reasonable quantitative agreement between theory and experiment was achieved, especially for dilute PBSQ solutions, despite the many complicating features involved in the experimental techniques and procedures and in their analysis as detailed above. The more difficult to analyze cases of DSQ and 2, 5-DMSQ were not as readily amenable to rigorous test, and, where appropriate, approximate forms of the ENDOR theory were applied. In general, however, the experimental results reported in this work were found to be fully consistent with the general trends pre-

dicted by the theory and expected from the magnitude and nature of the relaxation mechanisms obtained from the ESR studies. It is expected that in future work the detailed comparisons will be made even more precise.

ACKNOWLEDGMENT

We wish to thank Dr. M. R. Das for his very considerable help and advise regarding sample preparation during the early stages of this work.

*Supported in part by the Cornell University Material Science Center and by a grant from the National Science Foundation (Grant No. GP-13780). Based upon theses submitted by D. S. Leniart (1971) and H. D. Connor (1972) to Cornell University for partial fulfillment of the Ph.D. requirement.

[1]J. H. Freed, J. Chem. Phys. 43, 2312 (1965). References to this work are designated as I.

[2]J. H. Freed, J. Phys. Chem. 71, 38 (1967). References to this work are designated as II.

[3]J. H. Freed, D. S. Leniart, and J. S. Hyde, J. Chem. Phys. 47, 2762 (1967). References to this work are designated by III.

[4]J. H. Freed, J. Chem. Phys. 50, 2271 (1969). References to this work are designated by IV.

[5]J. H. Freed, D. S. Leniart, and H. D. Connor, J. Chem. Phys. 58, 3089 (1973).

[6]M. P. Eastman, R. G. Kooser, M. R. Das, and J. H. Freed, J. Chem. Phys. 51, 2690 (1969).

[7]M. P. Eastman, G. V. Bruno, and J. H. Freed, J. Chem. Phys. 52, 321 (1970).

[8]S. A. Goldman, G. V. Bruno, and J. H. Freed, J. Chem. Phys. 59, 3071 (1973).

[9]J. S. Hyde, J. Chem. Phys. 43, 1806 (1965).

[10]M. R. Das, H. D. Connor, D. S. Leniart, and J. H. Freed, J. Am. Chem. Soc. 92, 2258 (1970).

[11]D. S. Leniart, Ph.D. thesis, Cornell University, Ithaca, NY, 1971.

[12]H. D. Connor, Ph.D. thesis, Cornell University, Ithaca, NY, 1972.

[13]J. H. Freed, Am. Revs. Phys. Chem. 23, 265 (1972).

[14]J. R. Bolton and G. K. Fraenkel, J. Chem. Phys. 40, 3307 (1964).

[15]M. P. Eastman, Ph.D. thesis, Cornell University, Ithaca, NY, 1968.

[16]In some cases, spectroscopic information from the intensity differences of the high and low frequency ENDOR partner lines shed light on the various cross relaxation ($S_+I_\mp$ and $S_-I_\pm$) processes that are active. See, e.g., Ref. 1, and D. S. Leniart, J. C. Vedrine, and J. S. Hyde, Chem. Phys. Lett. 6, 637 (1970), and F. Gerson, J. Jachimowicz, K. Mobius, R. Biehl, J. S. Hyde, and D. S. Leniart, J. Mag. Reson. (to be published).

[17]J. W. H. Schreurs and G. K. Fraenkel, J. Chem. Phys. 34, 756 (1961).

[18]H. Wahlquist, J. Chem. Phys. 35, 1709 (1961).

[19]A preliminary report of these observations appears in Ref. 13. We have been informed by Atherton [N. M. Atherton, A. J. Blackhurst, and I. P. Cook, Chem. Phys. Lett. 8, 187 (1971)] that he has observed some similar phenomena. Beside the effect described above, he has observed a total inversion of the ENDOR line at high nuclear rf powers and high duty cycle. We have not succeeded in reproducing his results. We observed a line shape of type (C) in Fig. 6 with the nuclear rf field at 4.3 G, and the duty cycle at 50% for a dilute sample of DSQ in DME at $\tau = -30\,^\circ$C.

[20]J. H. Freed and G. K. Fraenkel, J. Chem. Phys. 39, 326 (1963).

[21]J. H. Freed and G. K. Fraenkel, J. Am. Chem. Soc. 86, 2477 (1964).

[22]G. K. Fraenkel, J. Phys. Chem. 71, 139 (1967).

[23]J. Gendell, J. H. Freed, and G. K. Fraenkel, J. Chem. Phys. 37, 2832 (1962).

[24]H. M. McConnell and J. Strathdee, Mol. Phys. 2, 129 (1959).

[25]D. S. Leniart and J. H. Freed (to be published).

[25a]Actually, more recent theoretical work [J. B. Pederson and J. H. Freed, J. Chem. Phys. 59, 2869 (1973)] has shown that $\tau_1 \cong d/D_\lambda$ for an exchange interaction of form $J_{(r')} = J_0 e^{-(r'-d)\lambda}$, where r' is the (variable) distance between the radical pair. Other modifications for large J_0 are also found.

[26]R. G. Kooser, W. V. Volland, and J. H. Freed, J. Chem. Phys. 50, 5243 (1969).

[27]M. R. Das, S. Wagner, and J. H. Freed, J. Chem. Phys. 52, 4675 (1970).

[28](a) S. Wagner, M. S. thesis, Cornell University, Ithaca, NY, 1969. (b) We note here that Eq. (3.25) of Ref. 5 for the average $\Omega^s_{n_\nu}\{M_\tau\}$ is actually less general than the conditions specified there. This is because the expressions for $\tilde{S}_{n_i n_j}$ which follow from Eqs. (A7'), (A8), and (A9) of V are rigorous only for the case of a single set of equivalent nuclei. When there is more than one set of equivalent nuclei, then the relaxation of the νth set of equivalent nuclei is, in general, affected by the alternate paths of relaxation made available by spin flips of other sets of equivalent nuclei $\tau \neq \nu$, and $\tilde{S}_{n_i n_j}$ becomes rather complex to calculate, although the expressions Eqs. (A4)–(A7) of V are fully applicable. Equation (3.25) of V will, however, always be an upper bound, and, when $\langle J^2_{\nu-}\rangle b_\nu \gtrsim \langle J^2_{\tau-}\rangle b_\tau$ it will usually be a reasonable approximation. When there are one or more sets of equivalent nuclei such that $\langle J^2_{\tau-}\rangle b_\tau \gg \langle J_{\nu-}\rangle b_\nu$, then Eq. (3.25) will usually overestimate $\Omega_{n^s_\nu}\{M_\tau\}$ by factors of the order of 2 or 3. Simple considerations show that in this latter limit Eq. 3.25 should be multiplied by the factor

$$\left(\prod_{\substack{\tau\neq\nu \\ \{J_\tau\}\,\mathrm{in}\,\{M_\tau\}}} D(J_\tau)^{-1}\right)\left(\prod_{\tau\neq\nu}\sum_{\{J_\tau\}\,\mathrm{in}\,\{M_\tau\}} D(J_\tau)\,[2J_\tau+1]^{-1}\right)$$

and τ refers only to the nuclei obeying $\langle J^2_{\tau-}\rangle b_\tau \gg \langle J^2_{\tau-}\rangle b_\nu$. The notation is discussed in Sec. II.B of Ref. 5. Also, the relative enhancements given by the expression on p. 3098 should be corrected for typographical errors to read

$$\langle \xi_e\rangle / \langle \Omega_e\rangle \approx \frac{\frac{1}{2} n_\nu d^2_{n_\nu} (\hbar W_e\{0\})^{-2}}{1 + d^2_{n_\nu}/b_\nu \hbar(b'')W_e\{0\}^2}\,.$$

The above-noted corrections to $\langle \Omega^s_{n_\nu}\rangle$ have no effect upon this expression for unsaturated NMR transitions, and this is the most important case for the average ENDOR theory. But, when the NMR transitions are appreciably saturated, the parameter b_ν^{-1} in this expression (which arises from the expression in Eq. 3.25 for $\langle \Omega^s_{n_\nu}\rangle$) must be modified as described above for $\langle \Omega^s_{n_\nu}\rangle$.

[29]P. S. Hubbard, Phys. Rev. 131, 1155 (1963).

[30]S. A. Goldman, G. V. Bruno, and J. H. Freed, J. Phys. Chem. 76, 1858 (1972).

[31]R. J. C. Brown, H. S. Gutowsky, and K. Shimomura, J. Chem. Phys. 38, 76 (1963).

[32]J. S. Hwang, R. P. Mason, L. P. Hwang, and J. H. Freed, J. Phys. Chem. (submitted).

[33]M. P. Eastman, G. V. Bruno, and J. H. Freed, J. Chem. Phys. 52, 2511 (1970).

[34]A. Abragam, *The Principles of Nuclear Magnetism* (Oxford U.P., London, 1961).

[35]H. C. Torrey, Phys. Rev. 92, 926 (1953).

[36]J. H. Freed, J. Chem. Phys. 43, 1710 (1965).